NUMERICAL SIMULATIONS OF SUBSONIC AEROELASTIC BEHAVIOR AND FLUTTER SUPPRESSION BY ACTIVE CONTROL

by

J. Alan Luton

Thesis submitted to the Faculty of the

Virginia Polytechnic Institute and State University

in partial fulfillment of the requirements for the degree of

Master of Science

in

Engineering Mechanics

APPROVED:

Dean T. Mook, Chairman

Ali H. Nayfeh

Scott L. Hendricks

December, 1991

Blacksburg, Virginia

NUMERICAL SIMULATIONS OF SUBSONIC AEROELASTIC BEHAVIOR AND FLUTTER SUPPRESSION BY ACTIVE CONTROL

by

J. Alan Luton

(ABSTRACT)

A method for predicting the unsteady, subsonic, aeroservoelastic response of a wing has been developed. The air, wing, and control surface are considered to be a single dynamical system. All equations are solved simultaneously in the time domain by a predictor-corrector method. The scheme allows nonlinear aerodynamic and structural models to be used and subcritical, critical, and supercritical aeroelastic behavior may be modeled without restrictions to small disturbances or periodic motions. A vortex-lattice method is used to model the aerodynamics. This method accounts for nonlinear effects associated with high angles of attack, unsteady behavior, and deformations of the wing. The vortex-lattice method is valid as long as separation or vortex bursting does not occur. Two structural models have been employed: a linear model and a nonlinear model which accounts for large curvature. Both models consider the flexural-torsional motion of an inextensional wing.

A series of simulations have shown the response of the wing as the velocity is increased while the angle of attack has been changed such that the lift is approximately constant. Below the flutter speed the oscillations decay while velocities above the flutter speed produce oscillations that grow exponentially at a common frequency.

Oscillations of the wing are suppressed by the motion of a control surface that is

governed by a feedback control law based on state values of the wing and prescribed gains. Flutter has been suppressed at velocities well beyond the flutter speed, but the response to random wind gusts cannot be completely controlled.

Acknowledgements

Many people have made my experience at Virginia Tech a rewarding one. Dr. Mook has offered his knowledge, guidance, encouragement, and perhaps most importantly, patience throughout my course of studies. His dedication to his profession is tremendous. Despite his many activities he always manages to find time for my questions and concerns. I am also indebted to Dr. Nayfeh and Dr. Hendricks for reading this manuscript and providing helpful suggestions. A special thanks is also in order to Dr. Kriz who has been a constant source of energy and ideas. His timely last minute help is greatly appreciated. In addition, Sally Shrader has performed many clerical services and has also provided helpful advice.

The support of Karen Brandes during my studies has been amazing. Her love, understanding, patience, and courage have made possible the goals I have achieved. She endured my long hours in the lab with a cheerfulness that was contagious. Her commitment has been an almost unlimited source of strength throughout our relationship.

The support of my family has also been deep and unwavering. Their praise of my accomplishments and encouragement in times of doubt has always been heartening. My parents Jim and Norma, my grandparents James and Edith, my sisters Barbara and Karen, and my brother Neil have all contributed in their own unique way.

Finally, I would like to acknowledge the people who have served as my role models: my father and Dr. Scott Northrup. Both exhibit exceptional character and morals and have had a profound influence on my life.

Table of Contents

List of Illustrations

Chapter 1 Introduction and Literature Review

1.1 Overview

In recent years the study of aeroelasticity has entered into the mainstream of aircraft design. In particular, the advancement of composite materials, while reducing weight, has led to more flexible aircraft. This in turn demands a closer investigation into possible structural-aerodynamic instabilities. These instabilities arise from the coupling between the aerodynamic forces, the elastic forces, and the inertial forces.

This study focuses on the aeroelastic behavior of high-aspect ratio wings in the subsonic regime. The wing and surrounding air are treated as a single dynamical system with the equations of motion for the wing and fluid solved simultaneously in the time domain. In contrast with solutions performed in the frequency domain, time-marching schemes allow the modeling of subcritical and supercritical aeroelastic behavior. The solution of the equations of motion must account for the coupling between the structure and the fluid. In other words, the aerodynamic loads depend upon the deformation and rate of deformation of the wing while the deformation and rate of deformation of the wing depend upon the aerodynamic loads. The coupled equations are solved by an iterative solution scheme based upon a predictor-corrector numerical integration algorithm.

An elastic wing that is free to bend and twist is examined. The elastic equations are linear with the bending and twisting motions uncoupled. In addition, a nonlinear formulation of an inextensional wing that accounts for large curvature effects is included.

Although the flexure and torsion are structurally uncoupled, they are coupled through the aerodynamic loads. The loads are provided by a vortex-lattice method and nonlinearities due to angle of attack and static or dynamic deformations are included. The geometry of the wake is part of the solution so the history of the motion is stored in the wake.

This study moves beyond merely predicting the aeroelastic behavior to suppressing the flutter of the wing by active feedback control. Control surfaces are added near the wing tips and moved in accordance with various control laws. These control laws are based on feedback that could be obtained by placing accelerometers near the wing tips. The response of the system to random wind gusts is also examined, with and without active control.

1.2 Aeroelastic Effects

Aeroelastic effects result from the interaction between aerodynamic, elastic, and inertial forces. Of course, each of these areas alone represents a field of study, that is, fluid mechanics, solid mechanics, and dynamics. It is also common to study the interactions between any two of these fields. The study of mechanical vibrations involves dynamics and solid mechanics, while the dynamic characteristics of rigid aircraft involve dynamics and aerodynamics. The study of the steady interaction between aerodynamic forces and elastic forces is known as static aeroelasticity. For the most general case, known as dynamic aeroelasticity, the aerodynamic, elastic, and inertial forces must all be considered.

Areas of concern in static aeroelasticity include stability, reversal of control, and

divergence. As an example of reversal of control, consider the right wing of an airplane attempting to bank to the left. The right aileron is rotated downward to increase the lift. For most wings this increase in lift causes a change in the twisting moment that rotates the leading edge downward, resulting in a loss of lift. At some critical speed the two changes in lift are exactly equal and the controls are rendered inoperative. A further increase in speed would result in a reversal in the sense of the controls.

The divergence of a wing is a static instability which is characterized by large deformations. Divergence is a result of the aerodynamic loads being greater than what the wing can support in any deformed position. This instability is usually not a concern since the divergence speed is generally greater than the flutter speed.

Unsteady aeroelasticity involves the influence of elastic structures on the stability and control of the aircraft, the response due to gusts and turbulence, and the motion of the lifting surface itself. Of great concern is the phenomenon known as flutter, in which the structure exhibits self-sustained oscillations. Types of flutter include control surface flutter, panel flutter, stall flutter, and classical flutter. Fung (1955) defines classical flutter as an "oscillatory instability in a potential flow, in which neither separation nor strong shocks are involved." This is the sense in which the term flutter is used. Descriptions of the flutter phenomenon are also given by Bisplinghoff, Ashley, and Halfman (1955) and Dowell et al. (1989). General discussions of classical flutter are given by Hancock and Wright (1985) and Niblett (1988). Garrick (1969) published a collection of classical papers concerning flutter. Physical mechanisms for flutter are offered in Pines (1958) and Biot and Arnold (1948).

The current work concerns the classical flutter of a cantilevered wing constrained to flexural and torsional motions. In general, the coupling of the flexural and torsional motions is essential for classical flutter. A wing constrained to flexure only will not flutter. A wing constrained to twisting motions will flutter only near the stalling angle of attack or for certain special mass distributions or locations of the elastic axis. The coupling between the flexure and torsion allows the wing to adjust in such a way that it may absorb energy from the freestream. The critical parameter is the phase difference between the two motions.

Below some critical speed, any disturbance given to the wing will decay; the phase difference is such that the net transfer of energy is from the wing to the air. Thus the wing is damped through aerodynamic effects even in the absence of structural damping and viscous effects. As the speed increases, there may be a point at which the net flow of energy between the wing and air is zero. This critical speed is known as the flutter speed and the state is neutrally stable. Any disturbance results in self-sustained harmonic oscillations. At subcritical speeds the frequencies of bending and twisting are distinct, but the frequencies are equal at and above the flutter speed. The value of the frequency is between the undamped natural frequencies of flexure and torsion. This is sometimes referred to as frequency coalescence and is a characteristic of classical flutter. A slight increase in speed will, barring nonlinear effects, lead to unbounded motions. This is a result of the wing gaining energy from the freestream. The following example, which closely follows one presented in Duncan (1959), illustrates the role of the phase difference in the energy exchange.

For the sake of simplicity, consider a symmetric, rigid wing initially at zero angle of attack and having two degrees of freedom: a vertical displacement perpendicular to the freestream and a rotation about some spanwise axis. Also let the aerodynamic loads be those due to pitch only. As noted before, the motions are harmonic and the frequencies are the same at the flutter speed. Now examine two different cases: one in which the phase difference between the two motions is zero and one in which the pitch rotation leads the vertical displacement by 90 degrees. The motion of the wing over one period for these two cases is shown in Figure 1.1. When the phase difference is 90 degrees, the lift is always in the same direction as the vertical displacement. Hence, the net work is positive, that is, the wing gains energy from the freestream and the system is unstable. However, when the phase difference is zero the net work is zero and the system is neutrally stable. Thus it is the coupling between the modes that is essential to understanding classical flutter and it is the phase difference between the motions that allows the wing to gain energy from the freestream.

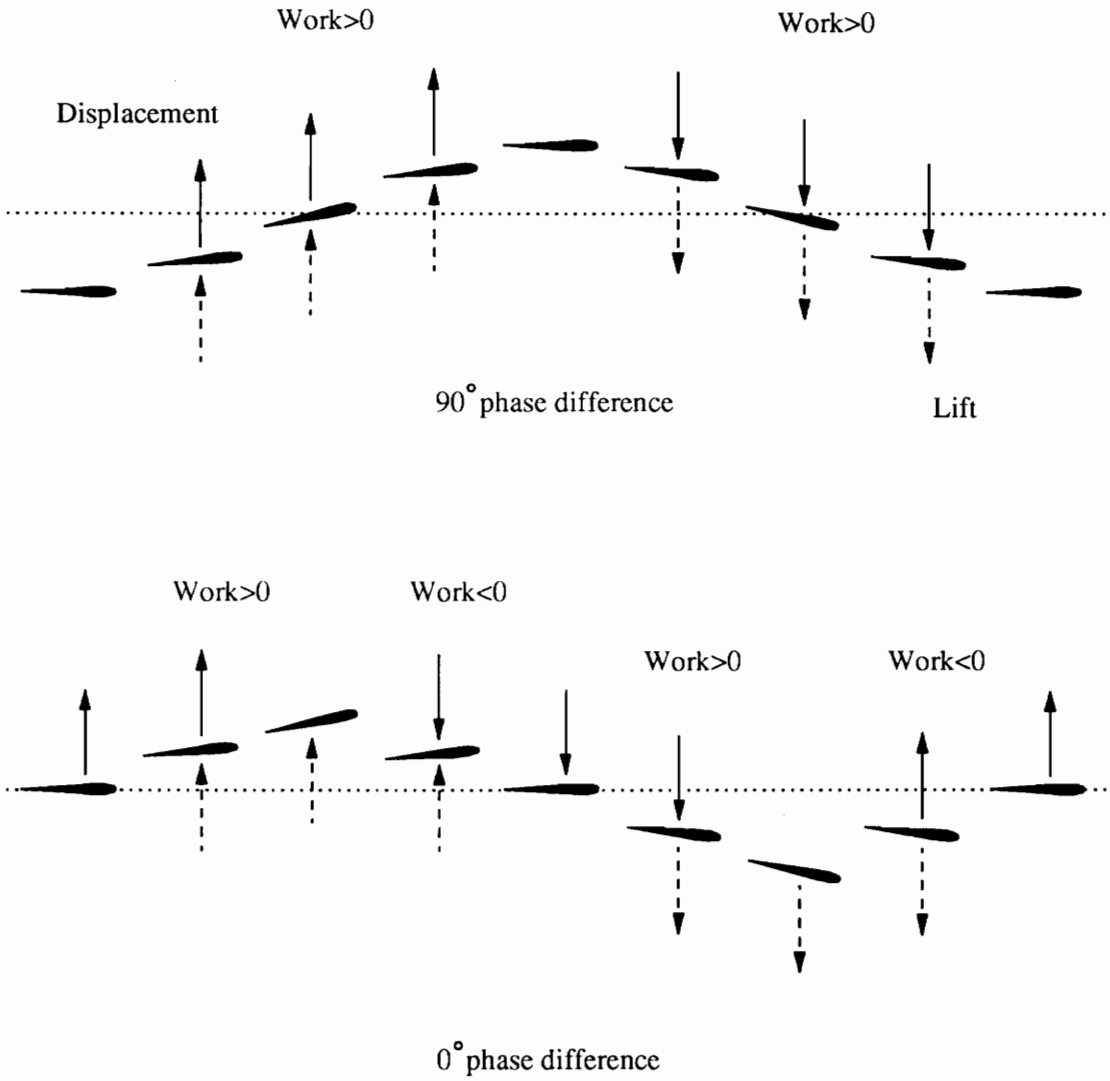

Figure 1.1 An example of the effect on flutter of the phase difference between the flexural and torsional displacements of a rigid wing. Work done by the air on the wing is defined as positive.

1.3 Aerodynamic Models

The current focus of aeroelastic research is primarily on the accurate determination of the unsteady aerodynamic loads, particularly in the transonic flow regime. This regime is of concern for two reasons: the critical dynamic pressures are typically lower and aerodynamic nonlinearities tend to be more important. Dowell and Ilgamov (1988) examined nonlinear aeroelasticity in the transonic regime and the conditions for which the nonlinearities are important. Cunningham et al. (1988) discuss flutter analysis using computational fluid dynamics methods while Borland and Rizzetta (1981) compare their CFD approach with more traditional methods of flutter analysis.

In the past there have been many different models used in aeroelasticity to find the unsteady aerodynamic loads. These include the kernel function, influence-coefficient, strip theory, piston theory, and doublet-lattice methods. The first to find a solution for an oscillating airfoil was Theodorsen (1935). Kussner (1940) laid the foundation for general nonstationary wing theory. He presented the basic idea of the kernel function, developed later by Watkins et al. (1955) and others. Most methods are, however, linear quasi-steady models. In the current work, a vortex-lattice method is used to obtain the aerodynamic loads. This allows aerodynamic nonlinear and unsteady effects to be included in the aeroelastic model. Thus, the effects of static deformations and large angles of attack may be incorporated into the model of the system.

The vortex methods are based on the theorems of Helmholtz (1858) who showed that in an inviscid fluid vortex filaments are always composed of the same fluid particles. Flow fields may be modeled as inviscid except where the vorticity is concentrated into

vortex filaments whose cross-sectional area is infinitely small. Sarpkaya (1989) gives an excellent review of the vortex methods including fundamental theory as well as practical applications. The vortex-lattice methods originated from the work of Belotserkovskiy (1966) who first approximated the free and bound vortex sheets with vortex lattices. His method could treat the unsteady flow about wings of arbitrary planform and deformation. Each element is associated with a horseshoe vortex with the semi-infinite vortices aligned with the free stream. Thus the geometry of the wake could not be modeled and the solution was limited to small angles of attack. Ermolenko (1966) was the first to model the wing tip vortex, but he neglected the trailing edge wake. Belotserkovskiy (1968) improved Ermolenko's model by including both the trailing edge and wing tip vortex sheets for steady flows. Belotserkovskiy and Nisht (1974) presented a nonlinear method for unsteady flow that solved for the geometry of the wake convected from the wing tips and trailing edge. Mook and Maddox (1974) modified Belotserkovskiy's model to include the effects of leading edge separation on highly swept wings. Although the leading edge free vortex sheet was force-free, the free vortex sheet from the trailing edge was not. Kandil (1974) and Kandil, Mook, and Nayfeh (1974) created an unsteady, nonlinear model for rectangular and delta wings with sharp edge separation. Thrasher et al. (1977) posed the problem in a body-fixed coordinate system and allowed the wings to perform arbitrary maneuvers. This method is completely general as long as separation occurs along the sharp edges and vortex bursting does not occur near the wing.

Thrasher (1979) combined the aerodynamic model with a predictor-corrector method to simultaneously predict the flow field, the motion of a hinged rectangular wing,

and the prescribed motion of a flap. Kandil et al. (1977) modified this approach for delta wings and developed a higher-order theory for the convection of the wake. Nayfeh et al. (1979) modified the method to include small harmonic oscillations about a steady-state angle of attack.

Konstandinopoulos (1984) and Konstandinopoulos, Mook, and Nayfeh (1985) describe a method for simulating one degree of freedom wing rock. Elzebda (1986) expanded the method to include two degrees of freedom for wing rock. The vortex-lattice method is also capable of modeling aerodynamic interference between multiple lifting surfaces as shown by Elzebda, Mook, and Nayfeh (1985) and Elzebda (1986).

In an approach similar to the one used in the current work, Strganac and Mook (1987) and Strganac (1987) used the vortex-lattice method and a predictor-corrector numerical integrator to solve the classical flutter problem for a rigid wing and an elastic wing. Nuhait (1988) incorporated feedback control in his model and also studied ground effects. Most recently, Dong (1991) used feedback control to suppress the flutter of a two dimensional wing section.

1.4 Structural Models

The current work concerns a cantilevered wing constrained to bending in the lateral direction and twist about its elastic axis. Bending in the chordwise direction is neglected due to the high stiffness. For rotor dynamics, however, this flexure can be important. Discussions of rotary-wing aeroelasticity are found in Dowell et al. (1989) and Ormiston (1988).

Two structural models are included in the present work: a linear model and a nonlinear model that accounts for large curvature effects. Nonlinear effects are frequently included in the aeroelastic study of rotorcraft. In addition to the previous references, Crespo da Silva and Hodges (1986) and Kaza and Kvaternik (1977) address the effect of nonlinearities. Hauenstein et al. (1990) show how structural nonlinearities can lead to complicated motions, including chaos. In the present work the nonlinear model is derived by an approach similar to that of Crespo da Silva and Glynn (1978). Material and inertial nonlinearities are not included in this formulation and the wing is assumed to be inextensional.

The deformation of the wing is traditionally represented in terms of generalized coordinates and the mode shapes. This procedure was first proposed by Loring (1941). The modes may be found by experiment, analytical means, energy methods, or finite element techniques. For complicated geometries or anisotropic materials it might be advantageous to use a finite element method directly with the fluid dynamics equations to find the deformation. The use of composite materials has created numerous opportunities in the field of aeroelastic tailoring. Weisshaar (1987) and Ashley et al. (1980) give a general description of this field, which is concerned with controlling various responses of the system by the incorporation of directional stiffnesses into the structure.

1.5 Aeroelastic Models

Aeroelastic formulations may be divided into two broad categories: frequency domain solutions and time domain solutions. Each has its own advantages and

disadvantages. Dowell et al. (1989) has a comprehensive study of the relative merits. The frequency domain solutions are the most popular. They are computationally more economical but only model the system at the critical condition. The slow development of the aerodynamic theory for general unsteady motions has hampered the progress of time domain solutions but they are rapidly gaining popularity. These solutions offer more physical insight into the problem and can model subcritical and supercritical behavior.

The frequency domain solutions usually rely on quasi-steady linear theory. Traditionally, the aeroelastic equations of motion are put in matrix form which may then be solved in many different ways. All solutions are based on the assumption that periodic motion exists. Theodorsen's method finds the flutter speed by breaking the flutter determinant into its real and imaginary parts and solving the equations for various values of k, the reduced frequency. The equations may also be solved by matrix methods or iteration. Goland and Luke (1949) used an iterative method to find the conditions under which an initial disturbance leads to nondecaying motions. Fung (1955) discusses many of the frequency domain techniques. Other solutions such as the p, k, and p-k methods are discussed in Richardson (1965) and Hassig (1971). The most common of the frequency domain solutions is the velocity-incremental damping (V-g) method originated by Smilg and Wasserman (1942). This method is discussed in Yates (1971) and Dowell et al. (1989). The solution is found by setting the determinant of the aeroelastic equations (the flutter determinant) equal to zero. A fictitious damping g is introduced whose value is such that the resulting motion is harmonic. The solution is found by varying the velocity and solving for g. The critical flutter speed occurs when g is equal to zero or

the actual damping of the system. For a three dimensional problem written in terms of n natural modes there are n corresponding functions g(V) and possibly more than one flutter point. Of course, the flutter point of interest is the one of lowest speed. It should be emphasized that the solution obtained with all frequency domain methods is only valid at the critical speed since periodic motion has been assumed.

The time domain solutions, while creating a more formidable problem, provide more physical insight into the nature of flutter. These methods find a solution by numerical time integration. This allows the structural equations to be solved simultaneously with the aerodynamic equations to give a time history of the motion of the system. Thus the subcritical and supercritical behavior of the system may also be found. The time domain solutions also allow a nonlinear flutter analysis as opposed to the frequency domain solutions. There are many different formulations for time domain solutions, mostly due to the effort in finding more efficient or stable algorithms. Dowell et al. (1989) give a general discussion of the time domain methods.

1.6 Control of Aeroelastic Responses

The aeroelastic response of an aircraft may be modified in such a way as to increase stability and performance while minimizing weight. The methods of controlling the aeroelastic responses fall into two categories: passive and active. Passive methods include changing the shape or mass distribution of a lifting surface, changing the stiffness, or reducing the flight speed. The use of composite materials has created many possibilities for altering the dynamic characteristics of a wing. However, passive control

is inherently limited to a single flight condition. The great advantage of active control is its usefulness over the entire flight envelope. Both methods may increase the flight envelope significantly. Active control involves moving control surfaces according to control laws based on output from sensors (usually accelerometers) placed on the wing. This discipline is commonly referred to as aeroservoelasticity. Most control systems are designed using classical feedback control techniques. Another approach is based on the aerodynamic energy method as first proposed in Nissim (1971). This method places the control surface at the spanwise location of maximum energy transferred between the wing and air.

Design approaches typically consist of three basic steps. First a full order optimal control law is developed. Linear quadratic Gaussian theory is the most widely used (see Mahesh et al. (1981) and Mukhopadhyay (1989)). However, due to the many state variables needed to model the system (rigid and elastic body modes, unsteady aerodynamic forces, etc.) the order of the control law is often reduced. There are many different methods of reduction. Mukhopadhyay et al. (1982) and Ohta et al. (1989) describe some of these. The reduced order system is then optimized. More complete discussions of aeroservoelasticity are found in Karpel (1981) and Noll (1990).

1.7 The Present Method

A general method for determining the unsteady subsonic aeroelastic response of a wing is presented herein. A modular approach allows different structural and aerodynamic models to be used if desired. The structural and aerodynamic equations are

solved simultaneously in the time domain. This creates a substantial advantage over the frequency domain techniques by providing physical insight into the problem. Thus a time history of subcritical, critical, or supercritical behavior may be obtained. The response due to atmospheric disturbances such as gusts and turbulence may also be modeled. In addition, an active control system is implemented in an effort to modify the response in a desirable way.

In Chapter 2 the unsteady vortex-lattice aerodynamic model is described. The equations are developed for any body performing arbitrary motions. Accuracy considerations and the range of validity are examined.

The structural equations are discussed in Chapter 3. Both linear and nonlinear models are presented. The wing is modeled as an inextensional cantilevered beam which is allowed two degrees of freedom: flexure and torsion. Euler-Bernoulli theory is used for the linear model while the nonlinear model accounts for large curvature effects.

The integration of the coupled structural and aerodynamic equations is the subject of Chapter 4. Generalized coordinates and normal modes are used to reduce the equations to ordinary differential equations. Both the static and dynamic solutions are found. The nonlinear static solution is solved by iteration while the dynamic solution is solved by an iterative scheme based on Hamming's predictor-corrector method.

In Chapter 5 several examples of static and dynamic solutions are presented for various freestream velocities and initial disturbances. The response due to random gusts is also studied. The effect of active control on gust response and flutter is demonstrated. The solutions are also shown graphically in a time sequence of the positions of the wing

and wake.

Conclusions drawn from the numerical simulations and the advantages and disadvantages of the present method are presented in Chapter 6.

This thesis is organized so that the figures appear at the end of the subsections in which they are first discussed.

Chapter 2 The Aerodynamic Model

2.1 Introduction

The unsteady vortex-lattice method is a fully three dimensional model that can simulate arbitrary subsonic maneuvers of thin finite wings of arbitrary planform at arbitrary angles of attack as long as stall or vortex bursting does not occur. It may also be used to model multiple coupled lifting surfaces and ground effects as shown by Elzebda (1986) and Nuhait (1988). Aerodynamic nonlinearities due to large angles of attack and static deformations can be included as well.

The unsteady vortex-lattice method models an irrotational and incompressible flow. Flows of this type are briefly discussed in the following sections.

2.2 The Governing Equation

For an incompressible and irrotational flow potential theory may be used and the continuity equation becomes

$$\nabla^2\phi=0 \tag{2.1}$$

where ϕ is the velocity potential and the velocity $\vec{V}$ is given by $\vec{V}=\nabla\phi$. The boundary conditions are

$$\vec{V} \rightarrow \vec{V}_\infty \qquad \text{away from } S_{LS} \text{ and } S_W \tag{2.2}$$

$$(\vec{V}-\vec{V}_{LS})\cdot\vec{n}=0 \qquad \text{on } S_{LS} \tag{2.3}$$

where $\vec{V}_\infty$ is the freestream velocity, $\vec{V}_{LS}$ is the velocity of the lifting surface (which is used to imitate the wing), S_{LS} represents the lifting surface, and S_W represents the surface of the wake. The first boundary condition states that the velocity approaches the freestream velocity as the distance from the wing and wake approaches infinity. The second boundary condition is the no-penetration condition. It is applied on the lifting surface and requires that the normal component of the relative velocity be zero.

2.3 The Biot-Savart Law

The basic tool of the vortex-lattice methods is the Biot-Savart law, which, for a straight vortex filament of constant strength, is given by

$$\vec{V}_P=\frac{\Gamma}{4\pi h}(\cos\theta_1-\cos\theta_2)\hat{e} \tag{2.4}$$

where $\vec{V}_P$ is the velocity at any arbitrary point P induced by the vortex filament with circulation Γ as shown in Figure 2.1. The vortex filament extends from point 1 to point 2. The vector $\hat{e}$ is a unit vector perpendicular to the plane containing points 1, 2, and P and in the direction of $\vec{\Omega}\times\vec{r}_1$, where $\vec{\Omega}$ is the vorticity. The variable h is the perpendicular distance from the point P to the vortex filament and θ_1, θ_2, and $\vec{r}_1$ are

defined in the figure. An examination of equation (2.4) shows that if the point $\boldsymbol{P}$ lies along the line $\boldsymbol{L}$ away from the vortex filament the induced velocity is zero. If the point $\boldsymbol{P}$ approaches the vortex filament then the induced velocity tends to infinity. There is a mathematical singularity, or infinite vorticity. The effects of finite vorticity and cross-sectional area cause the velocity to approach zero as shown in Figure 2.2. This is approximated by the addition of the following equation to the Biot-Savart law:

$$\vec{V}_P = 0 \qquad \text{if } h < h_0 \tag{2.5}$$

where h_0 is a user specified distance. Kelly (1977) studied the effect of this approximation.

The Biot-Savart law can be derived from the definition of vorticity by assuming an incompressible flow. The induced flow is also irrotational so the governing equation is satisfied. The far-field boundary condition is satisfied because the induced velocity decays inversely with distance. With the vortex-lattice methods the satisfaction of the no-penetration condition provides the values of the circulations around the individual, discrete vortex filaments from which the pressure on the lifting surface may be found.

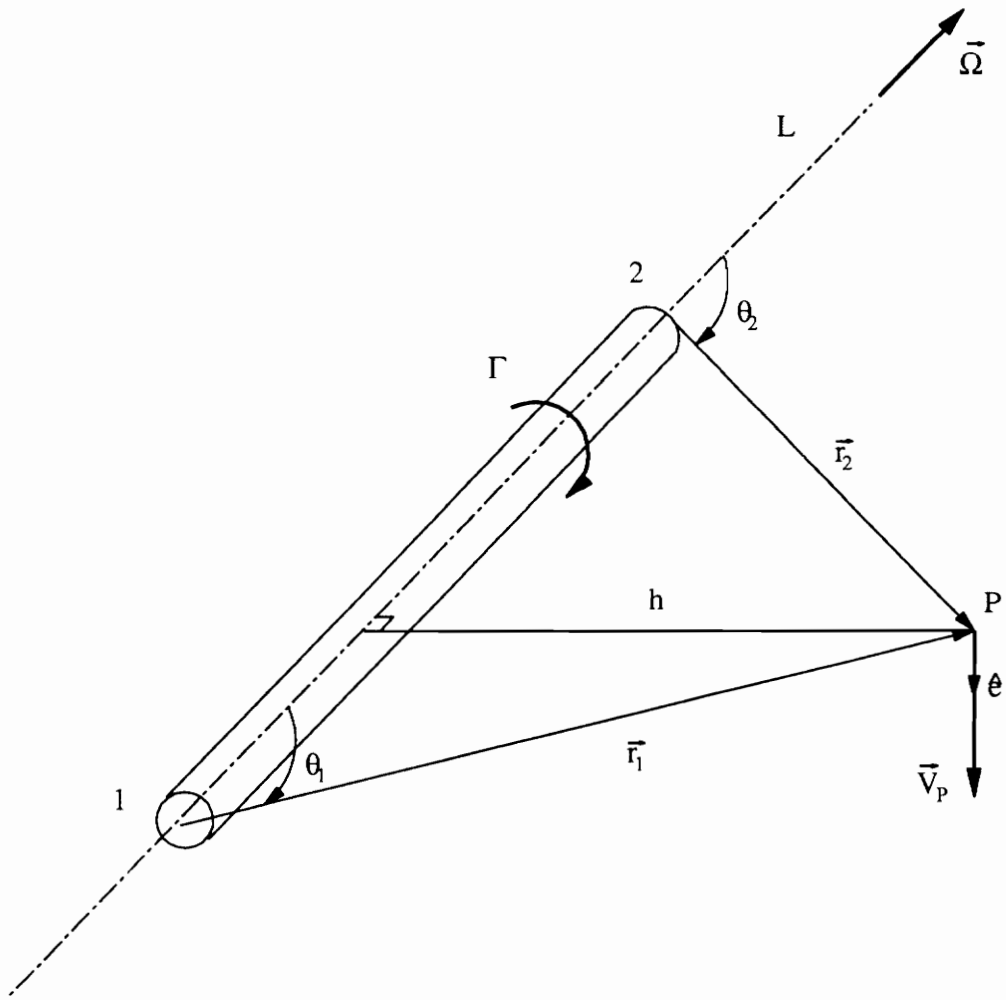

Figure 2.1 The Biot-Savart law.

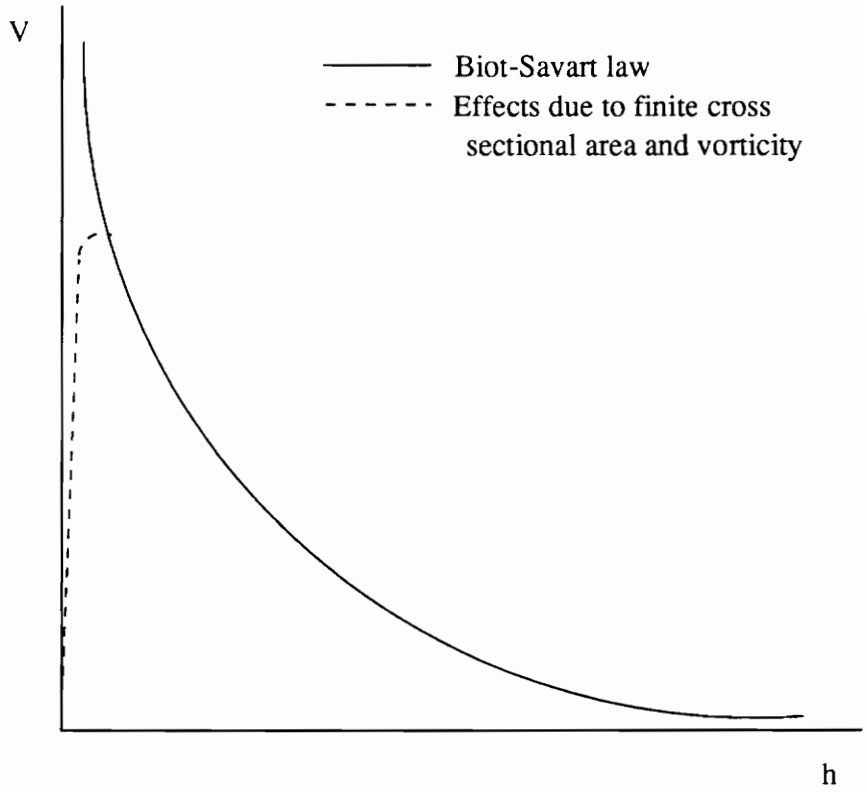

Figure 2.2 The velocity induced by a vortex filament of finite length.

2.4 The Unsteady Kutta Condition

For steady flows the Kutta condition requires the pressure difference, and therefore the circulation, to be zero along the edges of the wing. This forces the flow to leave the trailing edge smoothly. The unsteady Kutta condition requires that in order for the pressure difference to vanish along the edges the vorticity created along the edges must be shed. This shed vorticity convects away from the wing at the local particle velocity and forms the simulation of the wake. This point is discussed further in the following sections.

2.5 The Kelvin-Helmholtz Theorem and Spatial Conservation of Vorticity

Because vorticity is a divergenceless field, it can be shown that circulation must be spatially conserved. For a vortex filament, the circulation is constant along the filament at any instant in time. Consequently, vortex filaments cannot begin or end in a fluid. They must form closed loops or end at a boundary or infinity.

The Kelvin-Helmholtz theorem states that the circulation around any closed curve of fluid particles is constant for all times, or

$$\frac{D\Gamma}{Dt}=0 \tag{2.6}$$

Equation (2.6) applies only in the region of an inviscid flow where the relationship between the pressure and density is single-valued. The density is assumed to be constant while the pressure is continuous everywhere except across the lifting surface. The

implication is that vortex filaments in the wake are always composed of the same fluid particles. They are convected at the local particle velocity and can sustain no force. The discontinuity in pressure across the lifting surface gives the aerodynamic forces and moments.

2.6 The Unsteady Vortex-Lattice Method

2.6.1 Overview

As a body moves through a fluid, vorticity is generated in a thin region adjoining the surface known as the boundary layer. The rest of the flow field is considered irrotational and incompressible. The boundary layer may be modeled with a vortex sheet on the body. If the thickness of a wing is small compared with its chord, then the wing may be modeled as a single vortex sheet lying on the camber surface. Furthermore, the vortex sheet may be replaced by a finite number of vortex filaments that form a grid as shown in Figure 2.3. The grid is composed of closed loops of constant circulation, denoted by $\boldsymbol{G}$, as required by the spatial conservation of vorticity. The circulation around a vortex filament that is part of two loops is the difference between the loop circulations of the adjoining elements as shown in Figure 2.4.

The values of the loop circulations are found by imposing the no-penetration condition on the wing at the control points of the panels. The locations of the vortex filaments and the control points are based on the results for two dimensional steady flow

past a flat plate. An exact solution is known for a vortex sheet along a flat plate. If the sheet is replaced by a point vortex at the quarter-chord point and the no-penetration condition is enforced at the three-quarters-chord point, then the normal force and moment are in agreement with the exact solution. Thus, the grid of vortex filaments is shifted toward the trailing edge by a distance of one quarter of the chord length of one element as shown in Figure 2.3. The control point then becomes the centroid of the element.

However, the model is still incomplete. The unsteady Kutta condition requires that the vorticity generated along the edges be shed. This vorticity is convected at the local particle velocity in accord with the Kelvin-Helmholtz theorem. Thus a force-free wake is created which contains the vorticity (or circulation) shed from the wing. The wake therefore contains information from the past which affects the wing at the current time.

The lattice representing the wing is called the bound lattice because its position is specified and it can sustain a pressure difference. The lattice representing the wake is convected at the local particle velocity; it is, therefore, force-free and is referred to as the free lattice.

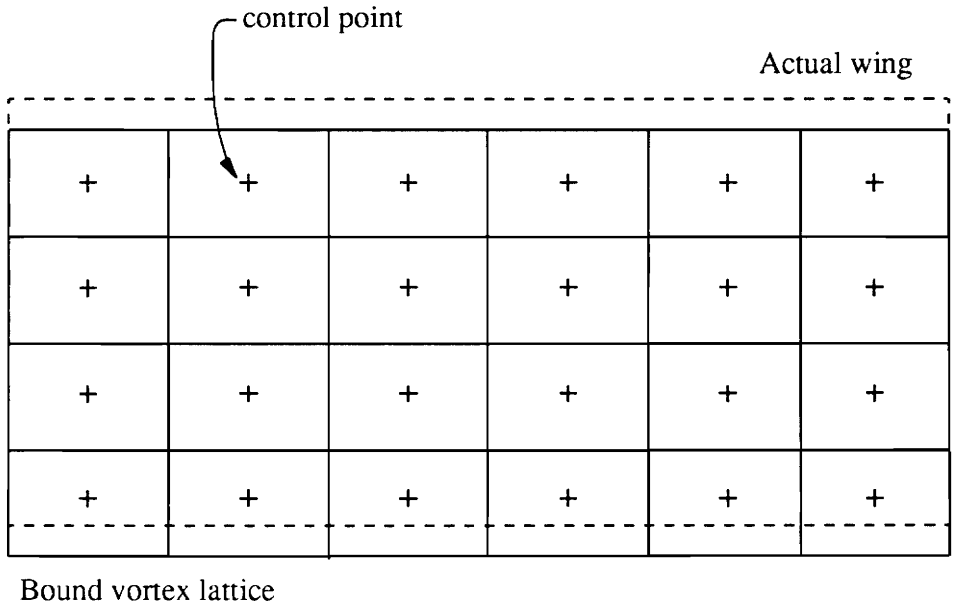

Figure 2.3 The bound vortex-lattice representation of the wing.

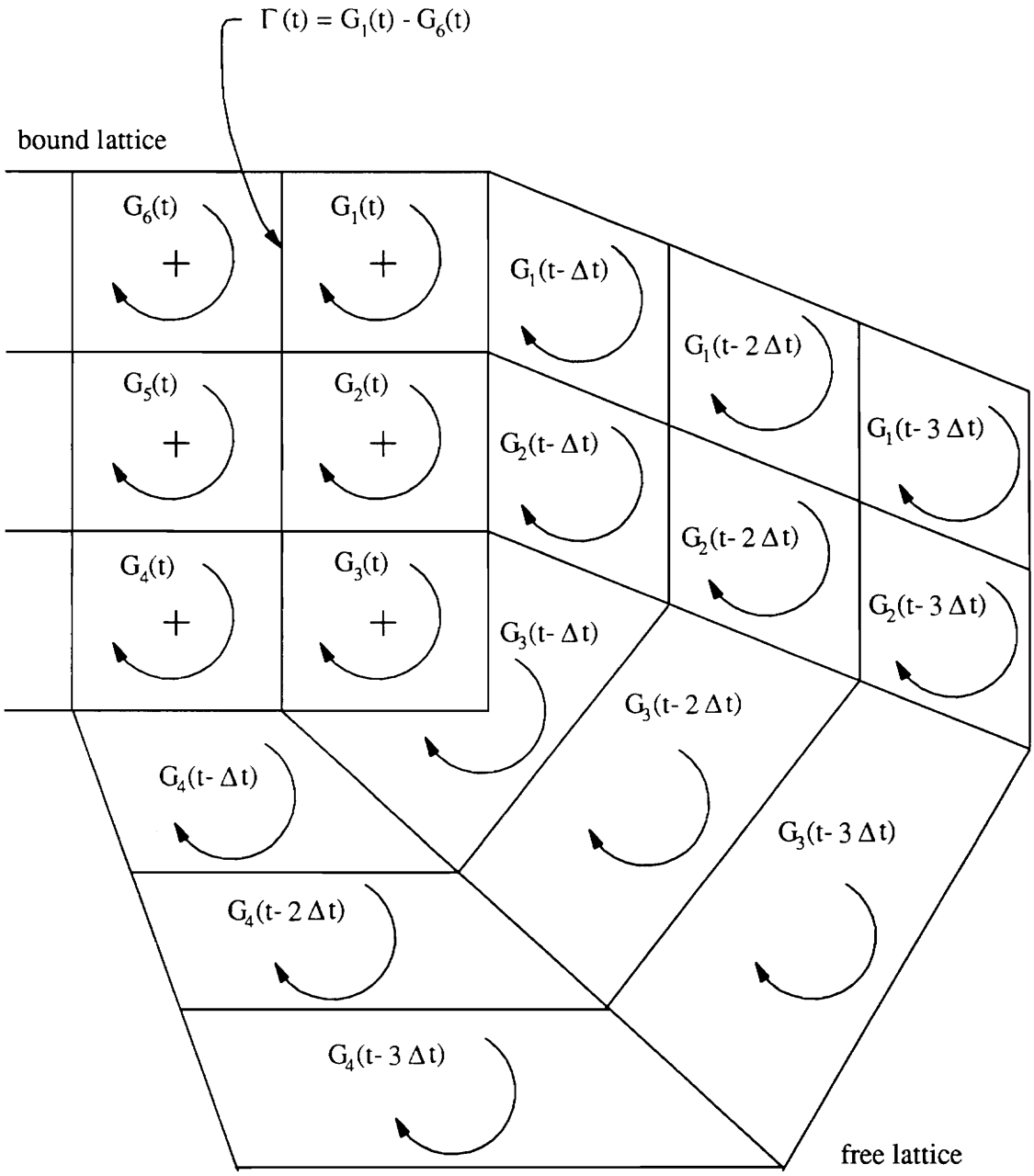

Figure 2.4 Convection of the wake.

2.6.2 Nondimensional Variables

The problem is nondimensionalized by using the following characteristic variables of length, velocity, and density:

L_c is the chordwise length of one element of the bound lattice.

V_c is the initial freestream velocity of the air.

ρ_c is the freestream density of the air.

From these definitions the characteristic time is defined as $T_c = L_c / V_c$. The choices for L_c and V_c are convenient for two reasons. First, an increase in the number of elements in the chordwise direction of the bound lattice automatically leads to a corresponding decrease in the physical time step. Second, a nondimensional time step of one creates wake elements of approximately the same dimensions as the elements on the wing.

2.6.3 Coordinate Systems

All equations are written in terms of a body-fixed coordinate system that moves with the aircraft as shown in Figure 2.5. The x axis is forward with the body of the aircraft, the y axis is in the spanwise direction, and the z axis is downward. The orientation of the body-fixed frame is given by a 3-2-1 set of Euler angles as described in Nuhait (1988). Initially the body-fixed frame $Ax_1y_1z_1$ is aligned with the ground-fixed frame $OXYZ$. As time progresses the body-fixed frame assumes a particular orientation in space defined by the following rotations:

1) A yaw-like rotation $\psi(t)$ about the z_1 axis to an orientation $Ax_2y_2z_2$.

2) A pitch-like rotation $\theta(t)$ about the y_2 axis to an orientation $Ax_3y_3z_3$.

3) A roll-like rotation $\phi(t)$ about the x_3 axis to the final orientation $Axyz$.

The unit vectors of the two reference frames are related by

$$\begin{bmatrix} \hat{i} \\ \hat{j} \\ \hat{k} \end{bmatrix} = [R_1(\phi)][R_2(\theta)][R_3(\psi)] \begin{bmatrix} \hat{I} \\ \hat{J} \\ \hat{K} \end{bmatrix} = [R] \begin{bmatrix} \hat{I} \\ \hat{J} \\ \hat{K} \end{bmatrix} \tag{2.7}$$

where $\hat{i}$, $\hat{j}$, and $\hat{k}$ are the unit vectors of the body-fixed frame and $\hat{I}$, $\hat{J}$, and $\hat{K}$ are the unit vectors of the ground-fixed frame. The rotation matrices are

$$[R_1(\phi)] = \begin{bmatrix} 1 & 0 & 0 \\ 0 & c\phi & s\phi \\ 0 & -s\phi & c\phi \end{bmatrix} \quad [R_2(\theta)] = \begin{bmatrix} c\theta & 0 & -s\theta \\ 0 & 1 & 0 \\ s\theta & 0 & c\theta \end{bmatrix} \quad [R_3(\psi)] = \begin{bmatrix} c\psi & s\psi & 0 \\ -s\psi & c\psi & 0 \\ 0 & 0 & 1 \end{bmatrix} \tag{2.8}$$

where c and s represent the cosine and sine functions. The matrix $[R]$ is the triple product of the rotation matrices:

$$[R] = \begin{bmatrix} c\psi c\theta & s\psi c\theta & -s\theta \\ -s\psi c\phi + c\psi s\theta s\phi & c\psi c\phi + s\psi s\theta s\phi & c\theta s\phi \\ s\psi s\phi + c\psi s\theta c\phi & -c\psi s\phi + s\psi s\theta c\phi & c\theta c\phi \end{bmatrix} \tag{2.9}$$

Since the origins of the body-fixed frame and ground-fixed frame do not coincide, equation (2.7) must be modified as follows:

$$\begin{bmatrix} x \\ y \\ z \end{bmatrix} = [R] \begin{bmatrix} X - X_A \\ Y - Y_A \\ Z - Z_A \end{bmatrix} \tag{2.10}$$

or

$$\begin{bmatrix} X \\ Y \\ Z \end{bmatrix} = [R]^T \begin{bmatrix} x \\ y \\ z \end{bmatrix} + \begin{bmatrix} X_A \\ Y_A \\ Z_A \end{bmatrix} \tag{2.11}$$

because the inverse of a rotation matrix is equal to its transpose (the transformation is orthonormal). Equation (2.11) transforms the position vector of a point in the body-fixed reference frame to the position vector of the same point in the ground-fixed reference frame.

Next the velocity at an arbitrary point $\boldsymbol{P}$ is examined. The position of the point in the ground-fixed frame is

$$\vec{R} = \vec{R}_A + \vec{r} \tag{2.12}$$

where $\vec{R}_A$ is the position of the origin of the body-fixed frame in terms of the ground-fixed frame coordinates and $\vec{r}$ is the position of point $\boldsymbol{P}$ in terms of the body-fixed frame as shown in Figure 2.5. Taking the time derivative produces

$$\vec{V} = \vec{V}_A + \vec{\omega} \times \vec{r} + \vec{v} \tag{2.13}$$

or

$$\vec{v} = \vec{V} - \vec{V}_A - \vec{\omega} \times \vec{r} \tag{2.14}$$

where $\vec{V}$ is the velocity at point P given by the Biot-Savart law, $\vec{V}_A$ is the velocity of the origin of the body-fixed frame, $\vec{v}$ is the velocity in the body-fixed frame, $\vec{\omega}$ is the angular velocity of the body-fixed frame, and $\vec{r}$ is the position in the body-fixed frame. Equation (2.14) can be used to compute the velocities relative to the body-fixed frame in terms of the velocities computed by using the Biot-Savart law. The equation for the calculation of the loads will also be altered as shown in section 2.6.6.

The angular velocity of the body-fixed frame can be expressed in the body-fixed or ground-fixed reference frame as

$$\vec{\omega} = \omega_x \hat{i} + \omega_y \hat{j} + \omega_z \hat{k} = \dot{\psi}\hat{k}_1 + \dot{\theta}\hat{j}_2 + \dot{\phi}\hat{i}_3 \tag{2.15}$$

which can be written as

$$\begin{bmatrix} \dot{\phi} \\ \dot{\theta} \\ \dot{\psi} \end{bmatrix} = \begin{bmatrix} 1 & \dfrac{s\phi s\theta}{c\theta} & \dfrac{c\phi s\theta}{c\theta} \\ 0 & c\phi & -s\phi \\ 0 & \dfrac{s\phi}{c\theta} & \dfrac{c\phi}{c\theta} \end{bmatrix} \begin{bmatrix} \omega_x \\ \omega_y \\ \omega_z \end{bmatrix} \tag{2.16}$$

Thus the angular velocities about the body-fixed axes may be transformed into the time derivatives of the Euler angles. Integrating gives the Euler angles and thus the orientation of the body-fixed frame.

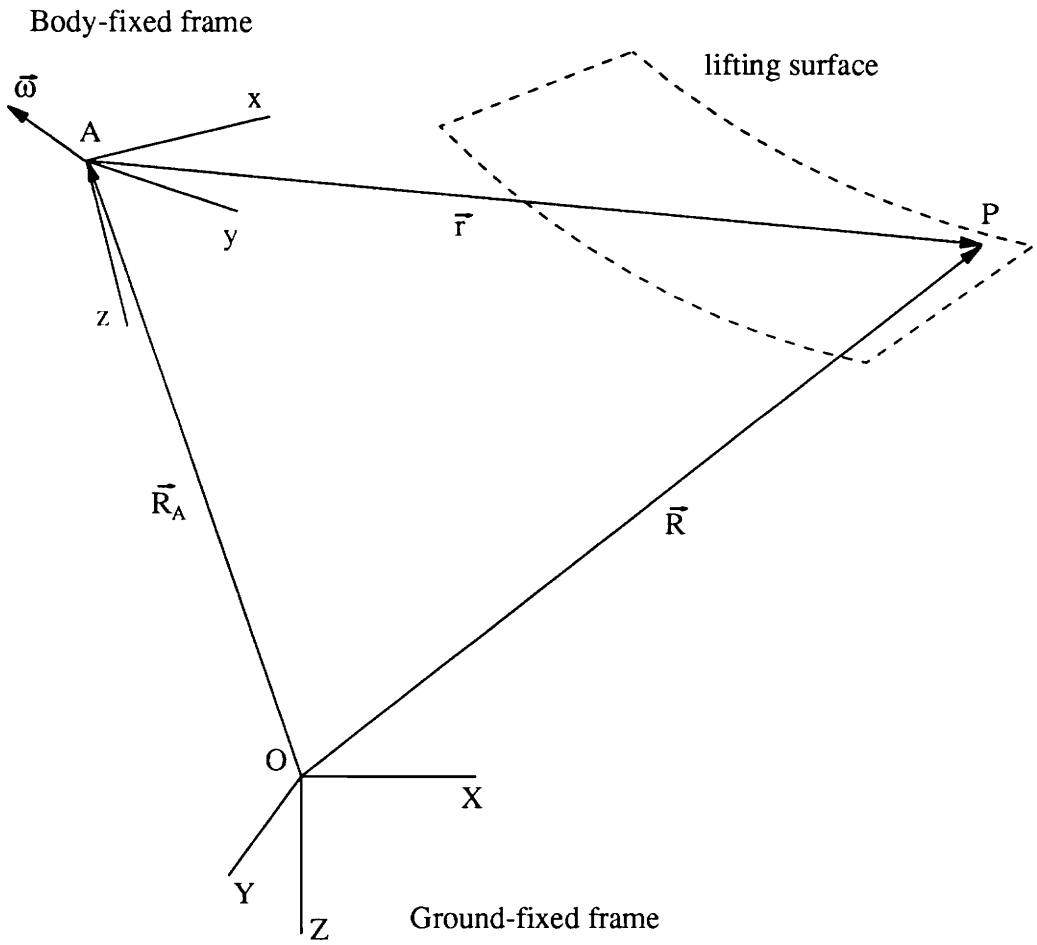

Figure 2.5 The coordinate systems.

2.6.4 Determination of the Bound Lattice Circulations

The solution of the problem requires the satisfaction of the no-penetration condition (2.3) at the control points of the bound lattice. The velocity at a control point can be broken into its known and unknown components and the equation written as

$$\vec{V}_{BL} \cdot \vec{n} = (-\vec{V}_{FL} + \vec{V}_{LS}) \cdot \vec{n} \tag{2.17}$$

where $\vec{V}_{BL}$ is the velocity due to the bound lattice, $\vec{V}_{FL}$ is the velocity due to the free lattice (the wake), $\vec{V}_{LS}$ is the velocity of the lifting surface, and $\vec{n}$ is the normal vector of an element. Equation (2.17) may also be written as

$$A_{ij} G_j = R_i \tag{2.18}$$

where A_{ij} is the influence coefficient matrix. It represents the normal velocity at control point i induced by a unit circulation around element j. The strength of the vortex filaments is contained in the unknown loop circulations G_j. The values of R_i are the known normal velocities relative to the wing at the control points. This system of equations is strongly diagonal and can be solved by Gauss-Siedel iteration. When integrating forward in time an accurate guess from the previous time step is known so convergence is rapid.

2.6.5 Convection of the Wake

The Kutta-Helmholtz theorem requires that in order for the wake to be force-free

it must be convected at the local particle velocity. A first-order explicit scheme is used to determine the displacements of points in the wake:

$$\vec{r}_i(t+\Delta t) = \vec{r}_i(t) + \vec{v}_i(t)\,\Delta t \tag{2.19}$$

where $\vec{r}_i(t+\Delta t)$ is the position of point i in the body-fixed reference frame at time $t+\Delta t$. The new position depends only upon values at the current time t. An implicit scheme could also be used which increases the accuracy to second-order but greatly increases the computational time as shown by Konstadinopoulos (1981). Comparisons of solutions obtained by the two methods suggest that a nondimensional time step of unity is small enough for very close agreement. The variable $\vec{v}_i(t)$ represents the velocity in the body-fixed frame induced at the point being convected due to every vortex filament in the bound and free lattices as calculated from the Biot-Savart law. It is found by using equation (2.14). In order to satisfy the unsteady Kutta condition the values of the loop circulation G are moved from the elements along the trailing edge and wing tips onto the first elements of the wake as shown in Figure 2.4.

2.6.6 Determination of the Loads

The loads on the wing are calculated from the pressure jumps at the control points of the elements of the bound lattice. The pressure jump is found by using the unsteady Bernoulli equation:

$$\left.\frac{\partial \phi^*}{\partial t^*}\right|_{\vec{R}} + \frac{1}{2}\vec{V}^* \cdot \vec{V}^* + \frac{p^*}{\rho_c} = H^*(t^*) \tag{2.20}$$

where the asterisks denote dimensional quantities. The velocity potential is represented by Φ^*, $\vec{V}^*$ is the absolute velocity, p^* is the unknown pressure, ρ_c is the reference density of the air, and $H^*(t^*)$ is an unknown function of time. The time derivative is calculated at a point fixed in the ground-fixed reference frame (constant $\vec{R}$). Using the reference values described in section 2.6.2, one can rewrite equation (2.20) in dimensionless form as follows:

$$\left.\frac{\partial \phi}{\partial t}\right|_{\vec{R}} + \frac{1}{2}\vec{V} \cdot \vec{V} + \frac{1}{2}p = H(t) \tag{2.21}$$

where

$$\phi = \frac{\phi^*}{V_c L_c} \qquad \vec{V} = \frac{\vec{V}^*}{V_c} \qquad p = \frac{p^*}{\frac{1}{2}\rho_c V_c^2} \qquad \vec{r} = \frac{\vec{r}^*}{L_c} \qquad \vec{\omega} = \frac{\vec{\omega}^* L_c}{V_c} \qquad t = t^* \frac{V_c}{L_c} \tag{2.22}$$

Equation (2.21) is written in terms of the ground-fixed reference frame yet the entire problem is posed in terms of the body-fixed frame. The pressure is needed at a point on the lifting surface, but such a point has a velocity relative to the ground-fixed frame because of the rigid-body motion and deformation of the wing. It is therefore necessary to express the time derivative at a point fixed in the ground-fixed frame in terms of the time derivative at a point fixed relative to the lifting surface. By definition,

$$\left.\frac{\partial\phi}{\partial t}\right|_{\vec{R}} \equiv \lim_{\Delta t \to 0} \frac{\phi(\vec{R}, t+\Delta t) - \phi(\vec{R}, t)}{\Delta t} \tag{2.23}$$

where $\left.\frac{\partial\phi}{\partial t}\right|_{\vec{R}}$ is the time derivative of the velocity potential of a point fixed in the ground-fixed reference frame. However, after a time Δt a point on the lifting surface has moved a distance $\Delta\vec{R}$. The value of the velocity potential at this new position may be found by a Taylor's series expansion.

$$\phi(\vec{R}+\Delta\vec{R}, t+\Delta t) = \phi(\vec{R}, t+\Delta t) + \nabla\phi(\vec{R}, t+\Delta t)\cdot\Delta\vec{R} + O(\Delta R^2) \tag{2.24}$$

or

$$\phi(\vec{R}, t+\Delta t) = \phi(\vec{R}+\Delta\vec{R}, t+\Delta t) - \nabla\phi(\vec{R}, t+\Delta t)\cdot\Delta\vec{R} + O(\Delta R^2) \tag{2.25}$$

Substituting equation (2.25) into equation (2.23) gives

$$\left.\frac{\partial\phi}{\partial t}\right|_{\vec{R}} = \lim_{\Delta t \to 0} \frac{\phi(\vec{R}+\Delta\vec{R}, t+\Delta t) - \nabla\phi(\vec{R}, t+\Delta t)\cdot\Delta\vec{R} - \phi(\vec{R}, t)}{\Delta t} \tag{2.26}$$

or

$$\left.\frac{\partial\phi}{\partial t}\right|_{\vec{R}} = \left.\frac{\partial\phi}{\partial t}\right|_{cp} - \nabla\phi(\vec{R}, t+\Delta t)\cdot\frac{d\vec{R}}{dt} \tag{2.27}$$

where $\left.\frac{\partial\phi}{\partial t}\right|_{cp}$ is the time derivative of the velocity potential at a given control point. The gradient of the velocity potential is the absolute velocity of the fluid and $\frac{d\vec{R}}{dt}$ is the

velocity of the control point due to the rigid-body motion and deformation of the wing, which is given by equation (2.14). Thus, equation (2.27) becomes

$$\left.\frac{\partial\phi}{\partial t}\right|_{\vec{R}} = \left.\frac{\partial\phi}{\partial t}\right|_{cp} - \vec{V}\cdot(\vec{V}_A + \vec{\omega}\times\vec{r} + \vec{v}) \tag{2.28}$$

Bernoulli's equation can now be written as

$$p = -2\left.\frac{\partial\phi}{\partial t}\right|_{cp} + 2\vec{V}\cdot(\vec{V}_A + \vec{\omega}\times\vec{r} + \vec{v}) - \vec{V}\cdot\vec{V} + 2H(t) \tag{2.29}$$

The pressure difference across the wing at a point is defined as the pressure above the bound vortex sheet minus the pressure below the bound vortex sheet. There is a jump in the tangential velocity across a vortex sheet equal to the strength of the sheet, or the circulation per unit length. The computed velocities relative to the lifting surface at the bound vortex sheet have no normal component because the no-penetration condition is satisfied. The computed velocities may be thought of as the mean velocities of the vortex sheet, so the velocities on the upper and lower surfaces may be written as

$$\vec{V}_U = \vec{V} + \frac{\Delta\vec{V}}{2} \quad \text{and} \quad \vec{V}_L = \vec{V} - \frac{\Delta\vec{V}}{2} \tag{2.30}$$

where the subscripts U and L represent the upper and lower surfaces respectively and $\Delta\vec{V}$ is the jump in tangential velocity across the vortex sheet. Now Bernoulli's equation may be written for the pressure jump, ΔC_p, between a point on the lower surface and its

opposing point on the upper surface:

$$\Delta C_p = p_L - p_U = 2\frac{\partial}{\partial t}(\phi_U - \phi_L) + 2\Delta\vec{V}\cdot(\vec{V} - \vec{V}_A - \vec{\omega}\times\vec{r} - \vec{v}) \tag{2.31}$$

There are still two terms, $\phi_U - \phi_L$ and $\Delta\vec{V}$, that must be considered. The first may be written in terms of the loop circulation. Using basic definitions only results in

$$\phi_U - \phi_L = \int_c d\phi = \int_c \nabla\phi\cdot d\vec{r} = \int_c \vec{V}\cdot d\vec{r} \tag{2.32}$$

where the integration is along a curve c from point a to point b. Point a is just below control point i and point b is just above as shown in Figure 2.6. The path of integration must not cross the vortex sheet where ϕ does not exist. Therefore, a path is chosen beginning at point a, moving toward the leading edge, around the leading edge, and back to point b. Because the points in question are an infinitesimal distance apart Stoke's theorem may be used and equation (2.32) may be written as

$$\phi_U - \phi_L = \Gamma \tag{2.33}$$

where Γ is the sum of the circulations of the vortex filaments enclosed by the path. A simple inspection will show that this can be written as

$$(\phi_U - \phi_L)_i = G_i \tag{2.34}$$

where the subscript i refers to a control point. The time derivative is evaluated by using a first-order finite difference scheme,

$$\frac{\partial G_i(t)}{\partial t} = \frac{G_i(t) - G_i(t-\Delta t)}{\Delta t} \tag{2.35}$$

The second term of Bernoulli's equation in question, $\Delta \vec{V}$, is equal to the strength of the vortex sheet. In this method the vortex sheet has been discretized by a set of vortex filaments. At a control point the strength of the bound lattice, or circulation per length, may be taken as the average of the circulations of the two neighboring vortex filaments divided by the distance between them. For the representative element shown in Figure 2.6 this becomes

$$\Delta V_x = \frac{F\Gamma_1 + \Gamma_3}{2\Delta x} \qquad \Delta V_y = \frac{\Gamma_2 + \Gamma_4}{2\Delta y} \tag{2.36}$$

where F is one unless Γ_1 lies along the leading edge, then F is two. On the leading edge no wake elements are convected so all of the circulation Γ_1 is associated with the element. These two equations may be combined into a single equation

$$\Delta \vec{V} = -\hat{n} \times [(F\Gamma_1 + \Gamma_3)\vec{L}_y + (\Gamma_2 + \Gamma_4)\vec{L}_x] / 2A \tag{2.37}$$

where $\hat{n}$ is the upward-pointing unit normal, A is the area of the element, and $\vec{L}_x$ and $\vec{L}_y$ are defined in Figure 2.6.

The Bernoulli equation may now be written in its final form

$$\Delta C_{p,i} = 2\frac{G_i(t) - G_i(t-\Delta t)}{\Delta t} + 2\Delta \vec{V}_i \cdot (\vec{V}_i - \vec{V}_A - \vec{\omega} \times \vec{r}_i - \vec{v}_i) \tag{2.38}$$

Now that the pressures are known the forces and moment around the elastic axis may be calculated. Summing the elements in a column (the elements that have the same y values) and multiplying by the chord gives the force per unit of length acting on the elastic axis at that position along the span. Because the location of the elastic axis within the wing is known the moment about the elastic axis may also be found.

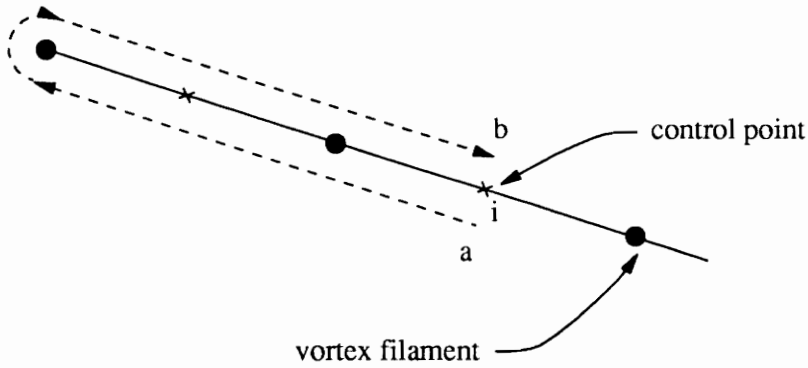

(a)

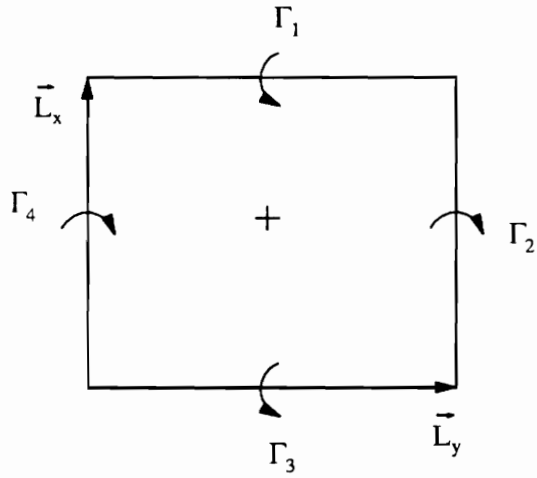

(b)

Figure 2.6 (a) Side view of the bound lattice showing the path of integration for the calculation of the time derivative of the velocity potential. (b) A representative element of the bound lattice.

2.6.7 The Impulsive Start

Initially the wing and the surrounding fluid are at rest. The circulations of the bound lattice are zero and there is no wake. At some instant in time, denoted by $t=0$, the aircraft assumes its full velocity. The circulations change according to equation (2.18) and a vortex filament is created along the sharp edges as required by the spatial conservation of vorticity. At the time $t=\Delta t$ the vorticity shed along the wing tip and trailing edge forms the first elements of the wake as required by the unsteady Kutta condition and the Kelvin-Helmholtz theorem. The particles are convected according to equation (2.19). At the next time step the circulations change again due to the normal velocity on the lifting surface induced by the wake. A new vortex filament is created along the sharp edges, which is also shed, and the elements in the wake are convected. This sequence of events is shown in Figure 2.7 and the notation is shown in Figure 2.4. The wake is thus grown to some finite length beyond which the vortex filaments have little effect on the wing and may be neglected.

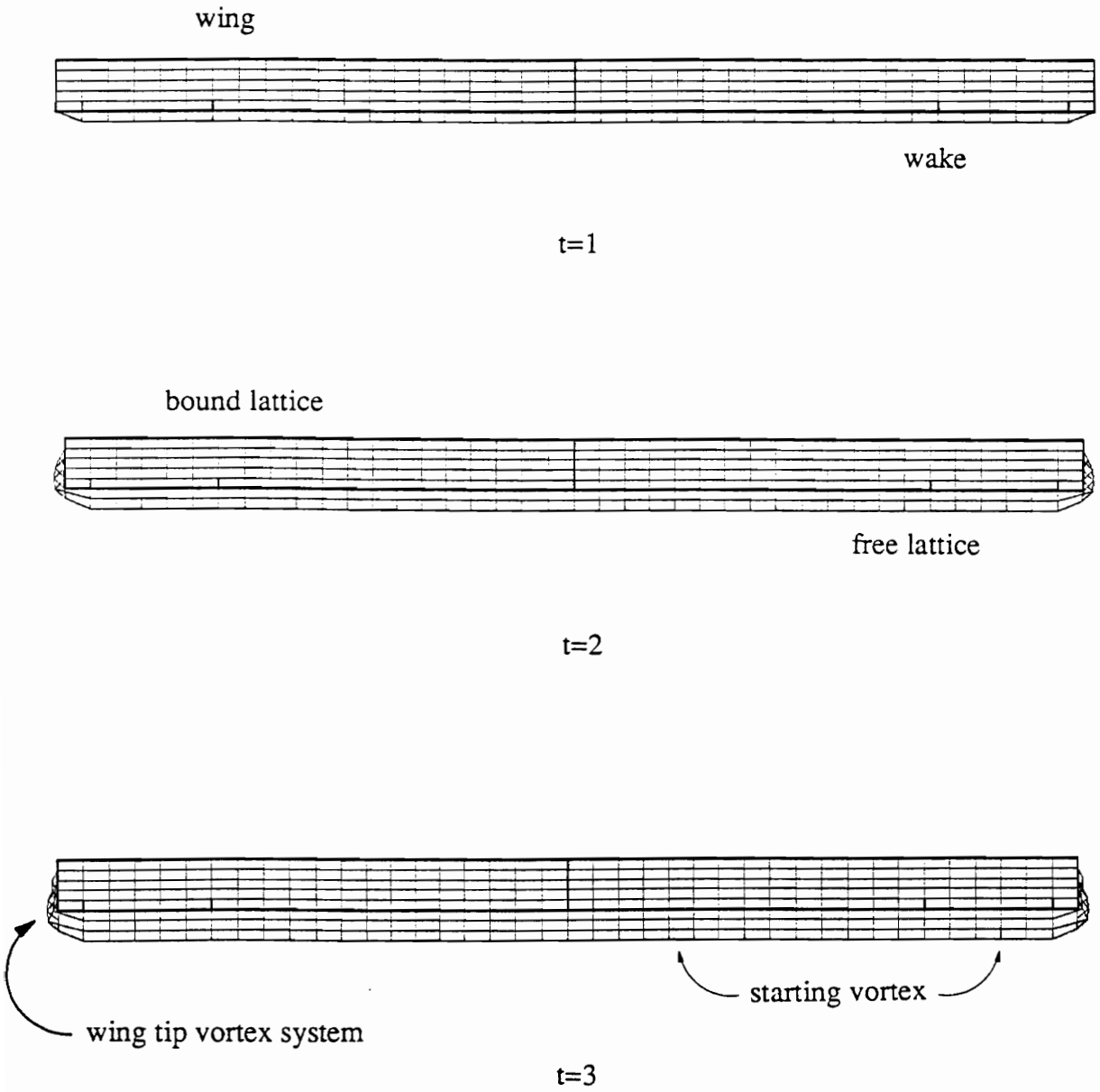

Figure 2.7 The first three time steps of an impulsive start (top view).

2.6.8 Accuracy Considerations

Several parameters affect the accuracy of the vortex-lattice method. These include the number of elements in the bound and free lattices, the size of the time step, and the method used to eliminate the singular nature of the vortex filaments. A complete discussion of these and other considerations is given in Kelly (1977).

Chapter 3 The Structural Models

3.1 Introduction

As shown in the following chapter, the solution scheme for the aeroelastic problem does not in any way limit the choice of a model for the dynamics of the wing. The numerical integration scheme is capable of handling any nonlinearities associated with aerodynamic, inertial, material, or geometric effects. Two different structural models are examined: a linear model of the wing and a nonlinear model which accounts for large curvature effects. The nonlinear model is not meant as a comprehensive study of the nonlinear effects but as a demonstration of the ability of the aeroelastic formulation to model structural nonlinearities. A complete nonlinear model should include extensional effects and coupling between bending and torsion. Both formulations developed here model the wing as a cantilevered beam which is allowed to bend and twist as shown in Figure 3.1. For simplicity the inertial axis is aligned with the elastic axis (which is assumed to be straight) to eliminate the inertial coupling between the bending and torsion. Also, material properties are assumed to be constant along the span.

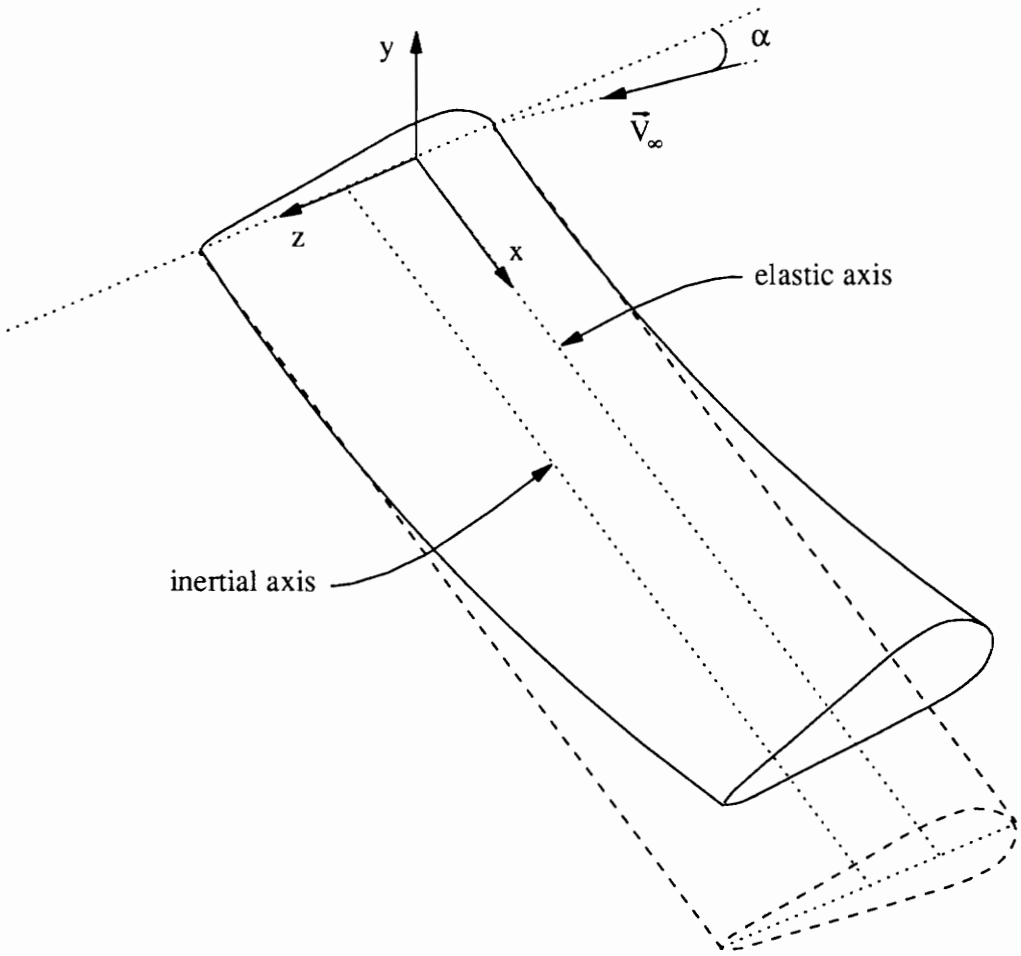

Figure 3.1 The two allowed degrees of freedom of the cantilevered wing.

3.2 The Coordinate System

The coordinate system for the determination of the equations of motion for an elastic wing is shown in Figure 3.1. The x and z axes lie in the plane of the undeformed wing with the x axis directed along the elastic axis toward the wing tip and the y axis directed upward. The lateral displacement is represented by v and ϕ represents the twist. The relationship between the xyz set of axes and the $x_a y_a z_a$ aerodynamic body-fixed axes is shown in Figure 3.2.

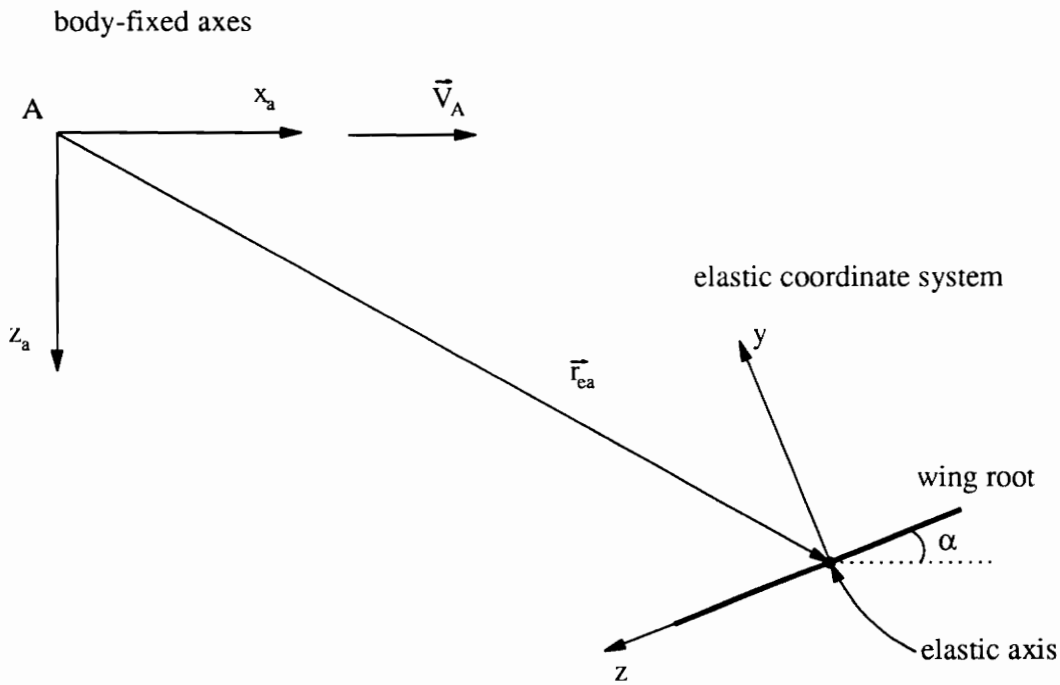

Figure 3.2 The body-fixed aerodynamic axes and the coordinate system used for the elastic equations.

3.3 The Equations of Motion

The cantilevered beam is allowed to have planar flexural-torsional motion: bending about the z axis and twist about the x axis. The flexural deflection about the y axis is neglected due to the much higher stiffness. The material is assumed to be linearly elastic. The equations for bending and torsion may be derived from Newton's second law or an energy approach. Although it is not necessary, the inertial coupling between flexure and torsion is eliminated by assuming that the inertial axis coincides with the elastic axis. In addition, the cross-sectional area, mass, and stiffness are assumed to be constant along the wing; these assumptions are also not necessary. Thus, for small shear strains, the equation for the torsional vibration of a beam has the well known form

$$J_0^* \ddot{\phi} - G^* J^* \phi'' = f_t^* \tag{3.1}$$

as shown in Rao (1986). The polar moment of inertia is represented by J^*, J_0^* is the mass polar moment of inertia, G^* is the shear modulus of elasticity, ϕ is the angle of twist, and f_t^* is the external twisting moment per unit length. The asterisks denote dimensional quantities and the primes denote differentiation with respect to x. Using the reference variables described in section 2.6.2, one may write equation (3.1) in dimensionless form as

$$\ddot{\phi} - D_t \phi'' = q_t Q_t \tag{3.2}$$

where

$$D_t = \frac{G^* J^*}{V_c^2 J_0^*} \qquad q_t = \frac{\rho_c L_c}{2 J_0^*} \tag{3.3}$$

The quantity D_t is known as the reduced torsional stiffness. The boundary conditions for a cantilevered beam are no deformation at the fixed end (x=0) and no moment at the free end, or

$$\begin{aligned} \phi(0,t) &= 0 \\ \phi'(L,t) &= 0 \end{aligned} \tag{3.4}$$

where L is the span or length of the beam.

The equations for the lateral vibration of the wing are developed for an inextensional beam. Only nonlinear terms due to curvature effects are included. Although the beam is inextensional, large curvature produces a significant displacement in the horizontal direction. Consider the free-body diagram in Figure 3.3 of an incremental element of length dx initially lying along the elastic axis. The vertical displacement is given by v and the horizontal displacement by u. The external forces on the element are represented by W, the weight, and Q_b, the aerodynamic force normal to the element per unit length. The variable M represents the bending moment and V represents the shear force. The effects of rotary inertia and shear deformation are neglected because the cross-sectional dimensions are small compared to the length of the wing. Summing the forces in the vertical direction leads to

$$m\ddot{v} = -mg + Q_b \cos\theta - (V\cos\theta)' \tag{3.5}$$

where m is the mass per unit length and g is the acceleration of gravity. Summing the moments around the mass center (while neglecting the rotary inertia) leads to the well known equation

$$V = M' \tag{3.6}$$

While it is common to neglect the nonlinear term in the expression for curvature (Euler-Bernoulli theory), this cannot be done for large deformations. For large curvatures the exact expression for curvature must be used, leading to

$$M = EI \frac{v''}{(1+v'^2)^{3/2}} \tag{3.7}$$

where E is the modulus of elasticity and I is the moment of inertia of the cross section about the x axis. From the geometry the following equations may be found:

$$\cos\theta = 1 + u' \tag{3.8}$$

and

$$dx^2 = (1+u')^2 dx^2 + v'^2 dx^2 \tag{3.9}$$

or

$$u'^2 + 2u' + v'^2 = 0 \tag{3.10}$$

The second equation is a result of the inextensionality assumption. It may be further reduced because u' is of order v'^2 and, hence, u'^2 is of order v'^4 and may be neglected if only terms up to cubic are kept. Integrating equation (3.10) gives

$$u(x) = -\frac{1}{2}\int_0^x v'^2 dx \tag{3.11}$$

where the boundary condition of no axial displacement at the fixed end has been used. Since u is a function of v only, the displacement in the x direction may be found from equation (3.11) after the lateral displacement has been found. Equation (3.11) has the same form when expressed in terms of dimensionless quantities.

The previous expressions allow equation (3.5) to be written in terms of a single unknown variable v. The equation may then be expanded in a Taylor series about the undeformed position $v=0$. The substitutions and expansion are performed by the program MACSYMA, a symbolic manipulator. The result, when keeping up to cubic terms, is

$$m\ddot{v} + EIv'''' - EI(2v'^2 v'''' + 10v'v''v''' + 3v''^3) = Q_b - mg - \tfrac{1}{2}Q_b v'^2 \tag{3.12}$$

Using the reference variables described in section 2.6.2, equation (3.12) may be written in dimensionless form as

$$\ddot{v}^* + D_b^* v^{*''''} - D_b^*(2v^{*'^2}v^{*''''} + 10v^{*'}v^{*''}v^{*'''} + 3v^{*''^3}) = q_b^* Q_b^* - W^* - \tfrac{1}{2} q_b^* Q_b^* v^{*'^2} \tag{3.13}$$

where

$$v^* = \frac{v}{L_c} \qquad D_b^* = \frac{EI}{mL_c^2 V_c^2} \qquad q_b^* = \frac{\rho_c L_c^2}{2m} \qquad W^* = \frac{gL_c}{V_c^2} \tag{3.14}$$

The asterisks represent dimensionless quantities and will now be dropped for convenience. The boundary conditions for a cantilevered beam are no deflection and slope at the fixed end and no bending moment and shear force at the free end. For a beam of uniform stiffness the boundary conditions become

$$\begin{aligned} v(0,t) &= 0 \\ v'(0,t) &= 0 \\ v''(L,t) &= 0 \\ v'''(L,t) &= 0 \end{aligned} \tag{3.15}$$

In summary, the nonlinear governing equations for the wing are

$$\ddot{\phi} - D_t \phi'' = q_t Q_t \tag{3.16}$$

$$\ddot{v} + D_b v'''' - D_b(2v'^2 v'''' + 10v' v'' v''' + 3v''^3) = q_b Q_b - W - \tfrac{1}{2} q_b Q_b v'^2 \tag{3.17}$$

$$u(x) = -\frac{1}{2}\int_0^x v'^2 dx \tag{3.18}$$

For the linear case the equations reduce to

$$\ddot{\phi} - D_t\phi'' = q_t Q_t \tag{3.19}$$

$$\ddot{v} + D_b v'''' = q_b Q_b - W \tag{3.20}$$

The following chapter describes the solution to these equations using the method of normal modes and an iterative integration scheme.

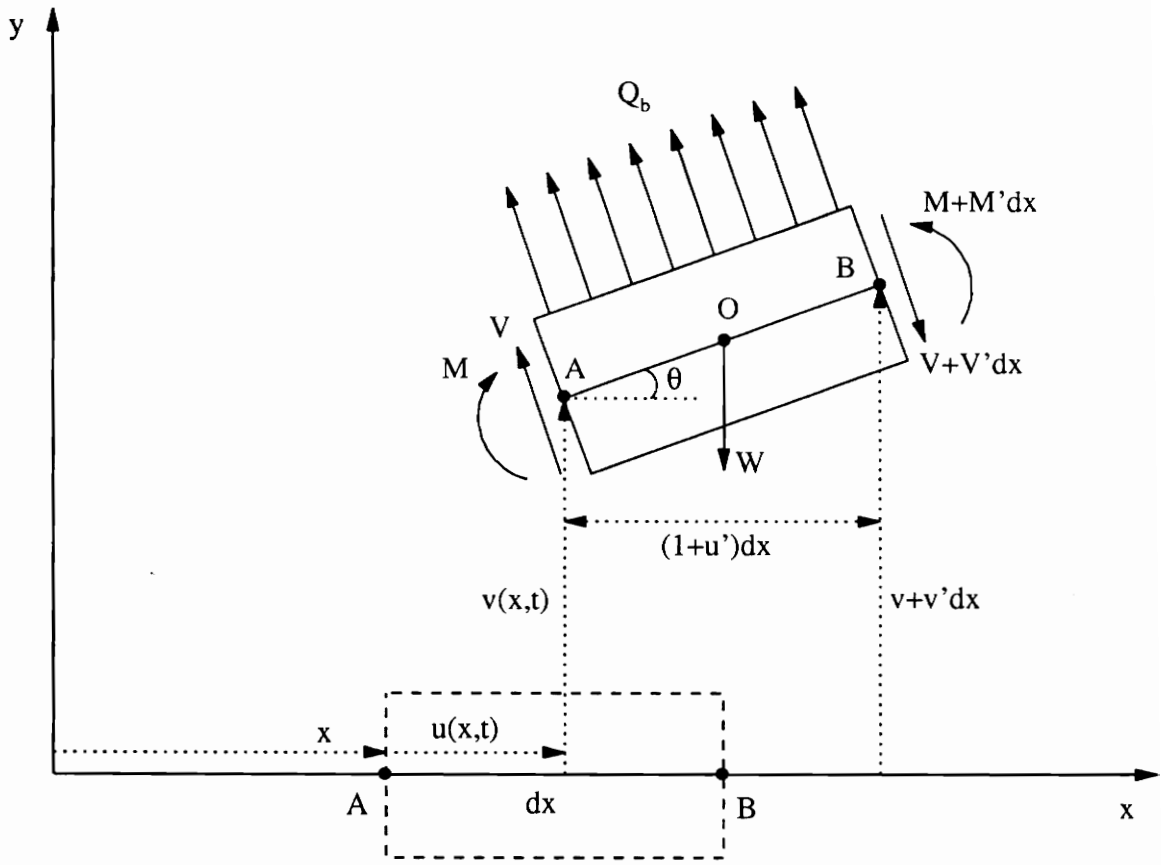

Figure 3.3 The free body diagram of an element initially lying along the elastic axis.

Chapter 4 The Numerical Solution

4.1 Introduction

The solution to the aeroelastic problem requires that the wing and surrounding air be treated as a single dynamical system. Thus, the aerodynamic and structural equations must be solved simultaneously. The equations are coupled because the deformation and rate of deformation of the wing depend on the aerodynamic loads, yet the loads depend upon the wing's deformation and rate of deformation. Moreover, while material, inertial, or geometric nonlinear structural effects might be neglected there are inherent nonlinearities introduced through the aerodynamic loads. Thus the problem consists of a coupled system of second-order, nonlinear, partial differential equations.

Section 4.2 describes how these equations may be transformed into a set of ordinary differential equations through the use of generalized coordinates and Galerkin's method, also known as the method of normal modes. In Section 4.3 the static solution to these equations is described. The velocity and acceleration of the deforming wing are assumed to be zero. The static solution is found with and without the geometric nonlinearities. In Section 4.4 the predictor-corrector scheme used to integrate the equations of motion is described. This scheme is valid regardless of the structural or aerodynamic models used. The algorithm for the entire aeroelastic, dynamical solution is discussed in section 4.5.

4.2 Generalized Coordinates

The use of generalized coordinates for the aeroelastic problem was first proposed by Loring (1941). The greatest advantage of this method is the reduction in the number of equations of the system. Although the wing has an infinite number of degrees of freedom, the deflection of the wing may be represented in terms of a small number of modes. Another advantage of the use of generalized coordinates is that the system of partial differential equations may be transformed into ordinary differential equations. The result is a small system of ordinary differential equations that may solved using a numerical integration scheme. As shown in the following section, this procedure leads to a set of uncoupled algebraic equations for the static case if the large curvature terms are neglected. For a more complete description of the method of normal modes, refer to Etkin (1972) and Nayfeh and Mook (1979).

The first step in the method of normal modes is to expand the torsional and lateral displacements in terms of the mode shapes, or

$$\phi(x,t) = \sum_{m=1}^{M} C_m(t)\,\chi_m(x) \tag{4.1}$$

$$v(x,t) = \sum_{m=1}^{N} B_m(t)\,\psi_m(x) \tag{4.2}$$

where ψ_m and χ_m are the linear undamped natural modes for bending and twisting respectively, and B_m and C_m are the generalized coordinates which are functions of time only. The mode shapes for a cantilevered beam are derived in the Appendix. By using

the mode shapes the boundary conditions are automatically satisfied. Substituting equation (4.1) into the governing equation for twist yields

$$\sum_{m=1}^{M} \ddot{C}_m \chi_m - D_t \sum_{m=1}^{M} C_m \chi_m'' - q_t Q_t = e_t \tag{4.3}$$

where e_t is the error introduced by choosing a finite number of modes. As shown in the Appendix,

$$\chi_m'' = -\frac{\omega_{t,m}^2 \chi_m}{D_t} \tag{4.4}$$

so equation (4.3) becomes

$$\sum_{m=1}^{M} (\ddot{C}_m + \omega_{t,m}^2)\chi_m - q_t Q_t = e_t \tag{4.5}$$

The variable $\omega_{t,m}$ represents the torsional reduced (nondimensional) natural frequency of the wing. One can now take advantage of the orthogonality of the modes by multiplying equation (4.5) by χ_n and integrating over the length of the wing.

$$\sum_{m=1}^{M} \int_0^L (\ddot{C}_m + \omega_{t,m}^2)\chi_m \chi_n dx - q_t \int_0^L Q_t \chi_n dx = \int_0^L e_t \chi_n dx \tag{4.6}$$

or

$$\ddot{C}_n + \omega_{t,n}^2 C_n = q_t \int_0^L Q_t \chi_n dx + \int_0^L e_t \chi_n dx \tag{4.7}$$

Since Galerkin's procedure requires that the error be orthogonal to the mode shapes, equation (4.7) becomes

$$\ddot{C}_n + \omega_{t,n}^2 C_n = E_n \tag{4.8}$$

where

$$E_n = q_t \int_0^L Q_t \chi_n dx \tag{4.9}$$

Following a similar procedure for the bending equation yields

$$\ddot{B}_n + \omega_{b,n}^2 B_n + (K_{1,n} B_1^3 + K_{2,n} B_1^2 B_2 + K_{3,n} B_1 B_2^2 + K_{4,n} B_2^3) D_b = D_n + F_n + H_{1,n} B_1^2 + H_{2,n} B_1 B_2 + H_{3,n} B_2^2 \tag{4.10}$$

where n=1,2 and

$$D_n = \int_0^L Q_b \psi_n dx \tag{4.11}$$

$$F_n = \int_0^L W \psi_n dx \tag{4.12}$$

The variable $\omega_{b,n}$ represents the flexural reduced natural frequency of the wing. The geometric nonlinearity creates the K_n and H_n terms which contain derivatives of the mode shapes and are not necessarily orthogonal to the modes so these terms might not be zero. Instead, they may introduce geometric coupling between the bending modes. The aerodynamic loads are represented in the D_n and H_n terms. The terms are evaluated

numerically and are given by

$$K_{1,n} = -\int_0^L \left[2\psi_1'^2\psi_1'''' + 10\psi_1'\psi_1''\psi_1''' + 3\psi_1''^3\right]\psi_n dx \tag{4.13}$$

$$K_{2,n} = -\int_0^L \left[2\psi_1'^2\psi_2'''' + 10\psi_1'\psi_1''\psi_2''' + 10\psi_1'\psi_1'''\psi_2'' + 9\psi_1''^2\psi_2'' + 4\psi_1'\psi_1''''\psi_2' + 10\psi_1''\psi_1'''\psi_2'\right]\psi_n dx \tag{4.14}$$

$$K_{3,n} = -\int_0^L \left[2\psi_2'^2\psi_1'''' + 10\psi_2'\psi_2''\psi_1''' + 10\psi_2'\psi_2'''\psi_1'' + 9\psi_2''^2\psi_1'' + 4\psi_2'\psi_2''''\psi_1' + 10\psi_2''\psi_2'''\psi_1'\right]\psi_n dx \tag{4.15}$$

$$K_{4,n} = -\int_0^L \left[2\psi_2'^2\psi_2'''' + 10\psi_2'\psi_2''\psi_2''' + 3\psi_2''^3\right]\psi_n dx \tag{4.16}$$

$$H_{1,n} = -\frac{1}{2}\int_0^L Q_b\psi_1'^2\psi_n dx \tag{4.17}$$

$$H_{2,n} = -\int_0^L Q_b\psi_1'\psi_2'\psi_n dx \tag{4.18}$$

$$H_{3,n} = -\frac{1}{2}\int_0^L Q_b\psi_2'^2\psi_n dx \tag{4.19}$$

In summary, the original set of partial differential equations has been transformed into the following set of ordinary differential equations:

$$\ddot{C}_m + \omega_{t,m}^2 C_m = E_m \qquad m = 1..M \tag{4.20}$$

$$\ddot{B}_n+\omega_{b,n}^2 B_n+(K_{1,n}B_1^3+K_{2,n}B_1^2B_2+K_{3,n}B_1B_2^2+K_{4,n}B_2^3)D_b=D_n+F_n+H_{1,n}B_1^2+H_{2,n}B_1B_2+H_{3,n}B_2^2 \tag{4.21}$$

where $n=1,2$. For the linear case these equations reduce to

$$\ddot{C}_m+\omega_{t,m}^2 C_m=E_m \qquad m=1..M \tag{4.22}$$

$$\ddot{B}_n+\omega_{b,n}^2 B_n=D_n+F_n \qquad n=1..N \tag{4.23}$$

where any number of modes may be used each equation. The aerodynamic loads appear in the E_m, D_n, and H_n which couple all of the equations. The loads are evaluated numerically by using the vortex-lattice method. The solution of these equations is the subject of the following sections.

4.3 The Static Solution

The equations of motion may be simplified if the velocity and acceleration of the wing due to deformation are assumed to be zero. For this situation two possibilities arise: either the wing assumes some steady deflection or there is aeroelastic divergence. Aeroelastic divergence occurs when the aerodynamic loads on the wing exceed the maximum load the wing can support in any deformed state. Divergence is generally not of practical concern because the divergence speed is usually greater than the flutter speed. For speeds less than the divergence speed the wing converges to a steady deflection. The long-time dynamic solution will approach the static solution if the wing is dynamically

stable. The static solution is generally valid for speeds below the flutter speed and is useful as an initial condition for a dynamical solution.

The equations of motion for the wing, without the acceleration terms, may be written as

$$B_n = \frac{1}{\omega_{b,n}^2}\left[-(K_{1,n}B_1^3 + K_{2,n}B_1^2B_2 + K_{3,n}B_1B_2^2 + K_{4,n}B_2^3)D_b + D_n + F_n + H_{1,n}B_1^2 + H_{2,n}B_1B_2 + H_{3,n}B_2^2\right] \tag{4.24}$$

where $n=1,2$ and

$$C_m = \frac{E_m}{\omega_{t,m}^2} \qquad m=1..M \tag{4.25}$$

Because the aerodynamic loads represented by the terms E_m, D_n, and H_n are functions of the shape of the wing, represented by the generalized coordinates B_n and C_m, an iterative procedure is used to solve equations (4.24) and (4.25). This algorithm is outlined in Figure 4.1.

The wing is initially undeformed (the generalized coordinates are zero). The wing is kept rigid and the corresponding aerodynamic steady state is calculated. The steady loads on the wing are then found and used in equations (4.24) and (4.25) to find the new generalized coordinates B_n and C_m. The current values of B_n are used in the right-hand side. The bending and twist deformations may be found from the normal mode expansions, equations (4.1) and (4.2). However, this new shape of the wing will produce

different loads. Also, equation (4.24) is not satisfied if the curvature terms are present. Therefore, the wing is moved to the deformed position and the new aerodynamic steady-state loads are found. Now equations (4.24) and (4.25) are again solved by using the current values of $\boldsymbol{B}_n$ in the right-hand side. The process is repeated until the position (i.e. $\boldsymbol{B}_n$) converges. Convergence is rapid and the computational time is short for this solution.

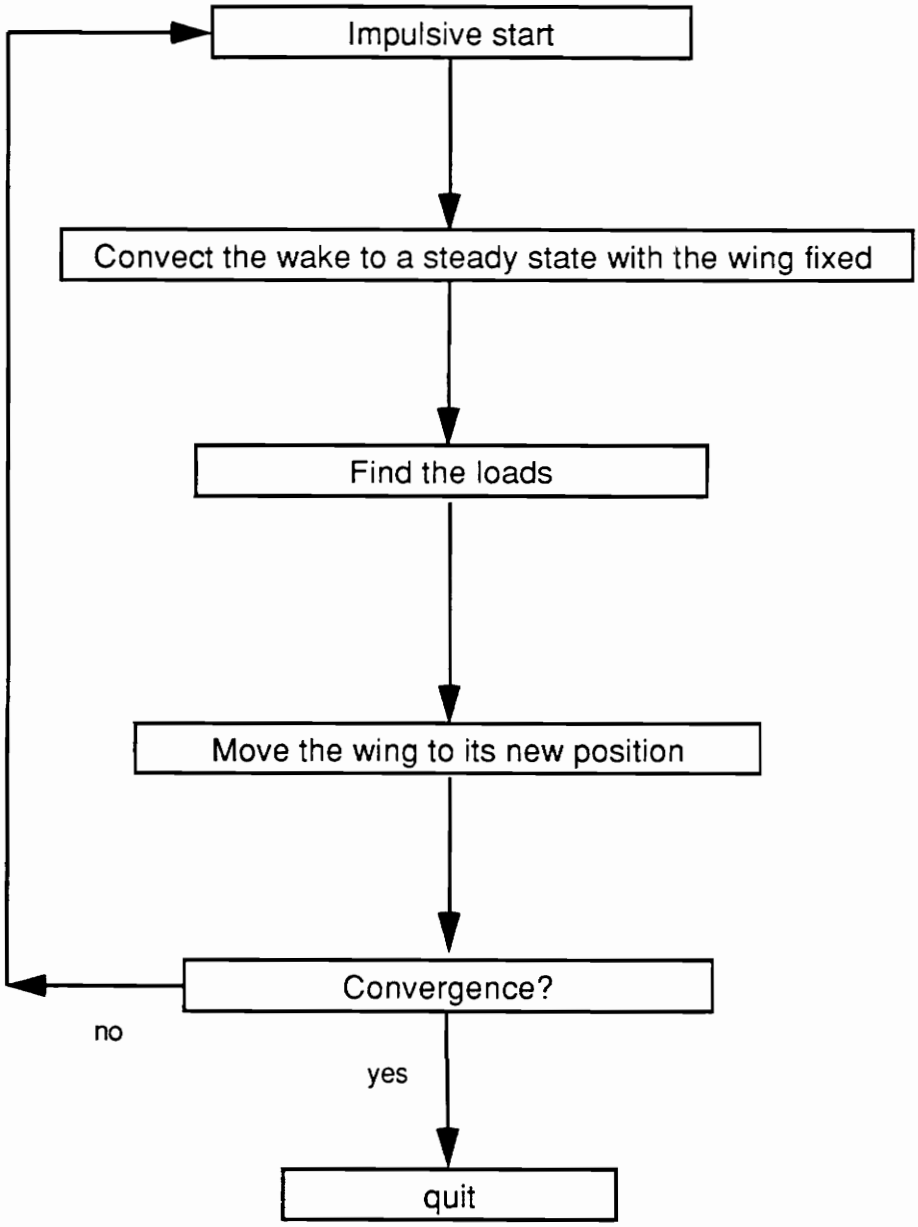

Figure 4.1 The algorithm for the static solution.

4.4 Hamming's Predictor-Corrector Method

The dynamic solution requires a numerical scheme to integrate the equations of motion. There are two important characteristics of these equations to consider in choosing a numerical integrator. By far the most computational time is spent finding the aerodynamic loads so this should be done as infrequently as possible. Also, the loads are only known at integral time steps which excludes schemes that evaluate the derivatives at fractional time steps, such as the Runge-Kutta methods. The scheme chosen is Hamming's forth-order predictor-corrector method as described in Carnahan (1969). This method has excellent accuracy and stability characteristics and requires as few as two iterations per time step. The algorithm requires the solution at the three previous time steps, so a separate algorithm is used to start the method. This starting routine is described in the following section. Now consider the general procedure when the solution is known at the current time i and at the three previous times $i-1$, $i-2$, and $i-3$.

First, the second-order equations of motion must be written as a system of first-order equations for the predictor-corrector method. To illustrate the numerical scheme, consider the general system of equations:

$$\dot{y}_n(t) = f_n(t, y_1, y_2, y_3, \ldots, y_N) \qquad n = 1..N \tag{4.26}$$

where N is twice the total number of bending and torsional modes. Equation (4.26) represents a system of fully coupled equations. The variable y may regarded as a vector.

First, the solution at time $i+1$ is predicted according to

$$y^*_{i+1,0} = y_{i-3} + \frac{4}{3}(2f_i - f_{i-1} + 2f_{i-2})\Delta t \tag{4.27}$$

where $y^*_{i+1,0}$ represents the predicted state. The state is then modified by using the local truncation error at the current time step, e_i, which is calculated at the end of the procedure.

$$y_{i+1,0} = y^*_{i+1,0} + \frac{112}{9}e_i \tag{4.28}$$

The variable $y_{i+1,0}$ represents the modification of the predicted state and is used as the initial guess to evaluate the derivative f. Next, the state is iteratively corrected by

$$y_{i+1,j+1} = \frac{1}{8}\{9y_i - y_{i-2} + 3[f(t_{i+1}, y_{i+1,j}) + 2f_i - f_{i-1}]\Delta t\} \qquad j=0..k \tag{4.29}$$

until the desired tolerance is reached. For the aeroelastic formulation, the aerodynamic problem must be solved each time the derivative $f(t_{i+1}, y_{i+1,j})$ is evaluated. This is a major investment in computational time. Fortunately, one iteration is usually sufficient so the derivative need only be calculated once. The truncation error is found by

$$e_{i+1} = \frac{9}{121}(y_{i+1,k} - y^*_{i+1,0}) \tag{4.30}$$

and a final modification to the state based on the truncation error is obtained from

$$y_{i+1} = y_{i+1,k} - e_{i+1} \tag{4.31}$$

The derivative f_{i+1} may now be found using y_{i+1}. Thus the complete solution at time $i+1$ is known.

4.4.1 Starting the Predictor-Corrector Method

The state variables and their derivatives at the first three time steps and the initial conditions must be known in order to start the full predictor-corrector method described in the previous section. Runge-Kutta schemes are commonly employed to find these values, but quantities must be calculated at fractional time steps, a procedure that produces inaccurate results for the vortex-lattice method. In the present scheme, the starting values are obtained by using Taylor series as discussed by Strganac (1987). His results are merely repeated here:

$$\begin{aligned} y_{n,1} &= f_{n,1}\Delta t + y_{n,0} \\ y_{n,2} &= \tfrac{4}{3}y_{n,1} - \tfrac{1}{3}y_{n,0} + (\tfrac{4}{3}f_{n,1} - \tfrac{2}{3}f_{n,0})\Delta t \\ y_{n,3} &= \tfrac{4}{3}y_{n,2} - \tfrac{1}{3}y_{n,1} + (\tfrac{4}{3}f_{n,2} - \tfrac{2}{3}f_{n,1})\Delta t \end{aligned} \tag{4.32}$$

where $n=1..N$ and the second subscript indicates the time step.

4.5 The Dynamic Solution

The algorithm for the dynamic solution by Hamming's predictor-corrector method is depicted in Figure 4.2. For initial conditions the static solution may be used or the undeformed wing may be impulsively started. For the first three steps the wake is convected and the aerodynamic loads found according to the vortex-lattice method. The state of the wing (deformation and rate of deformation) due to the aerodynamic loads is found by the start-up routine as discussed in the previous section. The general scheme for advancing the solution one time step involves convecting the wake to its new position and applying the predictor-corrector integrator. The wake is convected to its force-free position by using the solution at the current time step. A higher-order theory, where the wake position also depends on the solution at the next time step, could be employed. However, Strganac (1987) has shown that there is essentially no change in the results while the computational time increases greatly. To begin the predictor-corrector method the state variables (the deformed position and rate of deformation) at the next time step are predicted and then modified. Next the loads on the wing in its new state are found from the aerodynamic model and the state is corrected with these loads according to equation (4.29). This step is iterated until convergence. A final correction to the state is made and the loads on the wing in the final state are found. The complete solution at the next time step is now known so time may be incremented.

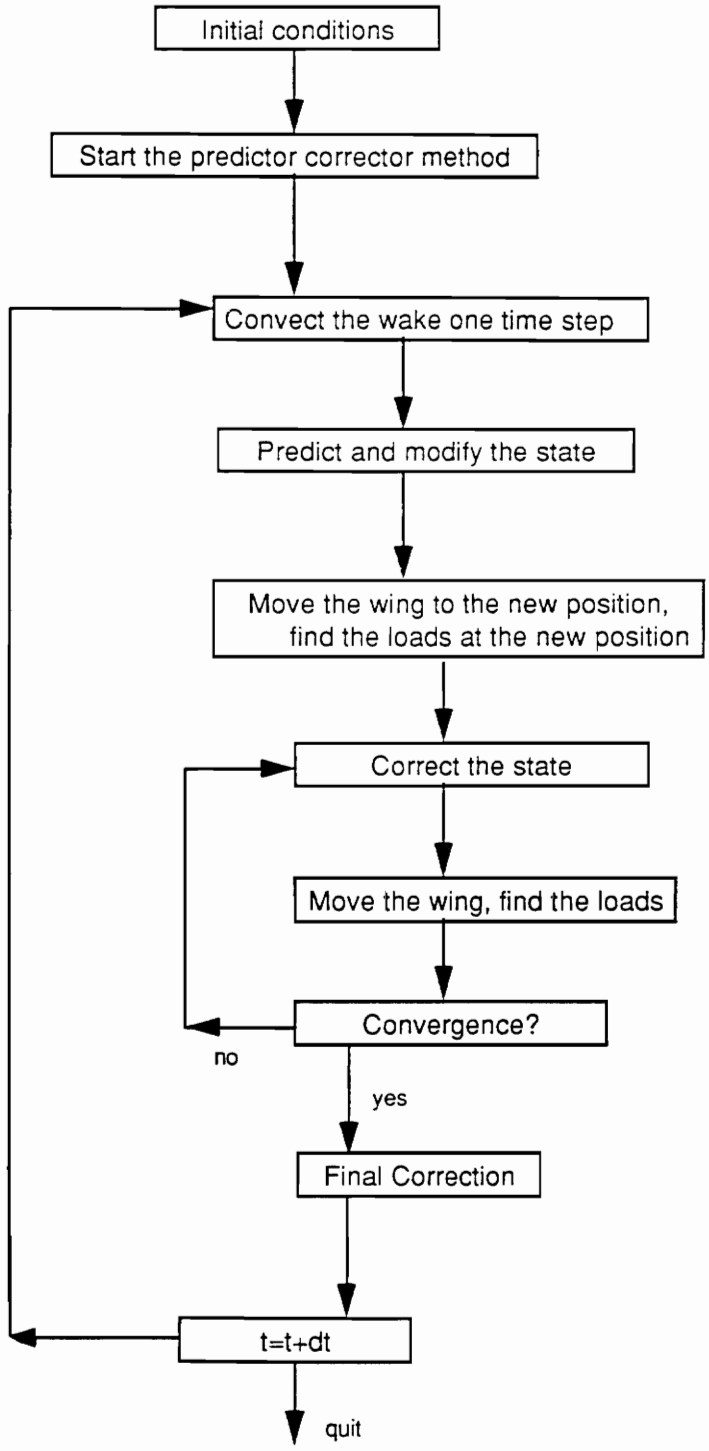

Figure 4.2 The algorithm for the dynamic solution.

Chapter 5 Numerical Examples

5.1 Introduction

Several examples are presented in the following pages to illustrate the aeroelastic model. The examples are presented in four different groups: static solutions, dynamic solutions, the suppression of flutter, and the alleviation of gust responses. Section 5.2 contains examples of solutions with both the linear and nonlinear structural models. The responses of a wing with varying speed and angles of attack chosen such that the lift is approximately constant are examined in Section 5.3. Both subcritical and supercritical responses are shown. Section 5.4 relates the effect of a control surface that is moved in an attempt to suppress the flutter of the wing. The control laws governing the motion of the control surface are discussed as well. Finally, Section 5.5 concerns the response of the wing to vertical perturbations of the free stream and the attempt to control the wing deformations by using feedback control.

The physical properties of the wing used in the examples are given in Table 5.1. For simplicity, the structural properties are assumed to be constant. Also, the inertial axis is coincident with the elastic axis. Neither of these assumptions is necessary. Four modes for bending and three modes for torsion are used in the expansions of v and ϕ. The modes and natural frequencies are derived in the Appendix.

Table 5.1 The physical properties of the wing used in the examples.

Chord	1.0 m
Aspect ratio	10.0
Elastic axis location (from leading edge)	30.5% of the chord
Elastic axis/inertial axis offset	0.0
Mass per unit length	10.0 kg/m
Mass moment of inertial per unit length	15.0 kg-m
Torsional stiffness	$0.2493(10^6)$ N-m^2
Bending stiffness	$0.3686(10^6)$ N-m^2
Freestream air density	1.0572 kg/m^3

Undamped natural frequencies (rad/s)

$\omega_{b,1} = 6.75$	$\omega_{t,1} = 20.26$
$\omega_{b,2} = 42.30$	$\omega_{t,2} = 60.79$
$\omega_{b,3} = 118.45$	$\omega_{t,3} = 101.25$
$\omega_{b,4} = 383.75$	

5.2 Static Solution Examples

This section presents examples of the static solution. The static solution represents a computationally efficient method of determining the equilibrium position of the wing (if one exists). If the velocity is at or above the divergence speed then the deformation of the wing will grow until structural failure occurs. Of course, the static solution gives no insight into the dynamic stability of the equilibrium position. The static solution may be used as initial conditions for the dynamic solution, with the magnitude of the initial disturbance governed by the convergence tolerance of the static solution.

The static solution is also a convenient way to compare linear and nonlinear beam theories. The higher-order terms of the nonlinear model are due to large curvature effects only. The following two examples compare two wings under identical conditions except for the angle of attack. In Figure 5.1 the static displacement of the elastic axis and the torsional deformation of the wing are shown for the linear and nonlinear models. The freestream velocity is 50 meters per second and the angle of attack is 3.5 degrees. In Figure 5.2 the angle of attack is increased to 5.9 degrees with a resulting increase in wing tip deflection of almost twice that of the previous case. In these examples the curvature terms have a negligible effect. It should also be noted that the twist of the wing has changed slightly despite the fact that the governing equation has not. This change in twist is due to the aerodynamic coupling between the bending and torsion loads.

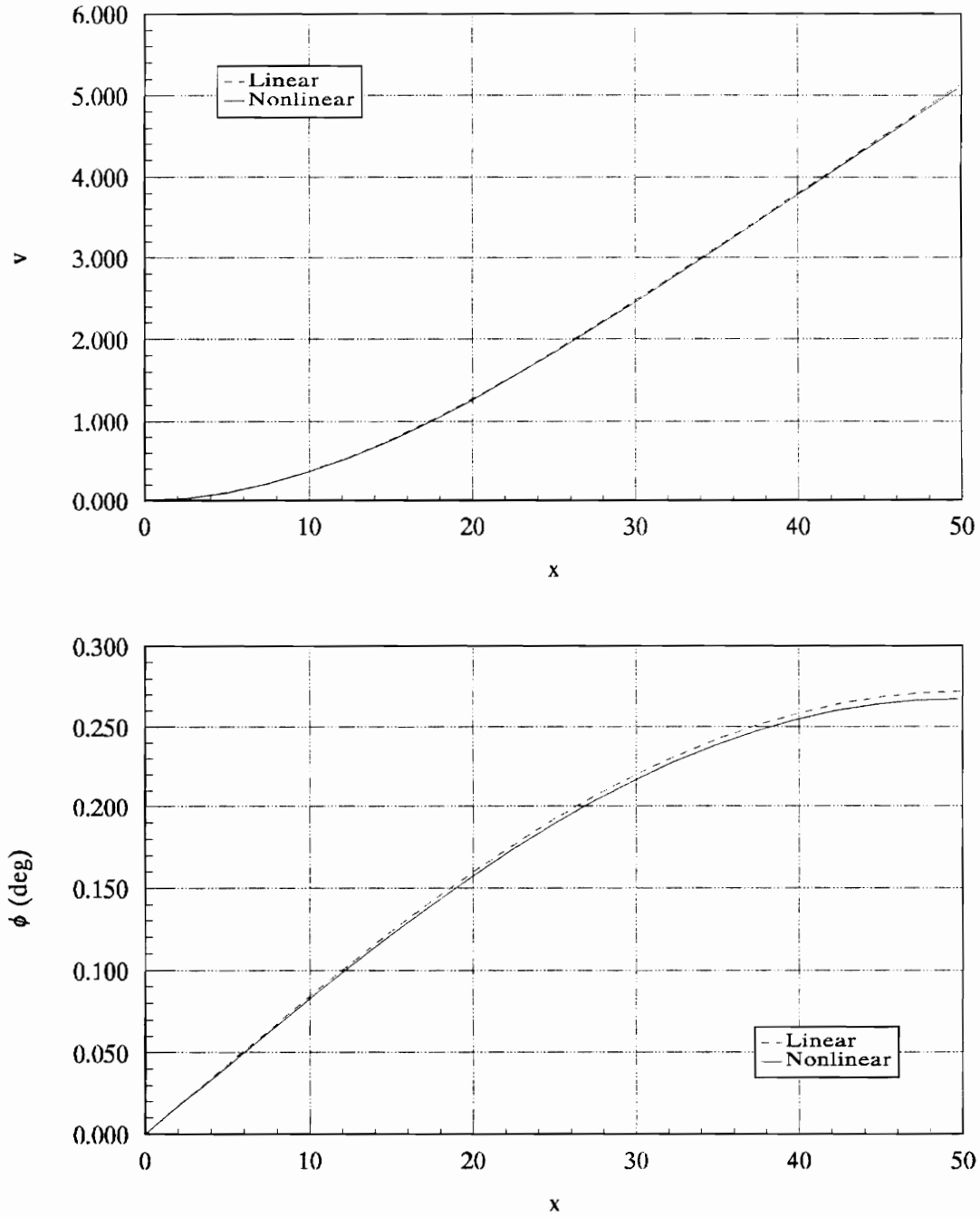

Figure 5.1 A comparison of the flexural and torsional deformations with the linear and nonlinear structural models. The velocity is 50 m/s and the angle of attack is 3.5 degrees.

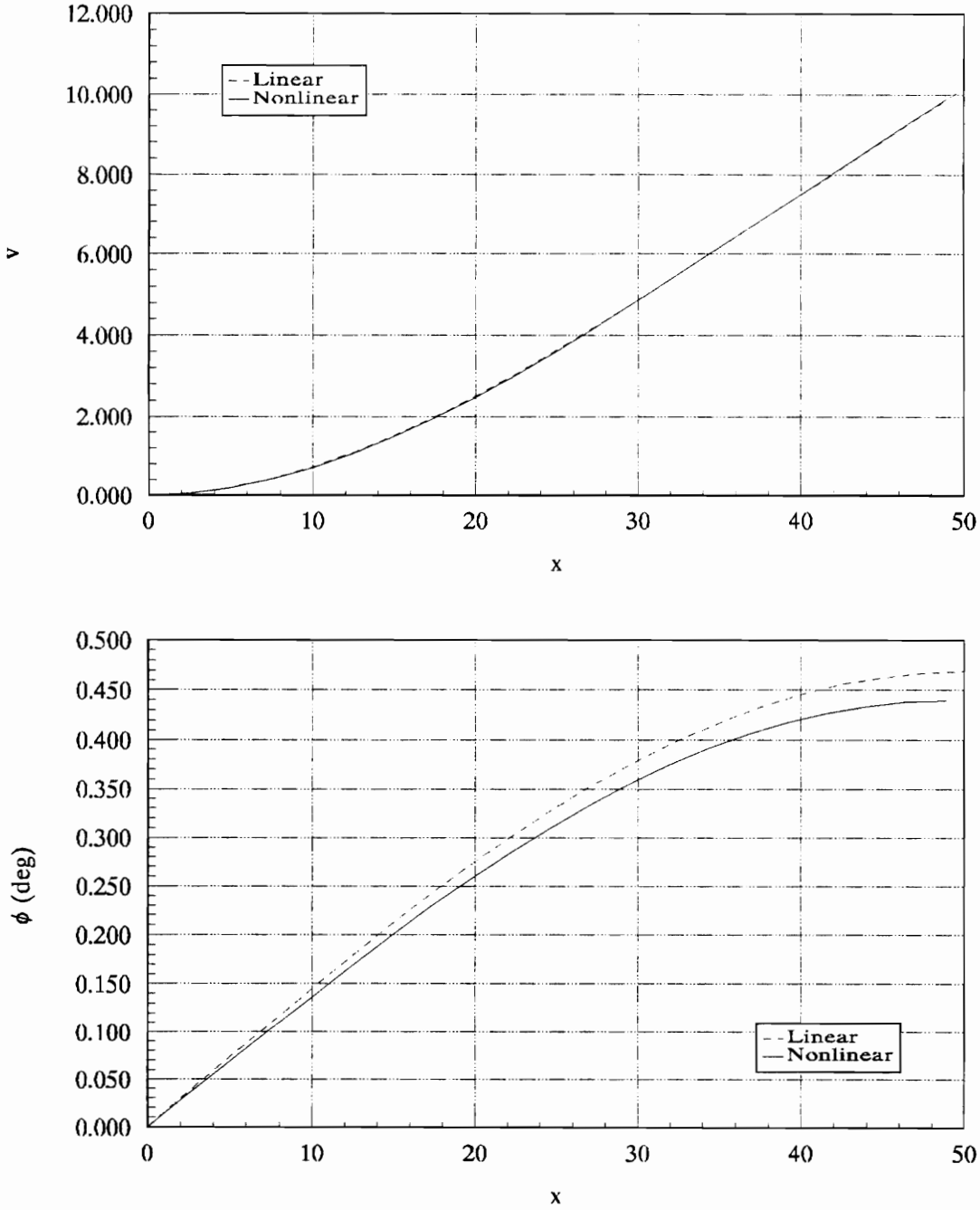

Figure 5.2 A comparison of the flexural and torsional deformations with the linear and nonlinear structural models. The velocity is 50 m/s and the angle of attack is 5.9 degrees.

5.3 Dynamic Solution Examples

The examples of this section show the dynamic response of a high-aspect ratio wing at various speeds and angles of attack. The following five cases model a wing at five different speeds: 50, 75, 100, 125, and 150 meters per second. The angle of attack has been changed to give approximately the same lift in each case. The angles of attack are 5.9, 2.4, 1.2, 0.65, and 0.35 degrees. The twist and percent bending deflection (vertical deflection divided by the span multiplied by 100) at the wing tip are shown as functions of dimensionless time for these five cases. In order to save computational time, the program is started near the static solution. For a velocity of 50 meters per second, the system is highly damped and oscillations decay quickly as shown in Figure 5.3. It is emphasized that all the damping is due to the aerodynamic loads (there is no structural damping in the present model). These loads are predicted by what is often called an "inviscid theory"; thus, there is "inviscid damping." The wing is twisting at a frequency corresponding to the first torsion mode. The twisting causes a small oscillation in the bending at the same frequency. The oscillations are about mean values equal to those found by the static solution. As shown in Figure 5.4, when the velocity is increased to 75 meters per second the system remains stable but the damping is lessened. A similar initial disturbance now takes approximately four times as long to decay to the same value. This condition is near the flutter speed. A further increase in velocity to 100 meters per second moves the system past the flutter speed as shown in Figure 5.5. The oscillations

appear to grow exponentially with a common frequency near the first torsional natural frequency. The phase difference between the motions is approximately 180 degrees. This phase difference is characteristic of flutter and allows energy to be extracted from the freestream as discussed in Chapter 1. Further increases in speed result in larger rates of growth. As shown in Figure 5.6 the bending and torsional motions quickly reach large values for a velocity of 125 meters per second. The frequency of both motions remains near the first torsional natural frequency (recall that the nondimensional time is based on the freestream velocity). The response at a velocity of 150 meters per second, shown in Figure 5.7, is similar but with a higher rate of growth. It is theoretically possible that there is another critical speed above which the system is stable. This is often noted in the frequency domain solutions by the curve g(V) possessing multiple roots. In the present study this does not appear to be the case. If unsuppressed these motions would quite likely lead to a catastrophic failure of the wing.

While the time histories of the wing tip deflections are easily interpreted, it is the generalized coordinates and their derivatives that completely describe the state of the wing. Figure 5.8 and Figure 5.9 show the time histories of the generalized coordinates and their first derivatives for the example corresponding to a velocity of 125 meters per second. The motion is dominated by the first mode for both flexure and torsion with higher modes not becoming significant until large oscillations are obtained.

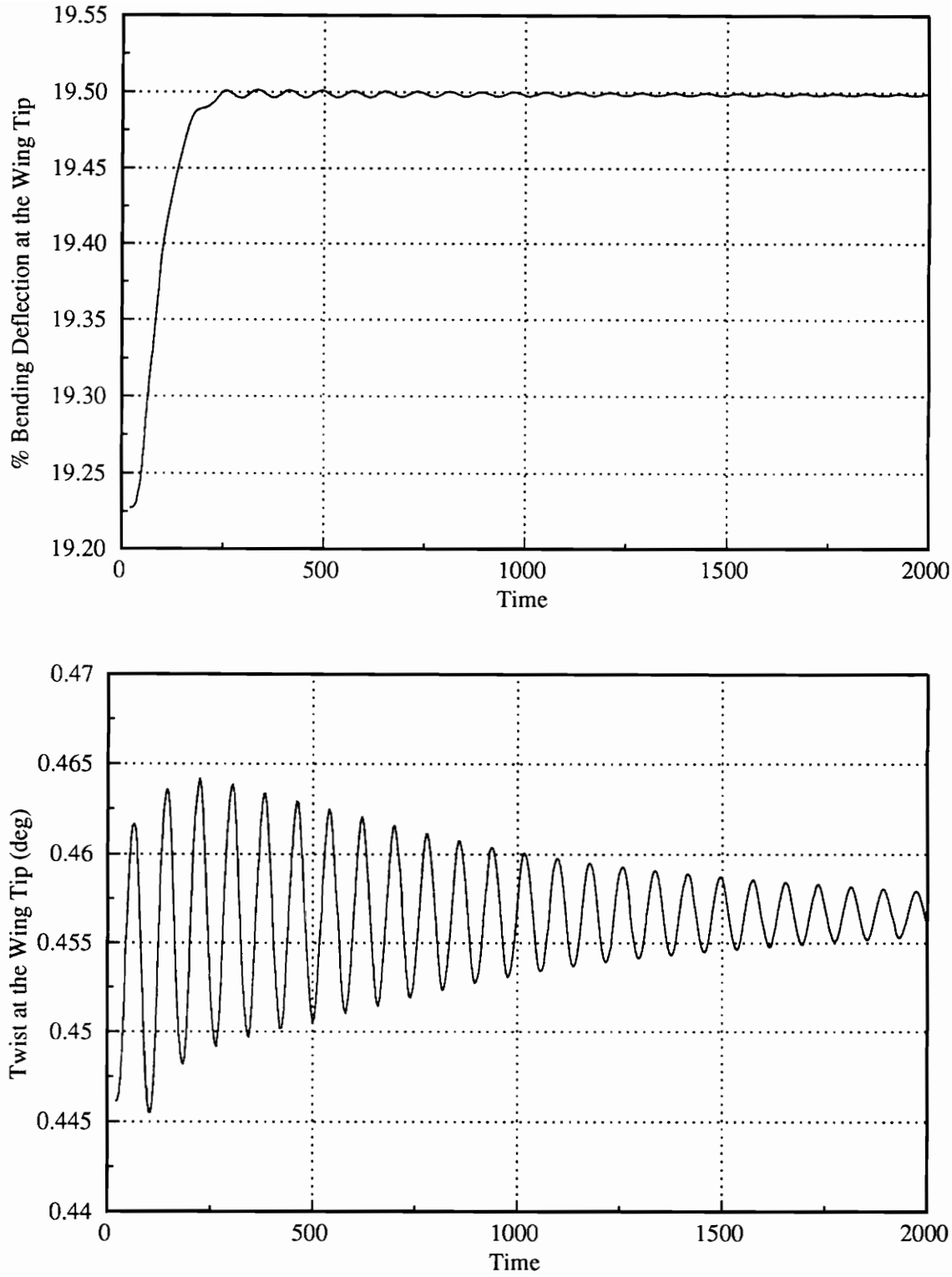

Figure 5.3 The response of the wing with a velocity of 50 m/s and angle of attack of 5.9 degrees.

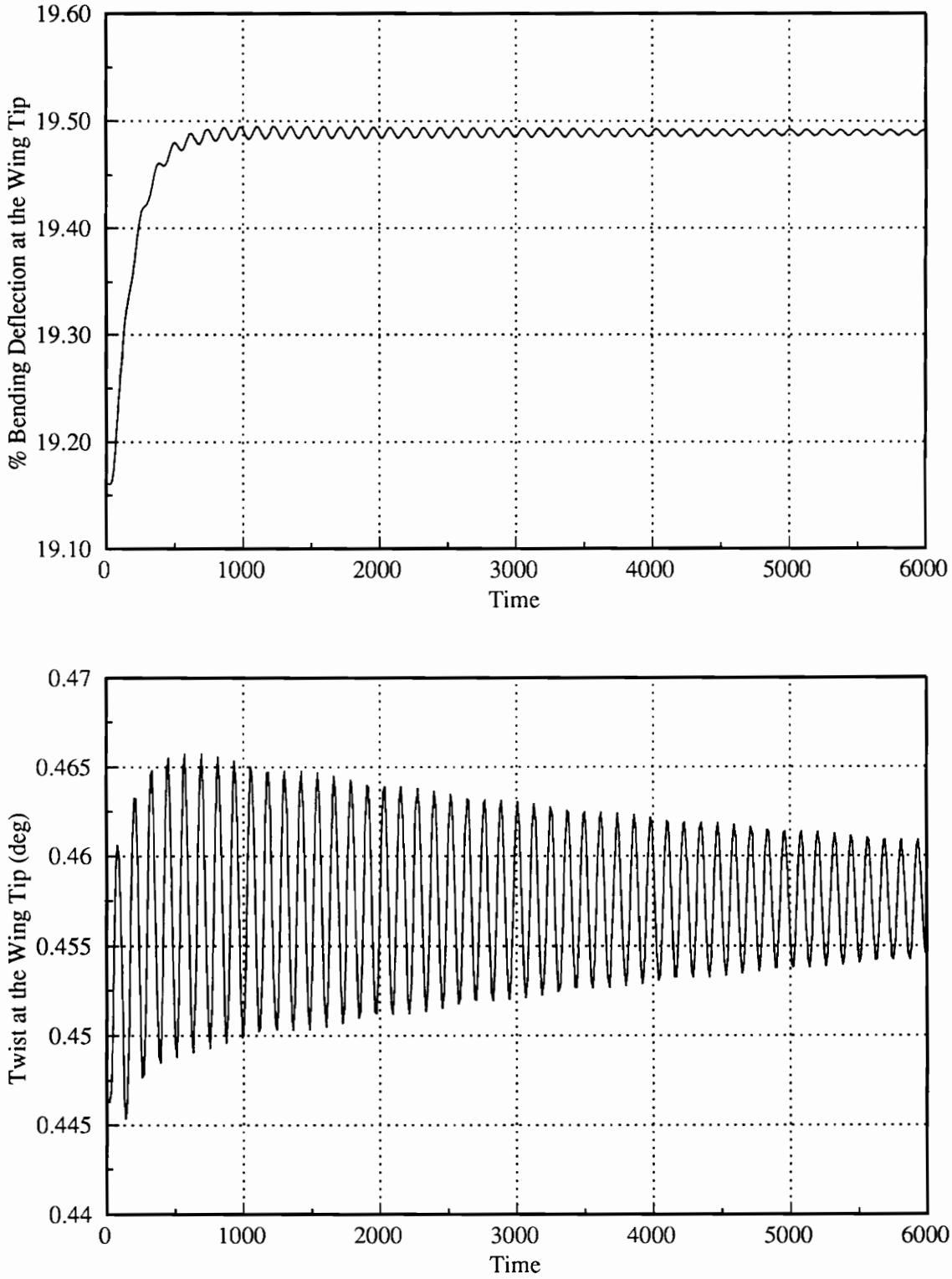

Figure 5.4 The response of the wing with a velocity of 75 m/s and angle of attack of 2.4 degrees.

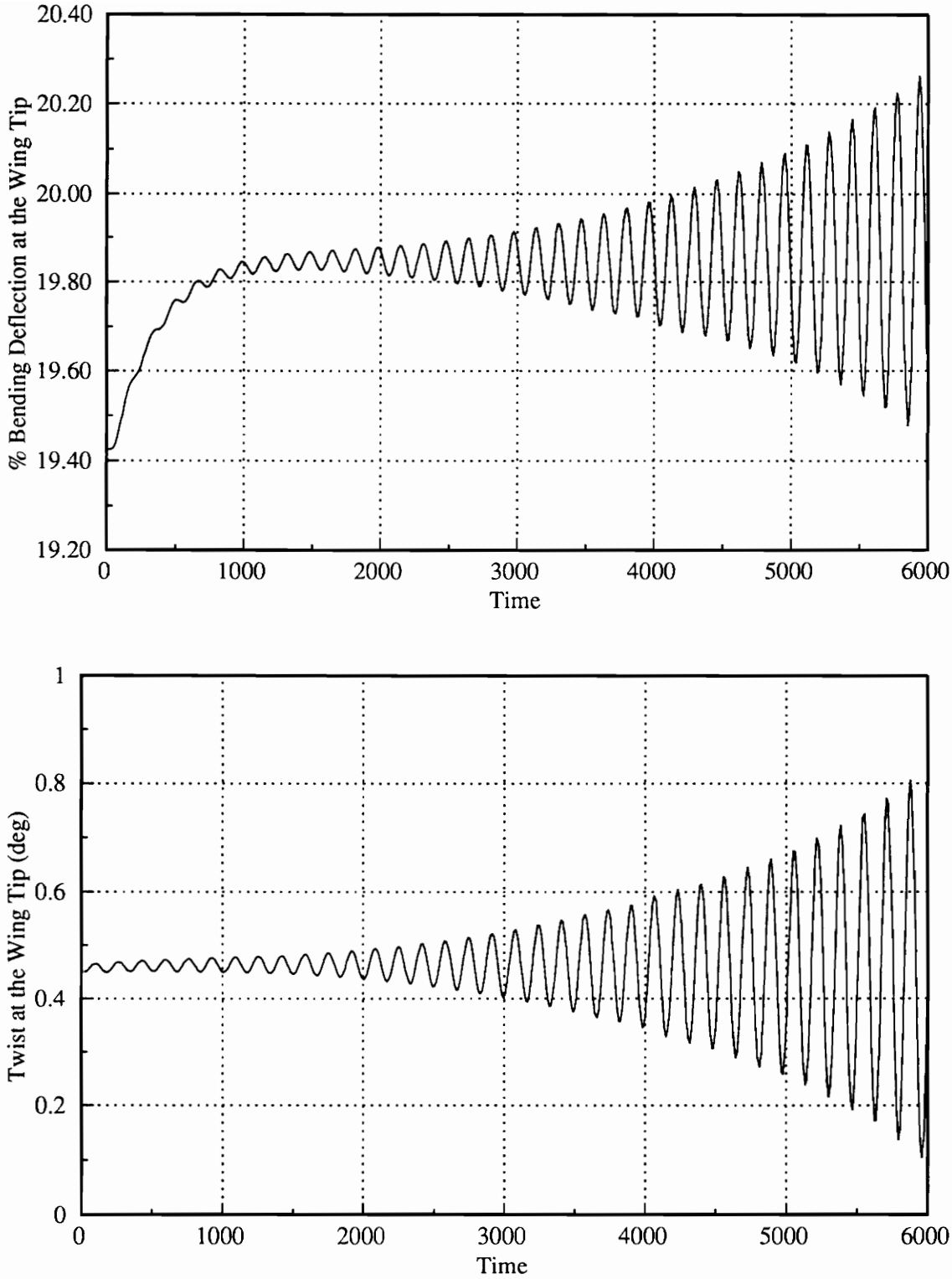

Figure 5.5 The response of the wing with a velocity of 100 m/s and angle of attack of 1.2 degrees.

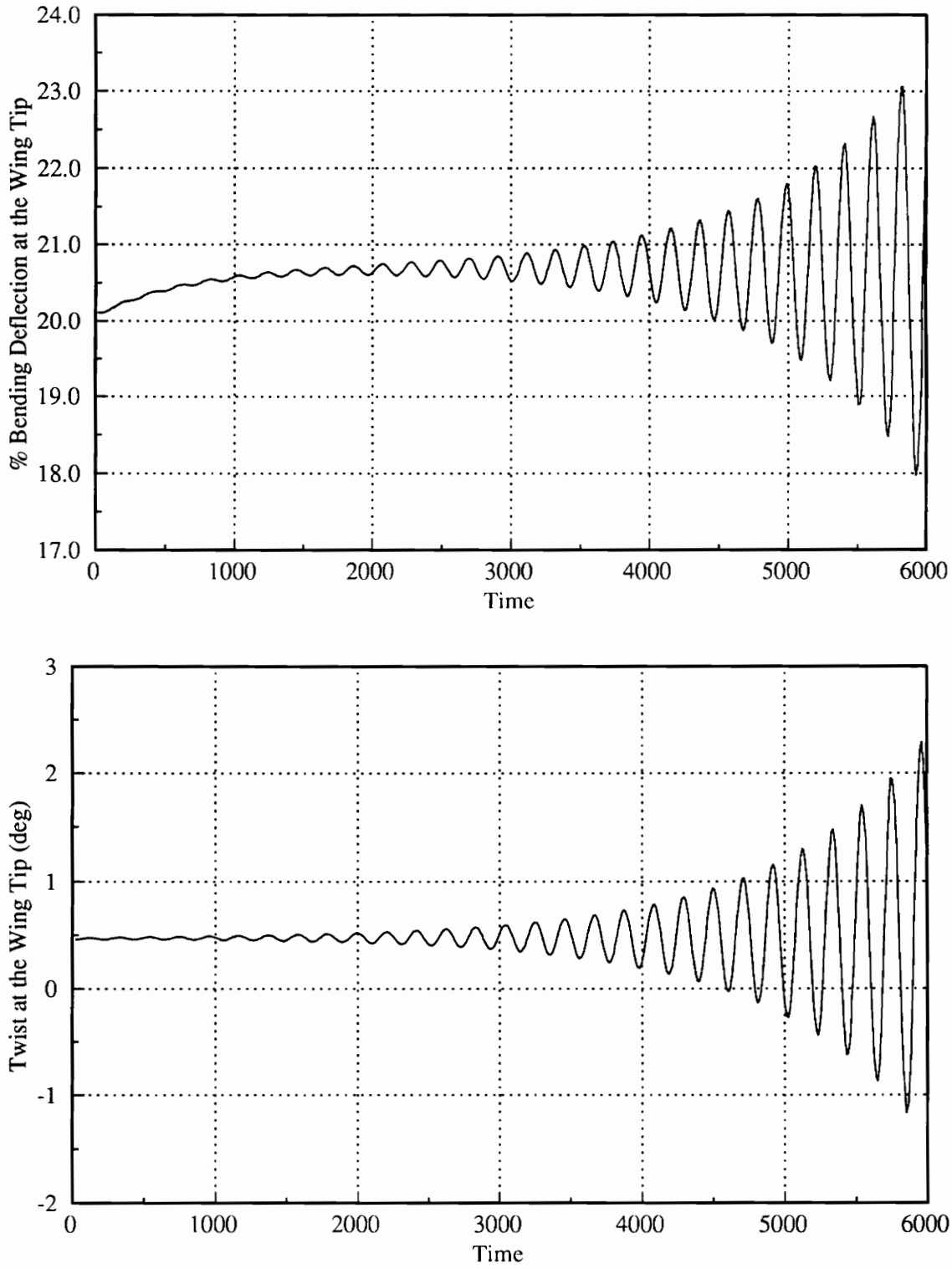

Figure 5.6 The response of the wing with a velocity of 125 m/s and angle of attack of 0.65 degrees.

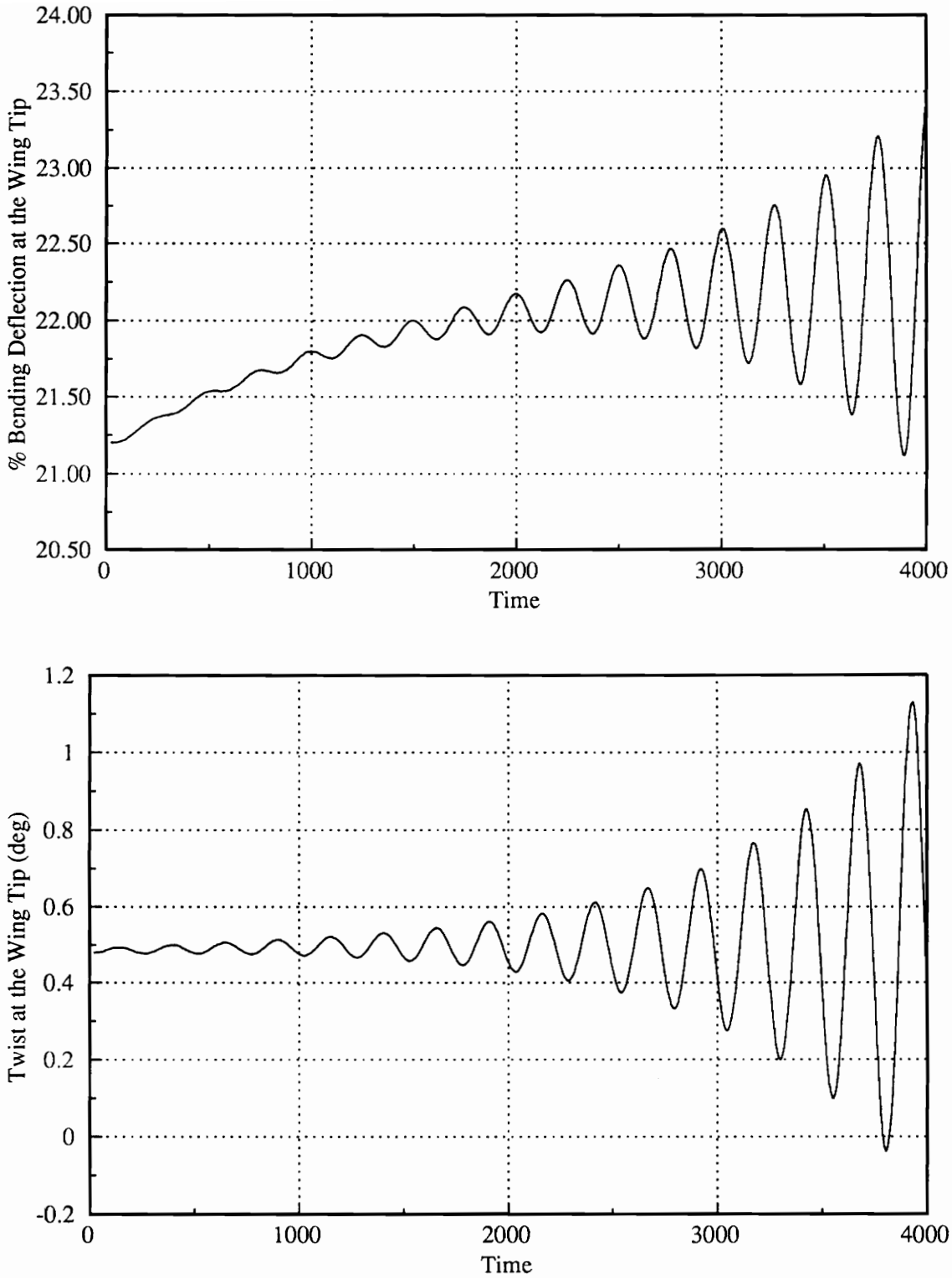

Figure 5.7 The response of the wing with a velocity of 150 m/s and angle of attack of 0.35 degrees.

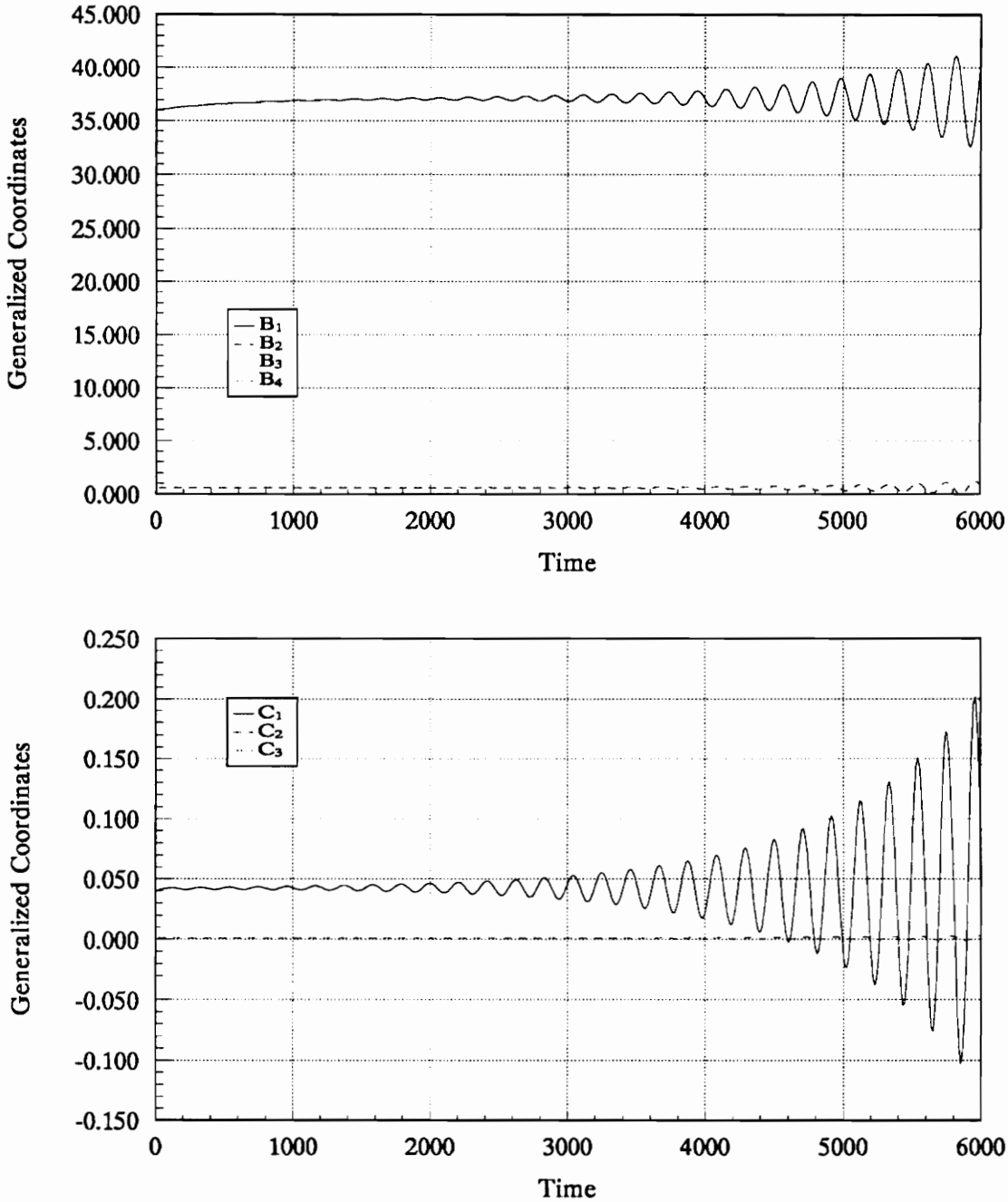

Figure 5.8 The time histories of the flexural and torsional generalized coordinates for the case with a velocity of 125 m/s and angle of attack of 0.65 degrees.

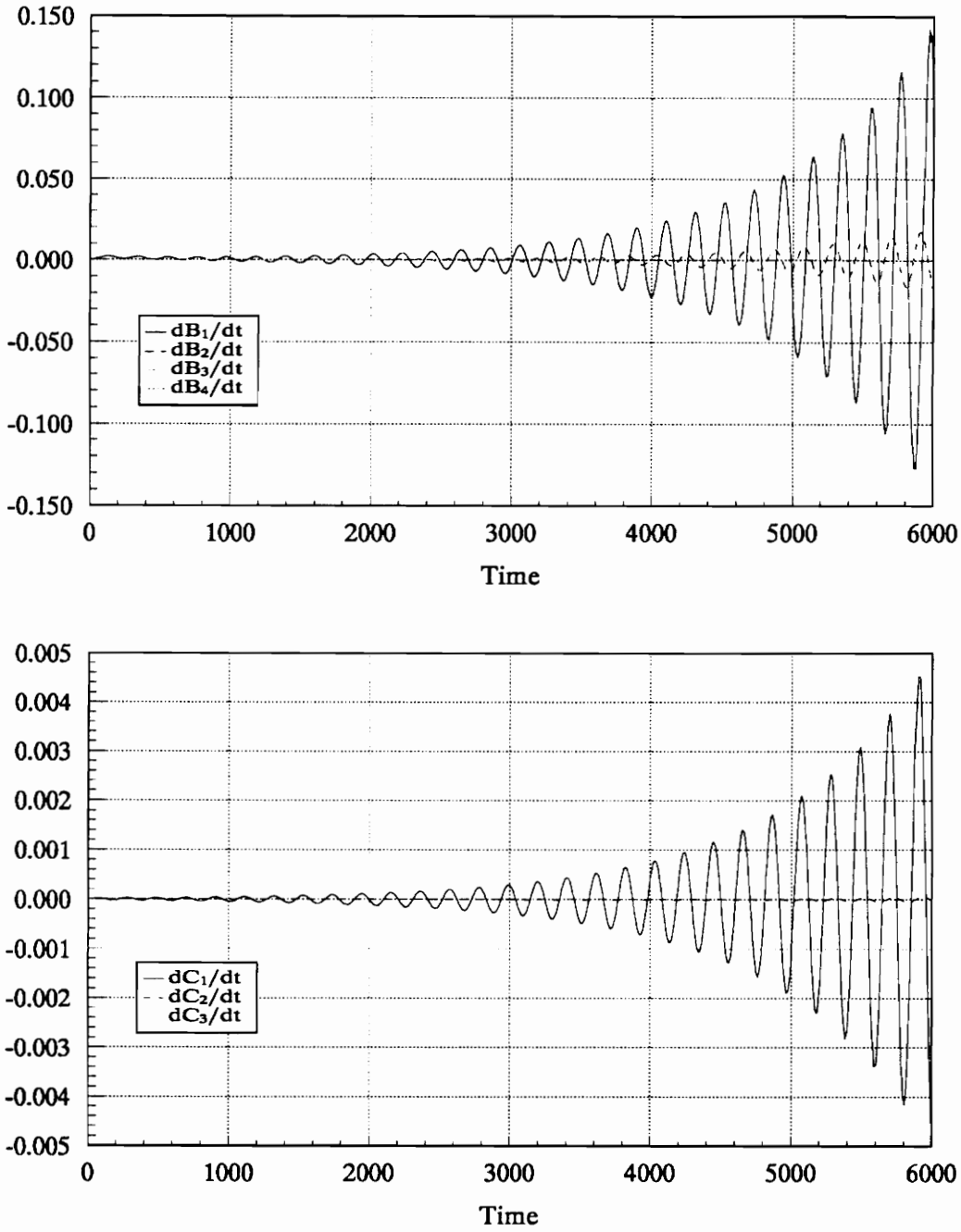

Figure 5.9 The time derivatives of the generalized coordinates for the case with a velocity of 125 m/s and angle of attack of 0.65 degrees.

5.4 Flutter Suppression

Flutter may be suppressed through active control by the appropriate motion of a control surface. Ailerons are placed near the wing tips and are moved as flaps according to a control law based on the wing tip velocity. The control law used in the present work has the form

$$\beta(t) = G_1 \dot{v}(t, 0.95L) + G_2 \dot{\phi}(t, 0.95L) \tag{5.1}$$

where $\beta(t)$ is the aileron deflection (positive downward) and G_1 and G_2 are the user-selected gains. For a trailing edge control surface $G_1<0$ and $G_2>0$. In the present work the gains are selected by trial and error. It was found that flutter may be suppressed for a wide range of gains.

The following five figures show the response of the system with and without feedback control. Three different speeds and two different sets of gains are used. The responses without active control correspond to the examples in the previous section. Figure 5.10 shows the responses of the wing at a freestream velocity of 100 meters per second and gains of -5 and 50. The control is turned on at a dimensionless time of 3000 and the oscillations are quickly suppressed. Despite the fact that the oscillations have already progressed to moderate values, the active control is able to stabilize the system. When the speed is increased to 125 meters per second the feedback control again stabilizes the system (Figure 5.11). At a speed of 150 meters per second, however, feedback control increases the response of the system dramatically, even though the control is activated when the wing is released from rest, before the oscillations have grown.

With different gains, however, the response is quite different. The responses of the wing at speeds of 125 and 150 meters per second using gains of -1 and 1000 are shown in Figure 5.13 and Figure 5.14. These gains create higher damping in the first case and a stable system in the second case. Once again the aileron deflections are quite reasonable and decay rapidly. Although the aileron deflection becomes small, control is still necessary for the stability of the system. If the aileron were fixed the large amplitudes would reappear because the system is unstable and, hence, any small disturbance would grow.

The time histories of the generalized coordinates and their first derivatives are shown in Figure 5.15 and Figure 5.16. The velocity is 125 meters per second and the gains are -1 and 1000. The second modes have a slight effect while higher modes are effectively zero. However, the generalized velocities of the higher modes have become large. As many as three modes appear to be important. The second torsional mode of velocity is now of the same order as the first mode. The increased values are a result of the aileron deflections. Larger aileron deflections could also cause the higher modes of deflection to become important. The implication is that the active control of an aeroelastic system increases the number of modes necessary to satisfactorily model the system. The phase plots of the first modes, with and without feedback control, are also shown in Figure 5.17.

The time domain solution allows a graphical representation of the history of the system. Figure 5.18 and Figure 5.19 show a sequence of time steps extracted from a computer animation of the aeroelastic simulation. The wing is released from an

undeformed position with a freestream velocity below the flutter speed. As the wing deforms under the influence of the aerodynamic loads the vorticity generated at the wing tip weakens. Then as the wing comes to rest in its equilibrium position the wing tip vortex begins to reform. This phenomenon has also been observed in flutter. The vorticity weakens as the wing rises and strengthens as the wing plunges.

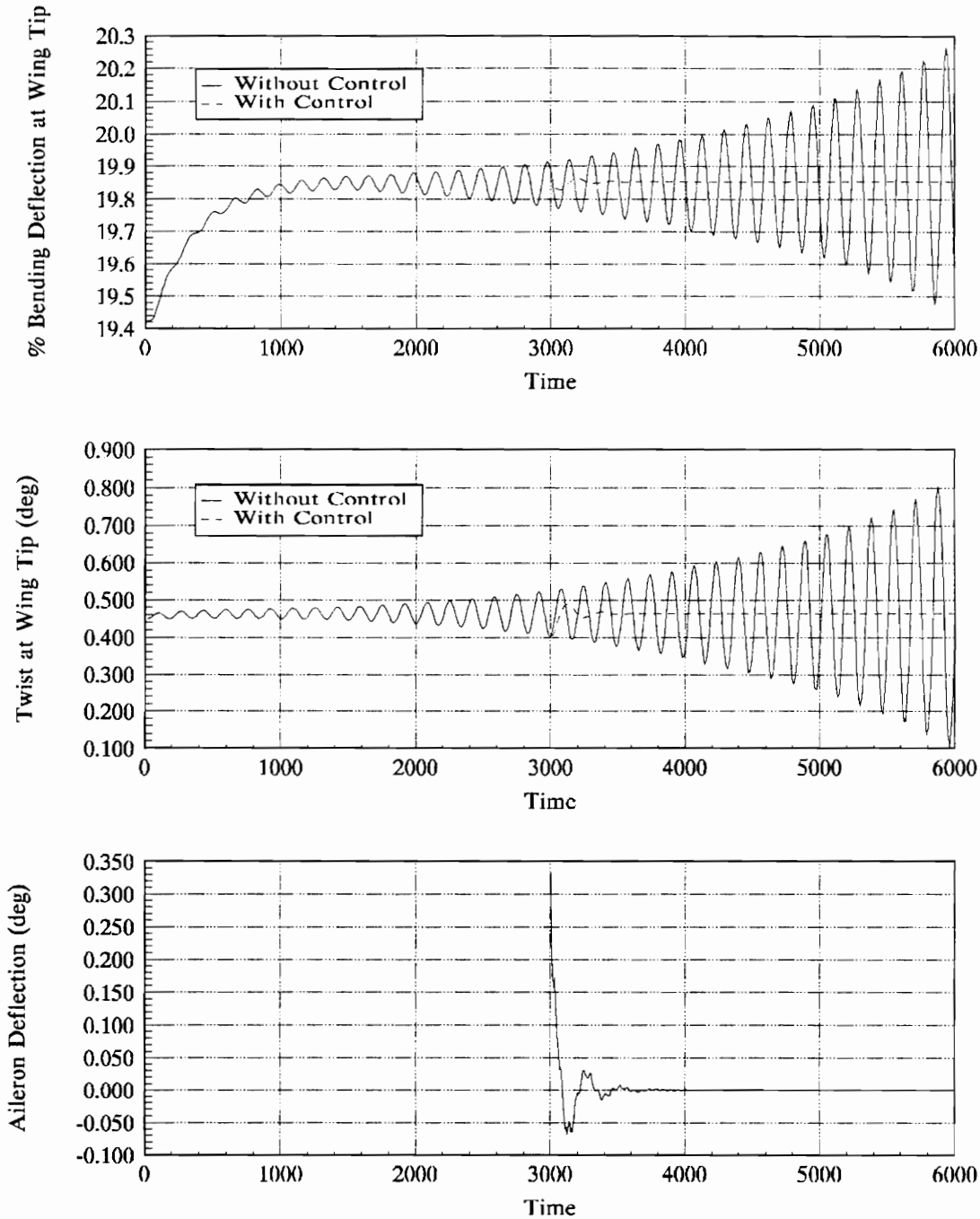

Figure 5.10 The response of the wing with and without control. The velocity is 100 m/s and the gains are -5 and 50.

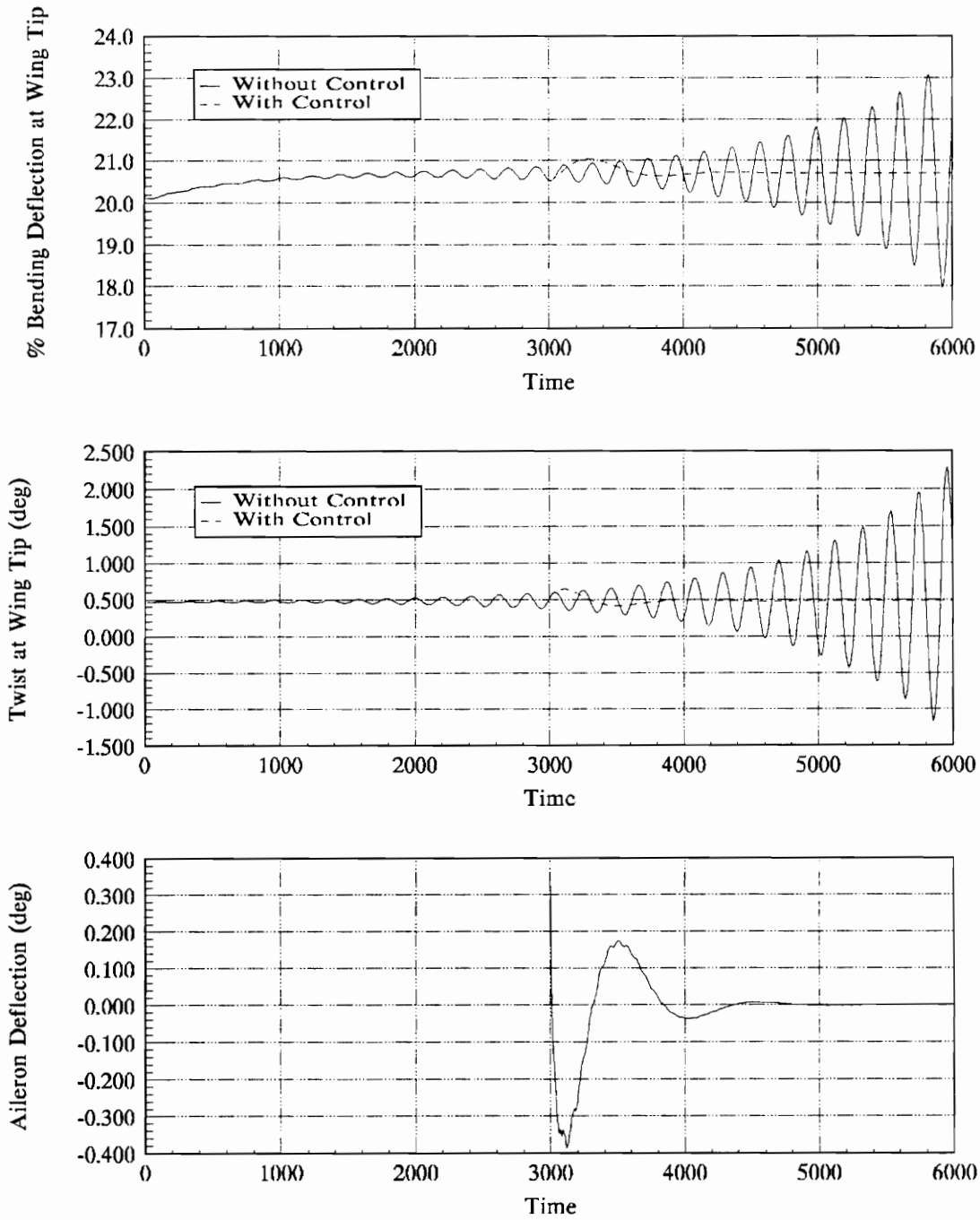

Figure 5.11 The response of the wing with and without control. The velocity is 125 m/s and the gains are -5 and 50.

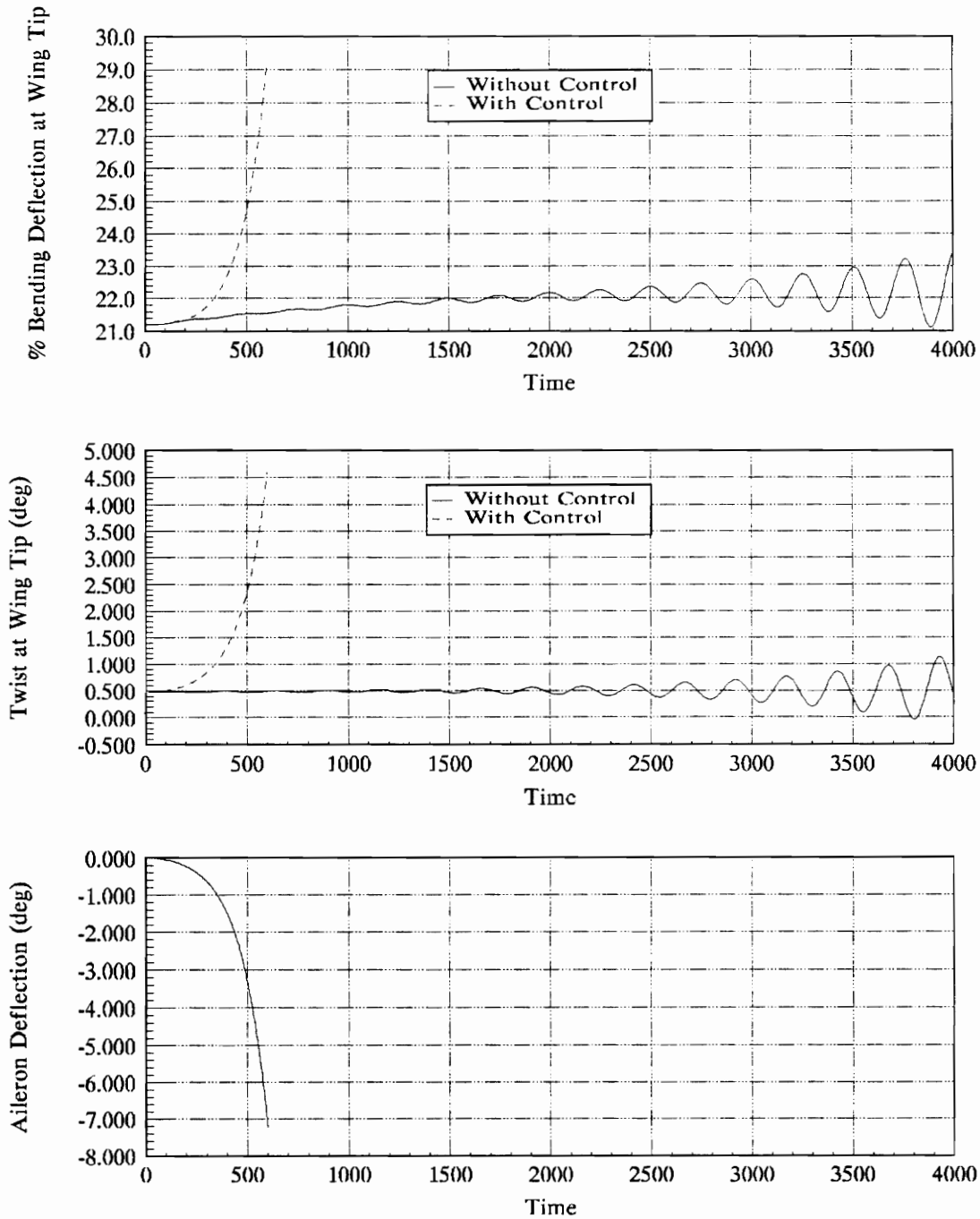

Figure 5.12 The response of the wing with and without control. The velocity is 150 m/s and the gains are -5 and 50.

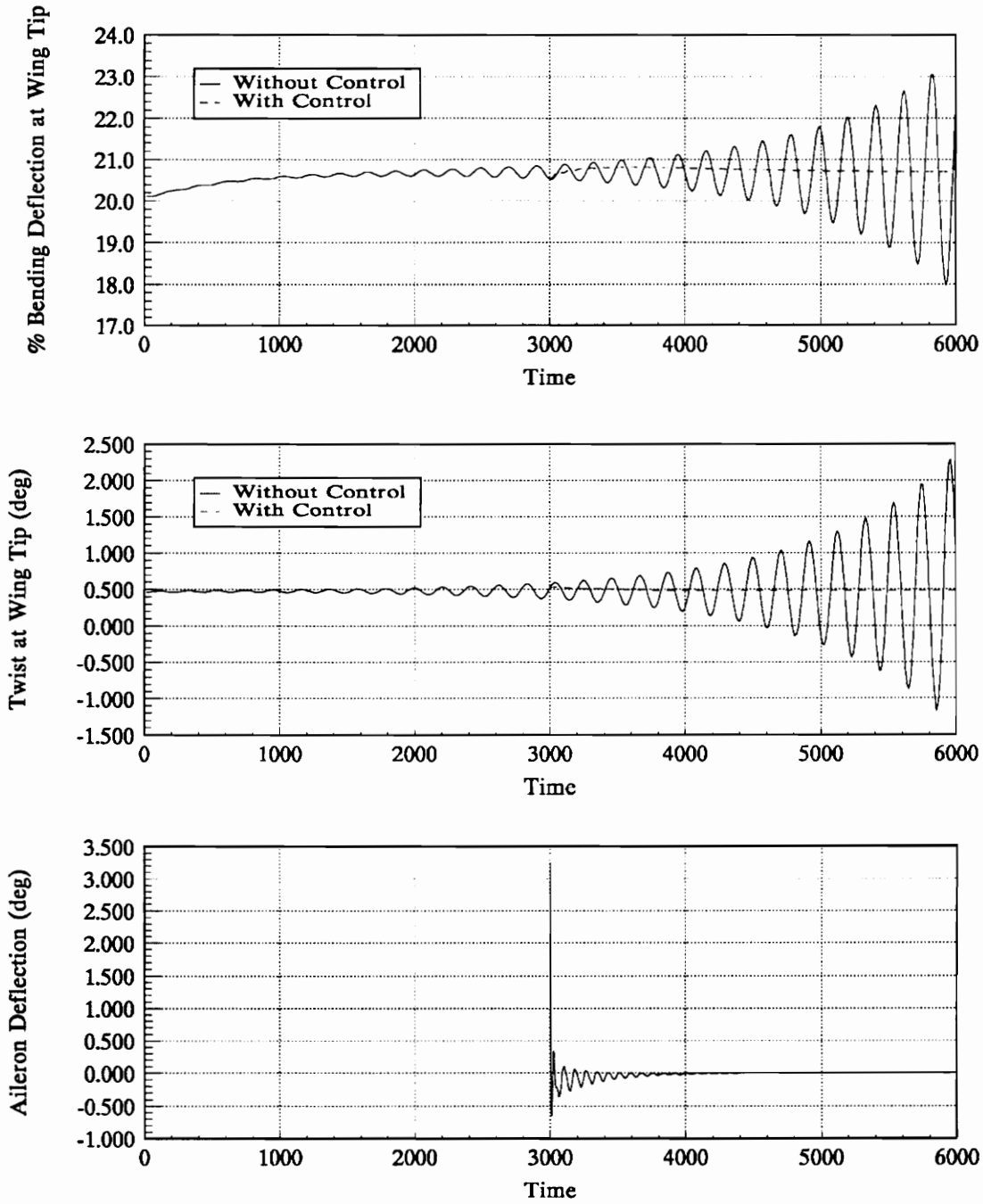

Figure 5.13 The response of the wing with and without control. The velocity is 125 m/s and the gains are -1 and 1000.

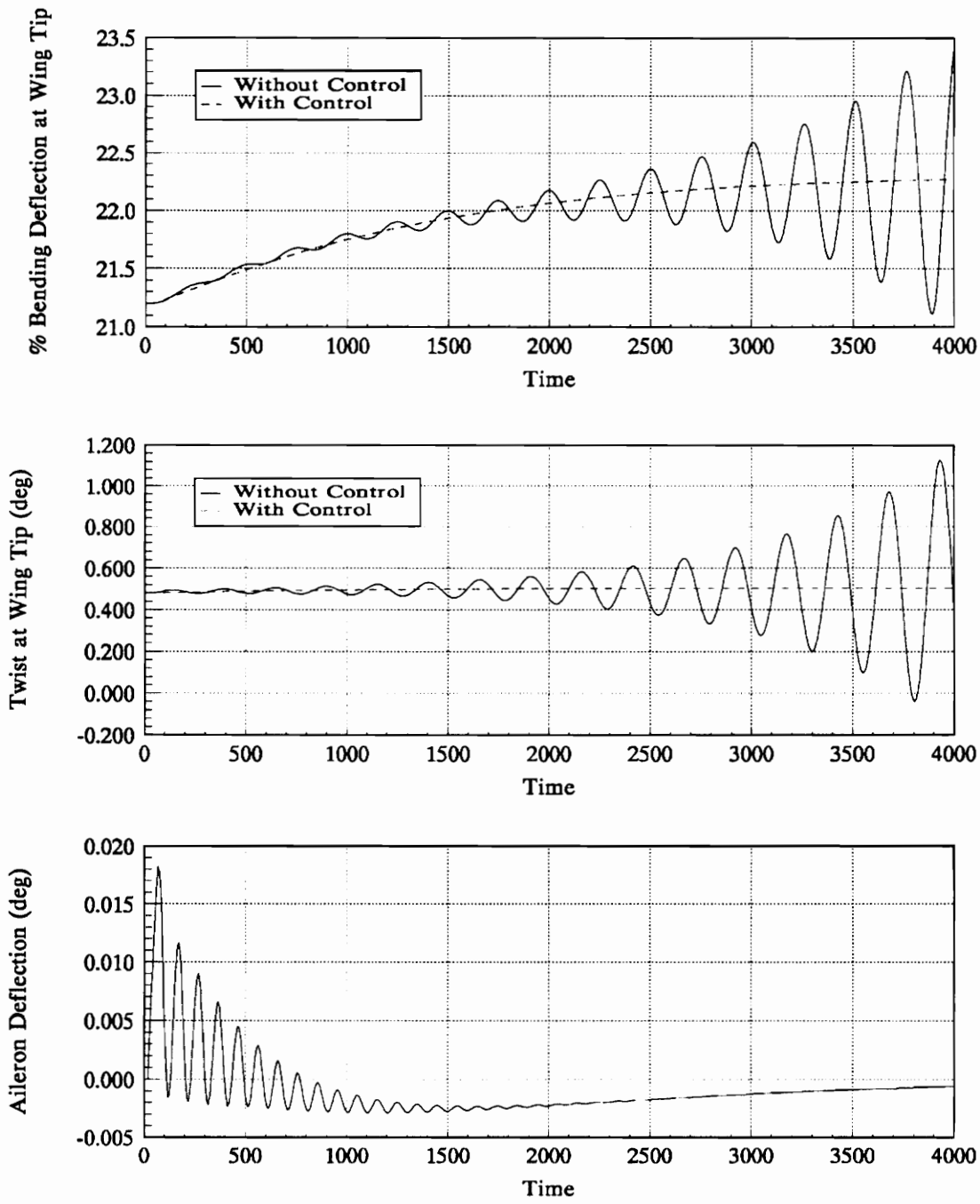

Figure 5.14 The response of the wing with and without control. The velocity is 150 m/s and the gains are -1 and 1000.

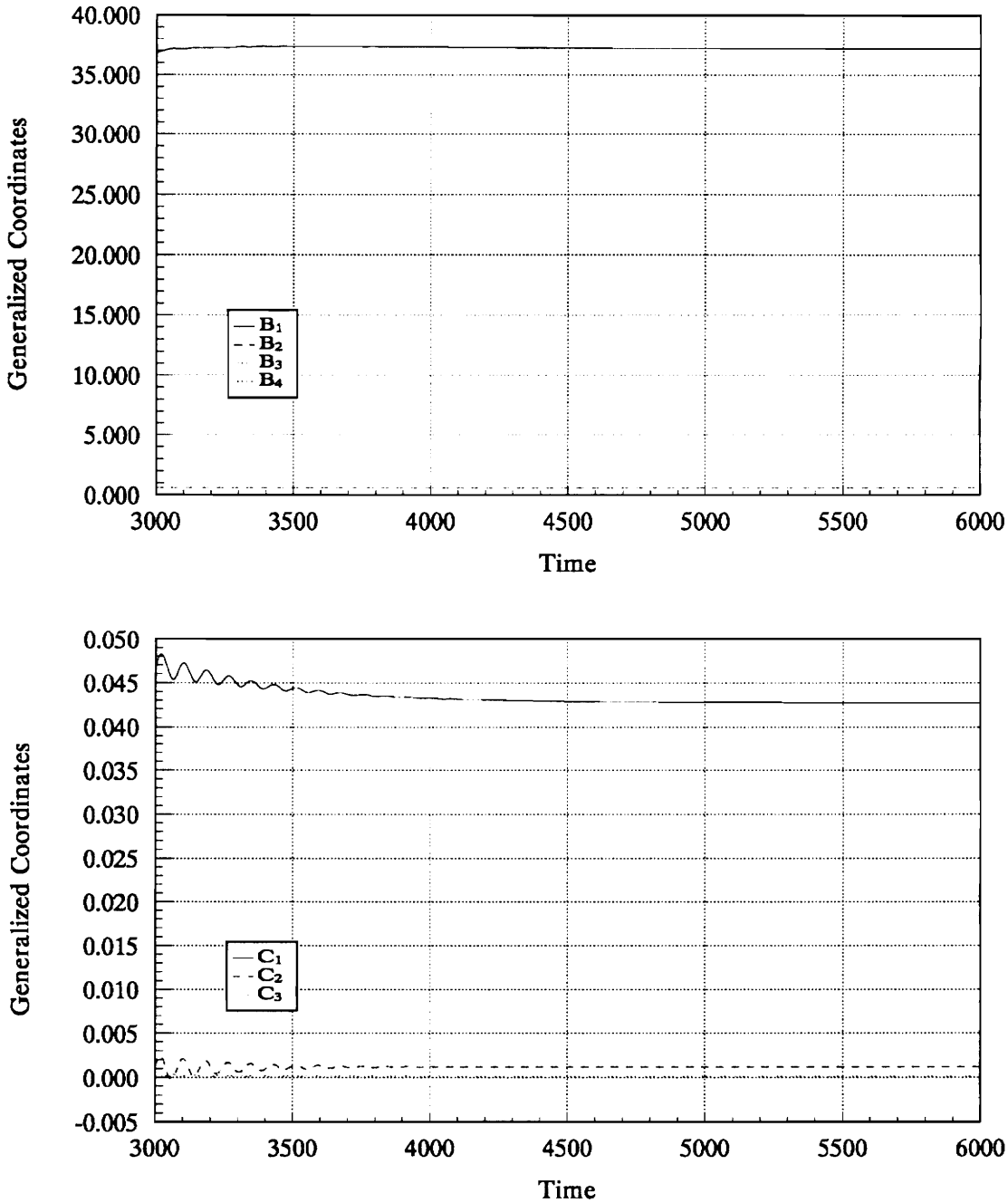

Figure 5.15 The time histories of the flexural and torsional generalized coordinates for a case with feedback control. The velocity is 125 m/s and the gains are -1 and 1000.

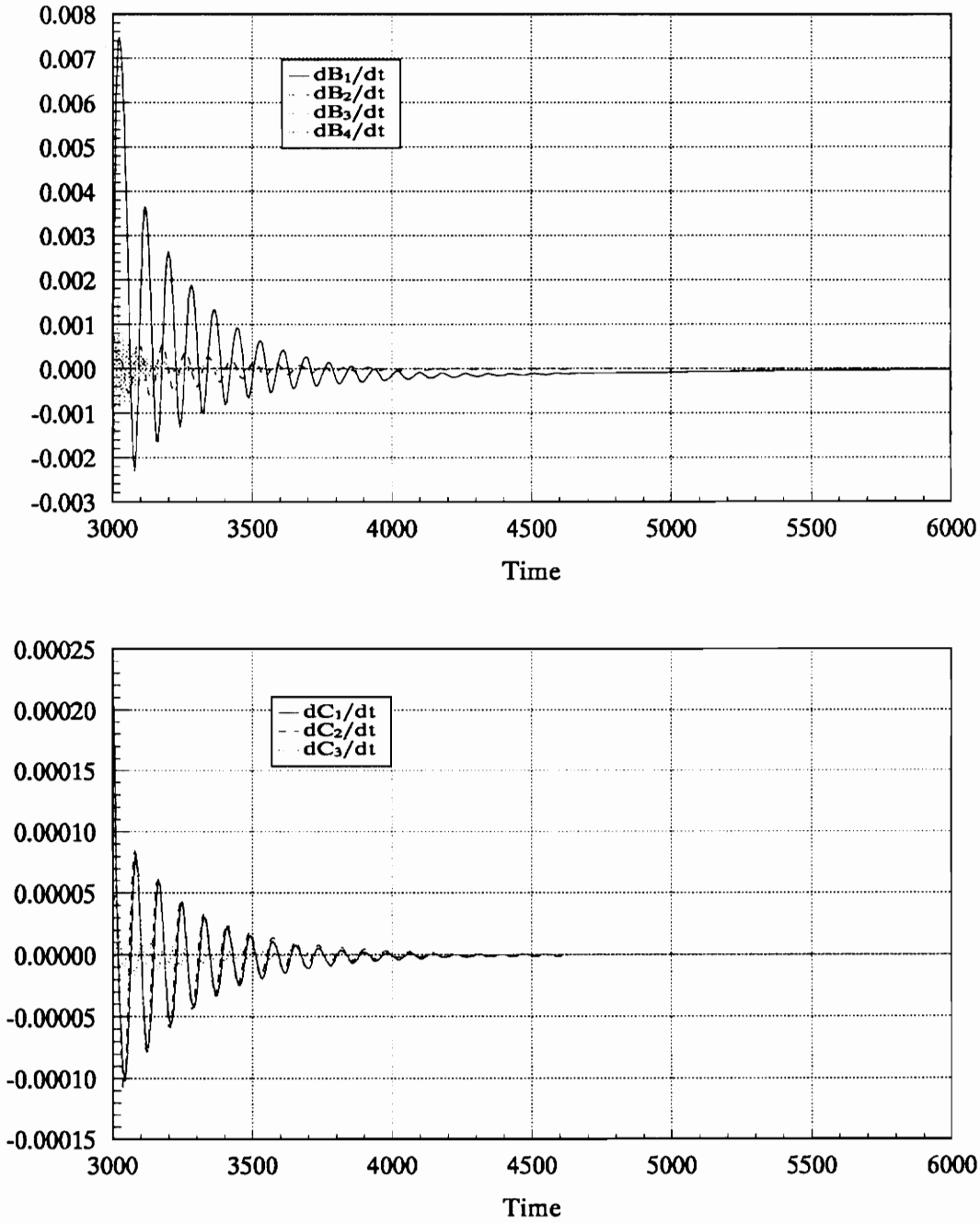

Figure 5.16 The time derivatives of the generalized coordinates for a case with feedback control. The velocity is 125 m/s and the gains are -1 and 1000.

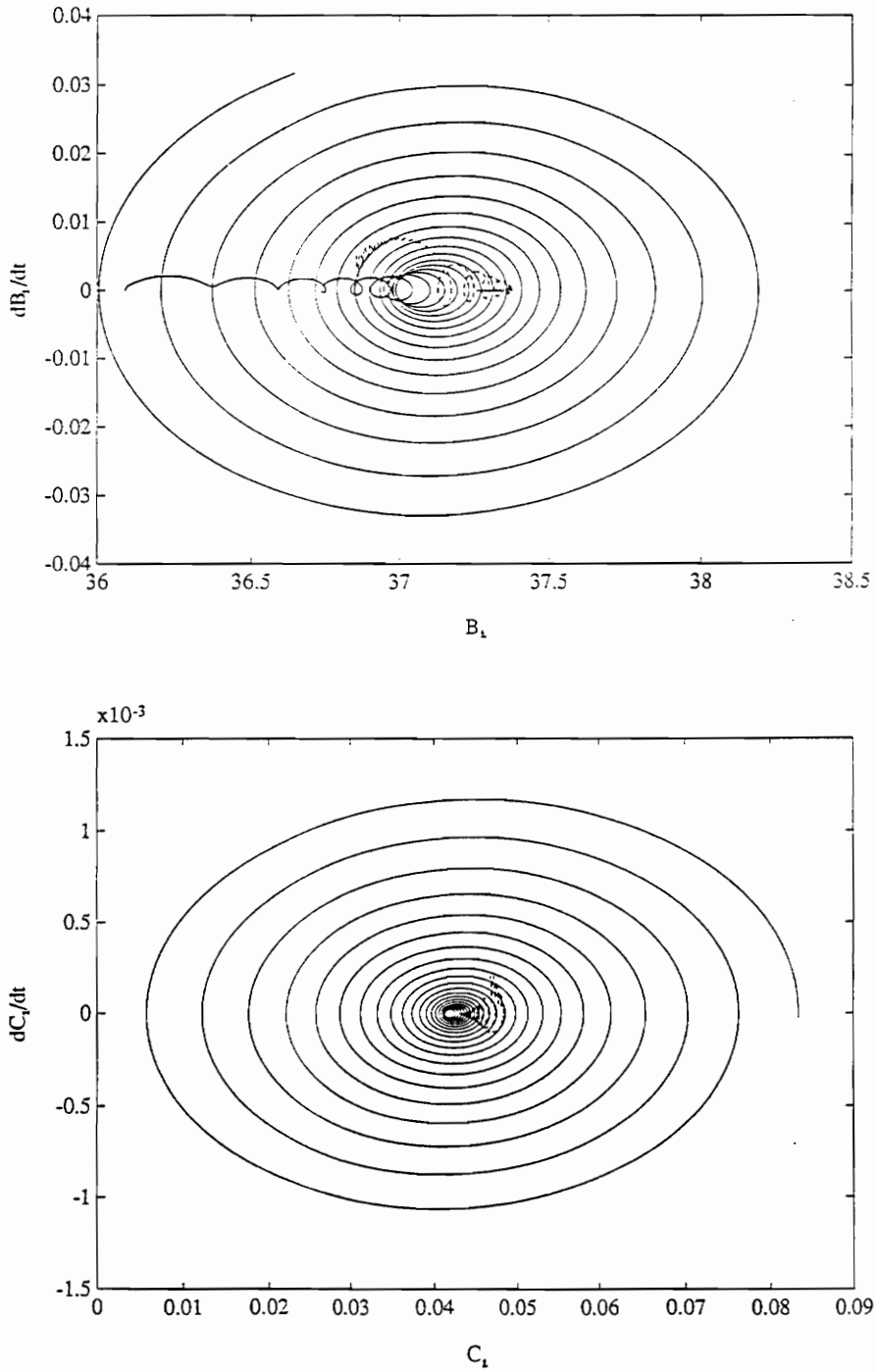

Figure 5.17 The phase plots with and without feedback control for the first generalized coordinates of flexure and torsion. The velocity is 125 m/s and the gains are -1 and 1000.

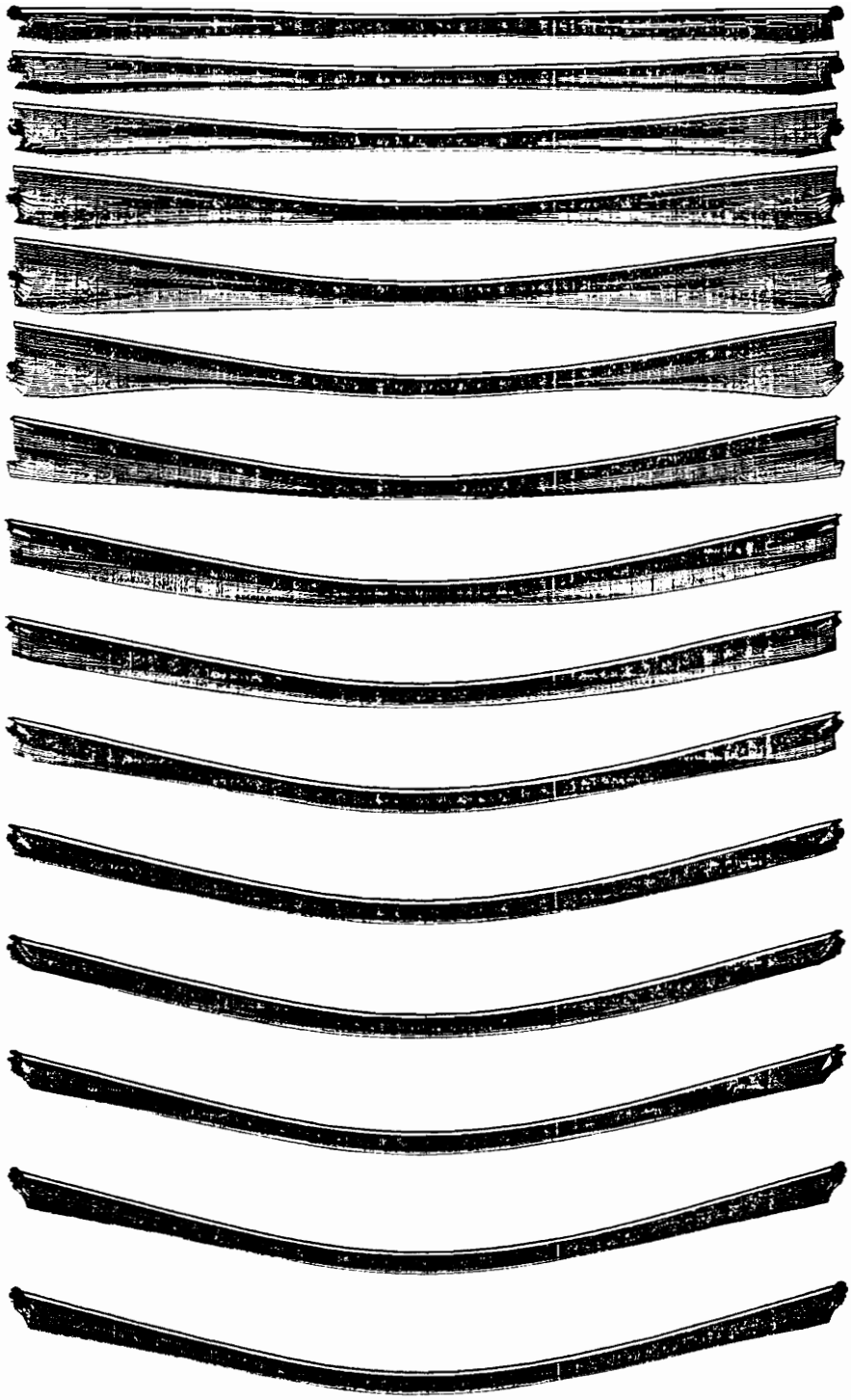

Figure 5.18 A time sequence of the wing and wake positions (front view).

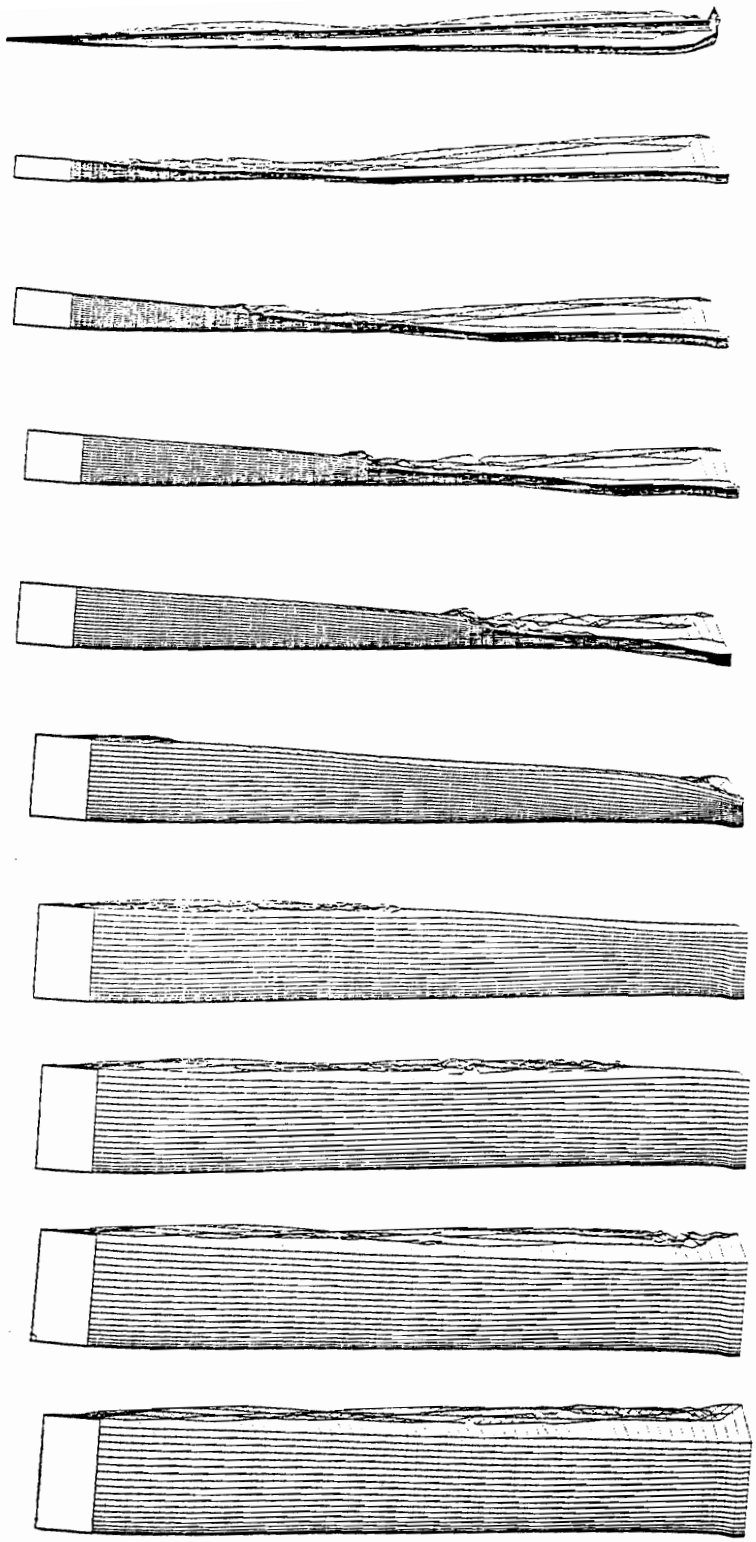

Figure 5.19 A time sequence of the wing and wake positions (side view).

5.5 Gust Alleviation

The control system used to suppress flutter may also be applied to disturbances such as wind gusts and turbulence. The disturbances are modeled as random perturbations in the vertical component of the freestream velocity. The response of a wing with and without wind gusts is shown in Figure 5.20. The mean velocity is 50 meters per second and the maximum magnitude of the gust velocity is 2.5 meters per second. The gust velocity is varied at every time step. The dominant frequency of the torsional deformation is the undamped natural frequency. The gust input containing many frequencies has been filtered by the aeroelastic system such that only gust frequencies near the natural frequency of the wing appear in the response. Figure 5.21 and Figure 5.22 show the responses of the system with and without feedback control and two different sets of gains. The gains used are -1 and 1000 for the first case and -10 and 0 for the second case. For these control systems the flexural and torsional motions could not simultaneously be reduced. In the first case the bending is somewhat reduced but only at the expense of higher angles of twist. Likewise, the twist is damped very well in the second case but the bending is essentially unchanged. Other control laws implemented have produced less satisfactory results.

The difficulty involved in designing an active control system for a trailing edge control surface may be partly explained by examining the aerodynamic coupling of the system. Consider a wing that receives a disturbance such that the wing tip moves upward. To counteract the motion the control surface should be moved upward, creating a negative change in lift. However, the change in lift creates a positive change in the

twisting moment, creating a positive change in the angle of attack and consequently a positive change in lift. The addition of a leading edge control surface would avoid this problem. Nevertheless, the current control system is very effective for the suppression of flutter.

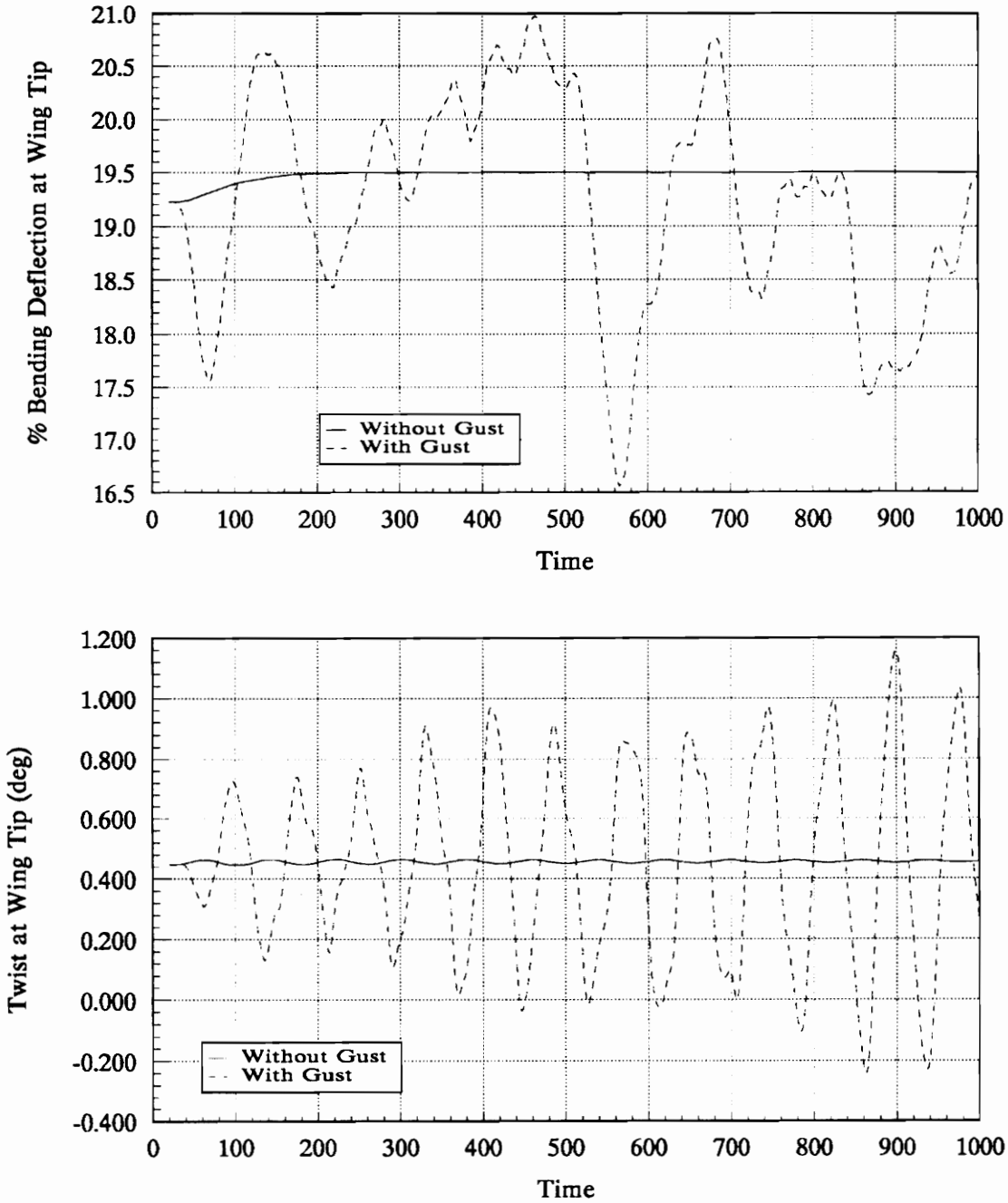

Figure 5.20 The tip deflections of a wing with and without wind gusts. The mean velocity is 50 m/s.

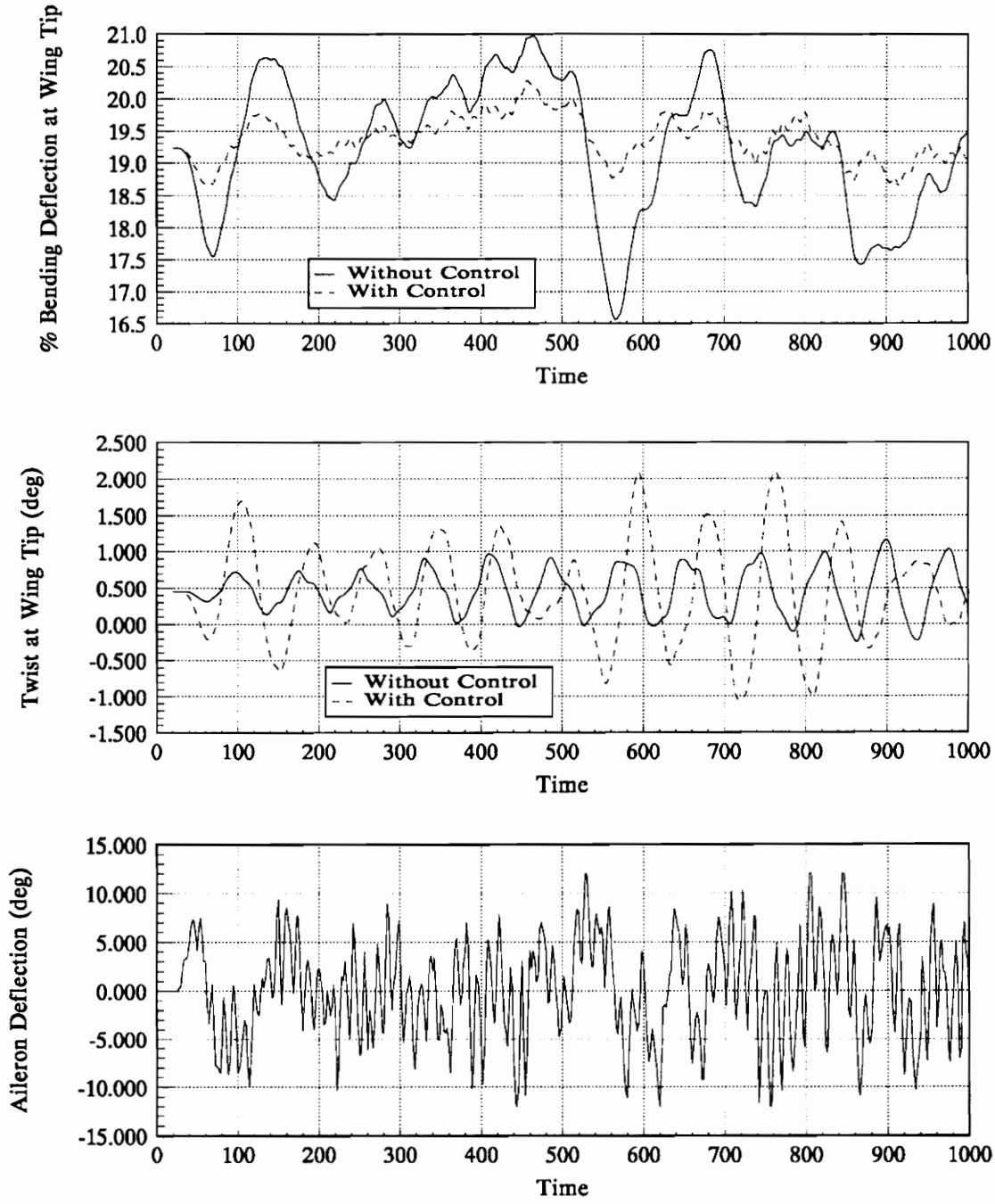

Figure 5.21 The response of the wing under the influence of wind gusts with and without feedback control. The velocity is 50 m/s and the gains are -1 and 1000.

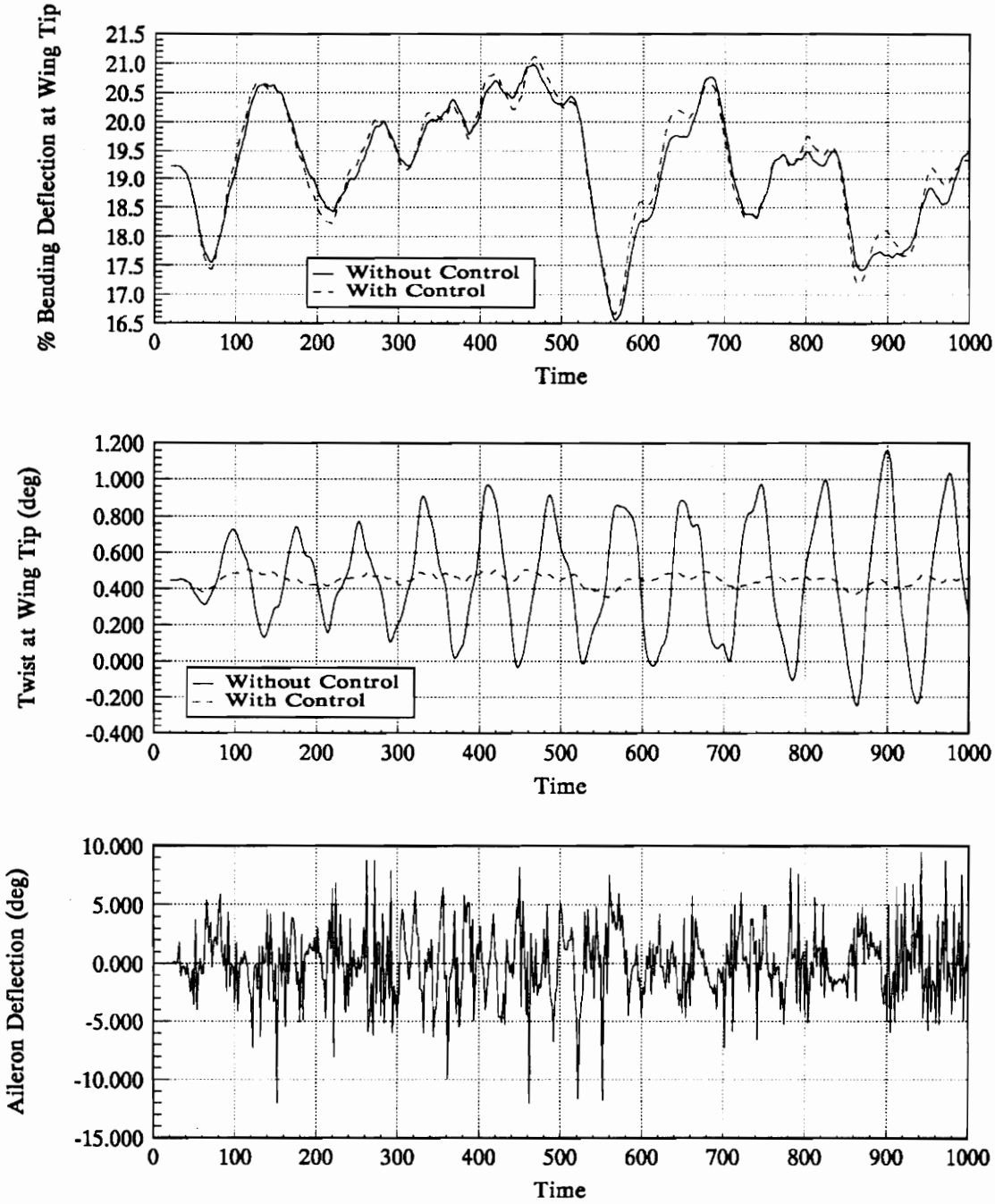

Figure 5.22 The response of the wing under the influence of wind gusts with and without feedback control. The velocity is 50 m/s and the gains are -10 and 0.

Chapter 6 Concluding Remarks

A general model for aeroservoelastic behavior has been presented. The numerical solution scheme is capable of incorporating almost any structural model or aerodynamic model whose solution is found in the time domain. Aerodynamic, material, inertial, or geometric nonlinear effects may be included. Obtaining a solution in the time domain provides a large degree of physical insight. Motions in the subcritical, critical, and supercritical regimes may be modeled with no prior assumptions as to the form of the solution (e.g. periodic motions).

The vortex-lattice method is used to find the aerodynamic loads. This model is valid in the subsonic regime as long as separation or vortex bursting does not occur. The vortex-lattice method is capable of accurately determining the unsteady loads and the position of the wake. The history of the wing deformations resides in the wake. Nonlinear effects due to angle of attack, static deformations, and dynamic deformations are also included.

Two structural models have been used in the aeroelastic formulation: a linear model and a nonlinear model that accounts for large curvature effects. In both cases the wing is modeled as an inextensional cantilevered beam which is allowed flexural-torsional motion. Simulations have shown that static solutions obtained by using the two different models agree closely for deflections up to 20% bending at the wing tip. Curvature effects appear to be negligible in the simulations examined in this work. A complete nonlinear study that includes flexural-torsional coupling and extensional effects should be performed to gain confidence in the relative importance of the nonlinearities. The current work is

intended to demonstrate the ability to include structural nonlinearities.

A feedback control system has been successfully used to suppress flutter. The control system consists of an aileron whose motion is based on the velocity of the wing tip ($\dot{v}$ and $\dot{\phi}$) and corresponding constant gains. The aeroelastic formulation is also capable of incorporating control laws with nonlinear and variable gains. The gains for the current study were selected by a trial and error procedure. It was found that a wide range of gains are effective in the suppression of flutter. The control system suppressed flutter at a velocity of almost twice the flutter speed. No upper bound to the flight speed has been found and velocities much higher might be obtained by selecting an appropriate control law and optimal gains. Although no attempt has been made to find the power requirements necessary for the aileron motion, it appears that only very small deflections are needed.

The response of the wing due to random vertical wing gusts has also been examined. The suppression of the wing motion was attempted by using the active control system. No gains were found that simultaneously suppressed the flexural and torsional motions, though one may be damped at the expense of the other. Large gust frequencies and amplitudes are possible explanations for the poor response characteristics. It should be noted that no attempt has been made to find the optimal gains. Optimization would almost certainly increase the performance of the system.

References

Ashley, H., Lehman, L. L., and Nathman, J. K., "The Constructive Uses of Aeroelasticity," AIAA Paper No. 80-0877, *AIAA International Annual Meeting and Technical Display*, 1980.

Batina, J. T., Seidel, D. A., Bland, S. R., and Bennett, R. M., "Unsteady Transonic Flow Calculations for Realistic Aircraft Configurations," AIAA Paper No. 87-0850, 1987.

Belotserkovskiy, S. M., "Calculating the Effects of Gusts on an Arbitrary Thin Wing," *Fluid Dynamics*, Vol. 1, No. 1, 1966.

Belotserkovskiy, S. M., "Calculation of the Flow around Wings of Arbitrary Planform in a Wide Range of Angles of Attack," NASA TT F-12291, May 1968.

Belotserkovskiy, S. M. and Nisht, M. I., "Nonstationary Nonlinear Theory of a Thin Wing of Arbitrary Planform," *Fluid Dynamics*, Vol. 9, No. 4, 1974.

Biot, M. A. and Arnold, L., "Low-Speed Flutter and Its Physical Interpretation," *Journal of the Aeronautical Sciences*, Vol. 15, April, 1948.

Bisplinghoff, R. L., Ashley, H., and Halfman, R. L., *Aeroelasticity*, Addison-Wesley Publishing Company, Inc., Cambridge, Massachusetts, 1955.

Bisplinghoff, R. L. and Ashley, H., *Principles of Aeroelasticity*, John Wiley & Sons, New York, 1962.

Borland, C. J. and Rizzetta, D. P., "Nonlinear Transonic Flutter Analysis," AIAA Paper No. 81-0608, *AIAA Dynamic Specialist Conference*, April 9-10, 1981.

Crespo da Silva, M. R. M. and Glynn, C. C., "Nonlinear Flexural-Flexural-Torsional Dynamics of Inextensionable Beams. I: Equations of Motion," *Journal of Structural Mechanics*, Vol. 6, 1978.

Crespo da Silva, M. R. M. and Hodges, D. H., "Nonlinear Flexure and Torsion of Rotating Beams, with application to Helicopter Rotor Blades -I. Formulation," *Vertica*, Vol. 10, No. 2, 1986.

Cunningham, H. J., Batina, J. T., and Bennett, R. M., "Modern Wing Flutter Analysis by Computational Fluid Dynamics Methods," *AIAA Journal of Aircraft*, Vol. 25, No. 10, October 1988.

Dong, B., "Numerical Simulations of Wakes, Blade-Vortex Interaction, Flutter, and Flutter Suppression by Feedback Control," Ph.D. Dissertation, Department of Engineering Science and Mechanics, Virginia Polytechnic Institute and State University, August, 1991.

Dowell, E. H. and Ilgamov, M., *Studies in Nonlinear Aeroelasticity*, Springer-Verlag, New York, 1988.

Dowell, E. H., Curtis, H. C. Jr., Scanlan, R. H., and Sisto, F., *A Modern Course in Aeroelasticity*, 2nd edition, Kluwer Academic Publishers, The Netherlands, 1989.

Dowell, E. H., "Nonlinear Aeroelasticity," AIAA Paper No. 90-1031, 1990.

Duncan, W. J., *AGARD Manual on Aeroelasticity*, Vol. 5, "Introductory Survey," 1959.

Elzebda, J. M., Mook, D. T., and Nayfeh, A. H., "Unsteady Aerodynamic Interference for Lifting Surfaces," AIAA Paper No. 85-1801, 1985.

Elzebda, J. M., "Two-Degree-of-Freedom Subsonic Wing Rock and Nonlinear Aerodynamic Interference," Ph.D. Dissertation, Department of Engineering Science and Mechanics, Virginia Polytechnic Institute and State University, August, 1987.

Etkin, B., *Dynamics of Atmospheric Flight*, John Wiley & Sons, New York, 1972.

Fung, Y. C., *An Introduction to the Theory of Aeroelasticity*, John Wiley & Sons, Inc., New York, 1955.

Garrick, I. E., "Aeroelasticity- Frontiers and Beyond," *Journal of Aircraft*, Vol. 13, No. 9, September, 1976.

Garrick, I. E., *Aerodynamic Flutter*, AIAA Selected Reprint Series, Vol. V, March 1969.

Goland, M., and Luke, Y. L., "A Study of the Bending-Torsion Aeroelastic Modes for Aircraft Wings," *Journal of the Aeronautical Sciences*, Vol. 16, No. 7, July, 1949.

Guruswamy, G. P., "Unsteady Aerodynamic and Aeroelastic Calculations for Wings Using Euler Equations," AIAA Paper No. 88-2281, *29th Structures, Structural Dynamics, and Materials Conference*, April 18-20, 1988.

Hancock, G. J., Wright, J. R., and Simpson, A., "On the Teaching of the Principles of Wing Flexure-Torsion Flutter," *Aeronautical Journal*, October, 1985.

Hassig, H. J., "An Approximate True Damping Solution of the Flutter Equation by Determinant Iteration," *Journal of Aircraft*, Vol. 8, No. 11, November, 1971.

Hauenstein, A. J., Laurenson, R. M., Eversman, W., Galecki, G., Qumel, I., and Amos, A. K., "Chaotic Response of Aerosurfaces with Structural Nonlinearities," AIAA Paper No. 90-1034, 1990.

Helmholtz, H., von, "On Integrals of the Hydrodynamic Equations Which Express Vortex Motion," 1858, Translation by P. G. Tait, 1867, *Philosophical Magazine*, Vol. 4.

James, R. M., "On the Remarkable Accuracy of the Vortex Lattice Method," *Computer Methods in Applied Mechanics and Engineering 1*, 1972.

Kandil, O. A., Mook, D. T., and Nayfeh, A. H., "Nonlinear Prediction of the Aerodynamic Loads on Lifting Surfaces," AIAA Paper No. 74-503, 1974.

Kandil, O. A., "Prediction of the Steady Aerodynamic Loads on Lifting Surfaces Having Sharp-Edge Separation," Ph.D. Dissertation, Department of Engineering Science and Mechanics, Virginia Polytechnic Institute and State University, 1974.

Karamcheti, K. K., *Principles of Ideal-Fluid Aerodynamics*, John Wiley & Sons, Inc., New York, 1980.

Karpel, M., "Design for Active and Passive Flutter Suppression and Gust Alleviation," NASA CR 3482, 1981.

Kaza, K. R. V. and Kvaternik, R. G., "Nonlinear Aeroelastic Equations for Combined Flapwise Bending, Chordwise Bending, Torsion, and Extension of Twisted Nonuniform Rotor Blades in Forward Flight," NASA TM 74059, August, 1977.

Kelly, S. G., "A Systematic Investigation of the Parameters Affecting the Accuracy of the Vortex-Lattice Method," M.S. Thesis, Department of Engineering Science and Mechanics, Virginia Polytechnic Institute and State University, May 1977.

Konstadinopoulos, P., "A Vortex-Lattice Method for General, Unsteady, Subsonic, Aerodynamics," M.S. Thesis, Department of Engineering Science and Mechanics, Virginia Polytechnic Institute and State University, July 1981.

Konstadinopoulos, P., "Numerical Simulation of the Subsonic Wing-Rock Phenomenon," Ph.D. Dissertation, Department of Engineering Science and Mechanics, Virginia Polytechnic Institute and State University, March 1984.

Konstadinopoulos, P., Mook, D. T., and Nayfeh, A. H., "Subsonic Wing Rock of Slender Delta Wings," *Journal of Aircraft*, Vol. 22, March 1985.

Kussner, H. G., "General Lifting Surface Theory," *Luftfahrtforschung*, Vol. 17, 1940.

Levin, D., "A Vortex-Lattice Method for Calculating Longitudinal Dynamic Stability Derivatives of Oscillating Delta Wings," AIAA Paper No. 81-1876, 1981.

Loring, S. J., "Outline of a General Approach to the Flutter Problem," *Society of Automotive Engineers Journal*, August, 1941.

Mahesh, J. K., Stone, C. R., Garrrard, W. L., and Dunn, H. J., "Control Law Synthesis for Flutter Suppression Using Linear Quadratic Gaussian Theory," *Journal of Guidance and Control*, Vol. 4, No. 4, July-August 1981.

Mook, D. T. and Maddox, S. A., "An Extension of a Vortex-Lattice Method to Include the Effects of Leading-Edge Separation," *Journal of Aircraft*, Vol. 11, No. 2, 1974.

Mook, D. T., "Unsteady Aerodynamics," *von Karman Institute for Fluid Dynamics Lecture Series 1988-07*, Vol. 1, *Unsteady Aerodynamics*, April 18-22, 1988.

Mukhopadhyay, V., Newsom, J. R., and Abel, I., "Reduced-Order Optimal Feedback Control Law Synthesis for Flutter Suppression," *Journal of Guidance*, Vol. 5, No. 4, July-August, 1982.

Mukhopadhyay, V., Perry, B. III, and Noll, T. E., "Flutter Suppression Control Law Synthesis for the Active Flexible Wing Model," NASA TM 101584, May, 1989.

Nayfeh, A. H. and Mook, D. T., *Nonlinear Oscillations*, John Wiley & Sons, Inc., New York, 1979.

Nayfeh, A. H., Mook, D. T., and Yen, A., "The Aerodynamics of Small Harmonic Oscillations Around Large Angles of Attack," AIAA Paper No. 79-1520, 1979.

Niblett, L. T., "A Guide to Classical Flutter," *Aeronautical Journal*, November, 1988.

Nissim, E., "Flutter Suppression Using Active Controls Based on the Concept of Aerodynamic Energy," NASA TN D-6199, 1971.

Noll, T. E., "Aeroservoelasticity," NASA TM 102620, March, 1990.

Nuhait, A. O., "Numerical Simulation of Wing in Steady and Unsteady Ground Effects and of Feedback Control," Ph.D. Dissertation, Department of Engineering Science and Mechanics, Virginia Polytechnic Institute and State University, October, 1988.

Ohta, H., Fujimori, A., Nikiforuk, P. N., and Gupta, M. M., "Active Flutter Suppression for Two-Dimensional Airfoils," *Journal of Guidance*, Vol. 12, No. 2, March-April, 1989.

Ormiston, R. A., "Survey of Army/NASA Rotorcraft Aeroelastic Stability Research," NASA TM 101026, 1988.

Pines, S., "An Elementary Explanation of the Flutter Mechanism," *Proceedings of the National Specialists Meeting on Dynamics and Aeroelasticity*, Institute of the Aeronautical Sciences, Fort Worth, Texas, November 6-7, 1958.

Rao, S. S., *Mechanical Vibrations*, Addison-Wesley Publishing Company, Inc., Reading, Massachusetts, 1986.

Rausch, R. D., Batina, J. T., and Yang, H. T. Y., "Euler Flutter Analysis of Airfoils Using Unstructured Dynamic Meshes," AIAA Paper No. 89-1384, *30th Structures, Structural Dynamics, and Materials Conference*, April 3-5, 1989.

Richardson, J. R., "A More Realistic Method for Routine Flutter Calculations," *AIAA Symposium on Structural Dynamics and Aeroelasticity*, Boston, Massachusetts, August 30 - September 1, 1965.

Sarpkaya, T., "Computational Methods with Vortices- The 1988 Freeman Scholar Lecture," *Journal of Fluids Engineering*, Vol. 111, March 1989.

Smilg, B. and Wasserman, L. S., "Application of Three-Dimensional Flutter Theory to Aircraft Structures," Air Force Technical Report 4798, 1942.

Strganac, T. W. and Mook, D. T., "A New Method to Predict Unsteady Aeroelastic Behavior," AIAA Paper No. 87-0736, *28th Structures, Structural Dynamics, and Materials Conference*, April 6-8, 1987.

Strganac, T. W., "A Numerical Model of Unsteady, Subsonic Aeroelastic Behavior," Ph.D. Dissertation, Department of Engineering Science and Mechanics, Virginia Polytechnic Institute and State University, August 1987.

Theodorsen, T., "General Theory of Aerodynamic Instability and the Mechanism of Flutter," NACA Report 496, 1935.

Thrasher, D. F., Mook, D. T., Kandil, O. A., and Nayfeh, A. H., "Application of the Vortex-Lattice Concept to General, Unsteady Lifting-Surface Problems," AIAA Paper No. 77-1157, 1977.

Thrasher, D. F., "Nonlinear Unsteady Aerodynamics with Application to Dynamic-Aerodynamic Interaction," M.S. Thesis, Department of Engineering Science and Mechanics, Virginia Polytechnic Institute and State University, 1979.

Watkins, C. E., Runyan, H. L., and Wollston, D. S., "On the Kernel Function of the

Integral Equation Relating the Lift and Downwash Distributions of Oscillating Finite Wings in Subsonic Flow," NACA Report 1234, 1955.

Weisshaar, T. A., "Aeroelastic Tailoring- Creative Uses of Unusual Materials," AIAA Paper No. 87-0976, *28th Structures, Structural Dynamics, and Materials Conference*, 1987.

Yates, E. C., Jr., "Flutter and Unsteady Lift Theory," NASA SP 258, 1971.

Yates, E. C., Jr., Wynne, E. C., and Farmer, M. G., "Measured and Calculated Effects of Angle of Attack on the Transonic Flutter of a Supercritical Wing," AIAA Paper No. 82-0647, 1982.

Appendix

The linear undamped equations of motion for the torsional and flexural free vibrations of a cantilever beam are uncoupled and may be solved using a separation of variables technique. For torsion, the governing equation reduces to

$$\ddot{\phi} - k^2\phi'' = 0 \tag{A.1}$$

with $k^2 = D_t$ and subjected to the boundary conditions

$$\phi(0,t) = 0 \tag{A.2}$$

$$\phi'(L,t) = 0 \tag{A.3}$$

where L is the length of the beam. Applying the method of separation of variables, ϕ is written as

$$\phi(x,t) = \chi(x)T(t) \tag{A.4}$$

where x is the distance along the elastic axis. Substituting into equation (A.1) leads to

$$\frac{\ddot{T}(t)}{T(t)} = k^2\frac{\chi''(x)}{\chi(x)} = -\omega_t^2 \tag{A.5}$$

Since the functions T and χ are independent of one another, they may only be equal if they are equal to some constant, denoted here as $-\omega_t^2$. Therefore equation (A.5) becomes

$$\ddot{T}(t) + \omega_t^2 T(t) = 0 \tag{A.6}$$

$$\chi''(x) + \frac{\omega_t^2}{k^2}\chi(x) = 0 \tag{A.7}$$

The first equation shows that ω_t is the reduced natural frequency. The solution of the second equation is

$$\chi(x) = A\cos(\frac{\omega_t}{k}x) + B\sin(\frac{\omega_t}{k}x) \tag{A.8}$$

where A and B are unknown constants. Applying the first boundary condition,

$$\phi(0,t) = \chi(0)T(t) = 0 \tag{A.9}$$

$$\chi(0) = A\cos(0) + B\sin(0) = 0 \tag{A.10}$$

$$\therefore \quad A = 0 \tag{A.11}$$

and

$$\chi(x) = B\sin(\frac{\omega_t}{k}x) \tag{A.12}$$

Applying the second boundary condition,

$$\phi'(L,t) = \chi'(L)T(t) \tag{A.13}$$

$$\chi'(L) = B\frac{\omega_t}{k}\cos(\frac{\omega_t}{k}L) = 0 \tag{A.14}$$

$$\therefore \quad \omega_t = \frac{k}{L}(n - \frac{1}{2})\pi \qquad \text{where} \quad n=1,2,3... \tag{A.15}$$

The constant $\boldsymbol{B}$ is chosen such that the mode shapes are normalized.

$$\int_0^L \chi^2(x)dx = 1 \tag{A.16}$$

$$B^2\int_0^L \sin^2(\frac{\omega_t}{k}x)dx = 1 \tag{A.17}$$

$$B^2\left[\frac{1}{2}L - \frac{k}{4\omega_t}\sin(\frac{2\omega_t}{k}L)\right] = 1 \tag{A.18}$$

The second term is identically zero, so

$$B = \sqrt{\frac{2}{L}} \tag{A.19}$$

Thus, the linear undamped natural mode shapes are

$$\chi_n(x) = \sqrt{\frac{2}{L}}\sin\left(\frac{\omega_{t,n}x}{\sqrt{D_t}}\right) \tag{A.20}$$

where

$$\omega_{t,n} = \frac{\sqrt{D_t}}{L}(n - \frac{1}{2})\pi \qquad n=1,2,3... \tag{A.21}$$

For linear, undamped, free vibration motion the governing equation for bending is

$$\ddot{v} + k^4 v'''' = 0 \tag{A.22}$$

with $k^4 = D_b$ and subjected to the boundary conditions

$$\begin{aligned} v(0,t) &= 0 \\ v'(0,t) &= 0 \\ v''(L,t) &= 0 \\ v'''(L,t) &= 0 \end{aligned} \tag{A.23}$$

Expressing the transverse displacement as

$$v(x,t) = \psi(x)T(t) \tag{A.24}$$

and substituting into equation (A.22) leads to

$$\frac{\ddot{T}(t)}{T(t)} = -k^4 \frac{\psi''''(x)}{\psi(x)} = -\omega_b^2 = -\lambda^4 \tag{A.25}$$

or

$$\ddot{T}(t) + \omega_b^2 T(t) = 0 \tag{A.26}$$

$$\psi''''(x) - \frac{\lambda^4}{k^4}\psi(x) = 0 \tag{A.27}$$

where ω_b is the reduced natural frequency. The solution of the second equation is

$$\psi(x) = A\cosh(\frac{\lambda}{k}x) + B\sinh(\frac{\lambda}{k}x) + C\cos(\frac{\lambda}{k}x) + D\sin(\frac{\lambda}{k}x) \tag{A.28}$$

where A, B, C, and D are constants. Utilizing the boundary conditions at the fixed end gives

$$\begin{aligned} C &= -A \\ D &= -B \end{aligned} \tag{A.29}$$

so that

$$\psi(x) = A\left[\cosh(\frac{\lambda}{k}x) - \cos(\frac{\lambda}{k}x)\right] + B\left[\sinh(\frac{\lambda}{k}x) - \sin(\frac{\lambda}{k}x)\right] \tag{A.30}$$

Applying the third and forth boundary conditions gives

$$\frac{B}{A} = -\frac{\cosh(\alpha) + \cos(\alpha)}{\sinh(\alpha) + \sin(\alpha)} \tag{A.31}$$

and

$$\frac{B}{A} = -\frac{\sinh(\alpha)-\sin(\alpha)}{\cosh(\alpha)+\cos(\alpha)} \tag{A.32}$$

where $\alpha = \frac{\lambda}{k}L$. Equating equations (A.31) and (A.32) yields

$$\cosh(\alpha)\cos(\alpha)+1=0 \tag{A.33}$$

The variable α may be found numerically. Rao (1986) lists the first four values as

$$\begin{aligned} \alpha_1 &= 1.875104 \\ \alpha_2 &= 4.694091 \\ \alpha_3 &= 7.854757 \\ \alpha_4 &= 10.995541 \end{aligned} \tag{A.34}$$

The reduced natural frequency is found from equation (A.33) as

$$\omega_{b,n} = \frac{\sqrt{D_b}\,\alpha_n^2}{L^2} \tag{A.35}$$

To obtain the mode shapes, substitute equation (A.31) into equation (A.30) to achieve

$$\psi_n(x) = \frac{1}{\sqrt{L}}\left\{\cosh(\frac{\lambda_n}{k}x)-\cos(\frac{\lambda_n}{k}x)-K_n\left[\sinh(\frac{\lambda_n}{k}x)-\sin(\frac{\lambda_n}{k}x)\right]\right\} \tag{A.36}$$

where

$$K_n = \frac{\cos(\frac{\lambda_n}{k}L) + \cos(\frac{\lambda_n}{k}L)}{\sinh(\frac{\lambda_n}{k}L) + \sin(\frac{\lambda_n}{k}L)} \tag{A.37}$$

and the constant $\boldsymbol{A}$ has been chosen to normalize the mode shapes.

Vita

The author was born in Oak Ridge, Tennessee on December 16, 1966. He attended Oak Ridge High School and served as captain of the soccer team. After graduating in 1985, he attended Tennessee Technological University to continue his academic and athletic careers. During his course of study he received the Tennessee Tech Academic Scholarship and the Martin Marietta Engineering Scholarship. After graduating magna cum laude with a baccalaureate degree in Mechanical Engineering he traveled extensively, exploring his passion of photography and the wilderness. He began graduate studies at Virginia Polytechnic Institute and State University and accepted the Virginia Tech Tuition Scholarship and Presidential Fellowship in August of 1989. He obtained his Master of Science degree in December of 1991 and is currently pursuing his doctorate degree at Virginia Tech. The author is a member of Kappa Mu Epsilon and Phi Kappa Phi.